

**Intestinal permeability and gut microbiota interactions of
phytochemicals from herbal drugs used in the treatment of
depressive, anxiety and sleeping disorders**

Inauguraldissertation

zur

Erlangung der Würde eines Doktors der Philosophie

vorgelegt der

Philosophisch-Naturwissenschaftlichen Fakultät

der Universität Basel

von

Antoine Chauveau

Basel, 2023

Genehmigt von der Philosophisch-Naturwissenschaftlichen Fakultät

auf Antrag von

Prof. Dr. Matthias Hamburger

Prof. Dr. Daniel Ricklin

Prof. Dr. Francisco A. Tomás-Barberán

Basel, den 14.11.2023

Prof. Dr. Marcel Mayor

Dekan

Acknowledgment

First of all, I would like to address my biggest gratitude to Prof. Dr. Matthias Hamburger for giving me the opportunity to conduct this PhD project at the department of Pharmaceutical Biology (University of Basel). His long-lasting experience as a professor in Pharmaceutical Biology, separation sciences and pharmaceutical sciences (among many others), has been crucial for the guidance of my PhD project. I also thank him for the nice atmosphere he has created in the lab. I have learned a lot by his side and I am honored that I was his last PhD student.

Secondly, I would like to address my big thanks Prof. Dr. Olivier Potterat (Pharmaceutical Biology, University of Basel), which was also involved in my global supervision, but also on a more daily basis. Olivier's experience was key to take good decisions, in research but also in technical aspects related to phytochemistry or separation sciences (among others). It has been a pleasure to interact with him over these PhD years.

I would like to warmly thank Prof. Dr. Robin Teufel (successor of Prof. Dr. Matthias Hamburger as head of Pharmaceutical Biology department, University of Basel) to allow me to complete my doctoral studies at the department. I would like to particularly thank him for being supportive and understanding by granting me a contract extension of several months, so that I could properly complete my PhD project.

I would like to warmly thank Prof. Dr. Daniel Ricklin (Molecular Pharmacy, University of Basel) for being my second supervisor over the whole project. His experience in Pharmaceutical Sciences and active listening were always appreciated.

I would like to thank Prof. Dr. Francisco A. Tomás Barberán (CEBAS-CSIC, Murcia) for being the external examiner of this thesis.

I address my warm thanks to Dr. Mouhssin Oufir (Pharmaceutical Biology, University of Basel); for the supervision of the bioanalytics part of the project, and also for his approach with industry-like standards of quality. His experience and vision in bioanalytics and ADME have been of great importance to launch well the project.

The next person I would like to warmly thank is Dr. Andrea Treyer (Pharmaceutical biology, university of Basel). Her experience in ADME, bioanalytics and cell culture was a key asset to the project. Her training for cell culture and Caco-2 assays was crucial. Furthermore, her approach of research was inspiring.

My big thanks also go to Dr. Annelies Geirnaert (Laboratory of Food Biotechnology, Institute of Food, Nutrition and Health, Department of Health Science and Technology, ETH Zurich) for her coordination and supervision of the gut microbiota related work. Her expertise and experience as microbiologist have been crucial over the whole PhD project. My thanks also go to her colleagues which conducted the batch fermentation experiments, Dr. Lea Bircher and Angela Babst, and to Alfonso Die for the analysis of the gut microbial metabolites.

I would like to warmly thank PD Dr. Ana Paula Simões-Wüst (Department of Obstetrics, University Hospital Zurich), for the global coordination and supervision she provided over the whole course of the ambitious Sinergia project "Herbal Safety in Pregnancy".

I also would like to warmly thank Prof. Dr. Carsten Gründemann (Translational Complementary Medicine, University of Basel), a key collaborator in the Sinergia project.

I would like to warmly thank my “PhD student” collaborators of the Sinergia project, Vanessa Abegg (Pharmaceutical Biology, University of Basel), Moritz Winker (Translational Complementary Medicine, University of Basel) and Deborah Spiess (Department of Obstetrics, University Hospital Zurich). Over these PhD years, we have developed a nice collaboration.

My thanks also go to the Swiss National Science foundation, which has provided the funding of the Sinergia project [CRSII5_177260; Herbal Safety in Pregnancy].

Additionally, I would like to thank my colleagues Dr. Morris Keller, Dr. Jakob Reinhardt and Orlando Fertig for the work related to the isolation of the escholtzine from California poppy.

I would like to thank Orlando Fertig for his help in daily lab organization, instrument troubleshooting and material ordering.

I thank very much Manuela Rogalski for her support with the administrative related aspects. Her help has been really appreciated over my stay at the Pharmaceutical Biology department.

I thank very much Tamara for her help with the translation of the abstract in German, and with the organization of my PhD defense.

My next thanks go to the co-workers I had the pleasure to share the labs, offices and coffee breaks over my PhD at the Pharmaceutical biology department (PhD students, PostDocs, scientists, visiting PhD scientists, and master’s students): Morris, Jakob, Nova, Pascaline, Ming, Halim, Ahmed, Teresa, Lara, Tanja, Eliane, Theresa, Justine, Ombeline, Tamara, Ruzhe, Maria, Natalie, Lars, Malik, Heiner, Lei, Sven, Andreas and Xinya. Particularly, I would like to thank Teresa, Halim and Ahmed, with whom I had nice and fun times inside or outside of the lab.

On a more personal note, I would like to thank friends that particularly counted for me over these PhD years: Tess, Pierre, Théo, Zdeněk, Anna, Maïté, Emre, Julien, Marina, Loren, Diego, Rafaëlle, Robert, Félix, Benoît, Charles, Bilel and Djerem.

To finish, I want to address huge thanks to my family, my mum, my dad, and my brother. They have always encouraged and supported me. My parents, on top of having provided me a good life (to me and my brother), have created from very early on, an environment that developed my curiosity, open-mindedness, critical thinking and autonomy, which is the best gift a son can wish for, and a good asset to complete big challenges in life. This thesis is dedicated to them.

Table of contents

Acknowledgment	3
List of abbreviations	7
Summary	9
Zusammenfassung	11
1 Aim of the work	14
2 Introduction	16
2.1 The intestinal absorption of xenobiotics	17
2.1.1 The gastrointestinal tract	18
2.1.2 The mucosa of the intestines	20
2.1.3 Permeation mechanisms of xenobiotics	22
2.1.4 Intestinal metabolism of xenobiotics	26
2.1.5 The Caco-2 cell model	27
2.1.5.1 Origin	27
2.1.5.2 Structural and functional features of differentiated Caco-2 cells	28
2.1.5.3 Permeability experiments	29
2.1.6 Other models to predict permeability of xenobiotics	31
2.1.6.1 Nonbiological models	31
2.1.6.2 Biological models	32
2.2 The gut microbiota interactions with xenobiotics	33
2.2.1 Gut microbiota composition	34
2.2.2 Functions of the gut microbiota	36
2.2.3 Microbiota-mediated biotransformation of xenobiotics	40
2.2.4 Impact of xenobiotics on gut bacterial metabolism	43
2.2.5 The <i>in vitro</i> PolyFermS model, an artificial gut microbiota	44
2.2.6 Other <i>in vitro</i> fermentation models of the human gut microbiome	47
2.3 Investigated herbal drugs and phytochemicals	48
2.3.1 Valerian	49
2.3.2 St John's wort	50
2.3.3 California poppy	51
3 Results and discussion	52
3.1 Intestinal permeability and gut microbiota interactions of pharmacologically active compounds in valerian and St. John's wort	53
3.2 Alkaloids in commercial preparations of California poppy – Quantification, intestinal permeability and microbiota interactions	65
4 Conclusions and outlook	76

References	81
Appendix	92
Supporting information of section 3.1	93
Supporting information of section 3.2.....	101
Curriculum Vitae	111

List of abbreviations

2/4/A1	Rat intestinal cell line
5-ASA	5-aminosalicylic acid
ABCs	ATP-binding cassette transporters
ADME	Absorption, distribution, metabolism, excretion
AMPs	Antimicrobial peptides
ASBT	Apical sodium-dependent bile acid transporter
ATP	Adenosine triphosphate
BBB	Blood-brain-barrier
BCRP	Breast cancer resistance protein
BDNF	Brain-derived neurotrophic factor
BSA	Bovine serum albumin
Caco-2	Human colon adenocarcinoma cell line
Caco-2/HT29-MTX	Co-culture of Caco-2 and HT29-MTX
clogD	Calculated logD
clogP	Calculated logP
CNS	Central nervous system
CoA	Coenzyme A
CR	Control reactor
CYP	Cytochrome P450
DC	Dendritic cells
DHAP	Dihydroxyacetonephosphate
EMA	European Medicine Agency
ENT	Equilibrative nucleoside transporter
ER	Efflux ratio
FFARs	Free fatty acid receptors
GABA _A	γ-aminobutyric acid
GDNF	Glial cell line-derived neurotrophic factor
GI	Gastrointestinal
GLP1	Glucagon-like-peptide 1
GST	Glutathione-S-transferase
HITChip	Human Intestinal Tract Chip
HT29-MTX	Human colon adenocarcinoma mucus producing cell line
IEC	Intestinal epithelial cell
IESC	Intestinal epithelial stem cell
IR	Inoculum reactor
ITC	International Transporter Consortium
lag-time	Time for an oral compound to appear in systemic circulation

MCT	Monocarboxylate transporter
MDCK	Madin-Darby canine kidney cell line
MDCK-BCRP	Madin-Darby canine kidney cell line overexpressing BCRP
MRP	Multidrug resistance protein
M-SHIME	Mucosal-simulator of the human intestinal microbial ecosystem
MW	Molecular weight
NGF	Nerve growth factor
NSAID	Nonsteroidal anti-inflammatory drug
OATP2B1	Organic anion transporting polypeptide
OST	Organic solute transporter
PAMPA	Parallel artificial membrane permeability assay
P_{app}	Apparent permeability coefficient
P_{appAB}	P_{app} in the absorptive direction (from apical to basolateral)
P_{appBA}	P_{app} in the secretory direction (from basolateral to apical)
PEP	Phosphoenolpyruvate
PEPT	Peptide transporter
Pg-p	P-glycoprotein
PolyFermS	Polyfermentor Intestinal Model
PYY	Peptide YY
RT	Retention time
SCFA	Short-chain fatty acid
SHIME®	Simulator of the human intestinal microbial ecosystem
sIgA	Secretory immunoglobulin A
SIHUMIx	Simplified human intestinal microbiota
SIMGI	Simulator of the gastrointestinal tract
SLCs	Solute carriers
SULT	Sulphotransferase
TC7	Late passaged human colon adenocarcinoma cell line
TFF3	Trefoil factor 3
THTR	Thiamine transporters
TIM-2	TNO in vitro model of the colon
t_{max}	Time to reach the C_{max}
TR	Test reactor
UGT	Uridine diphospho-glucuronosyltransferase
UHPLC/MS-MS	Ultrahigh-performance liquid chromatography coupled with tandem mass spectrometry
USA	United States of America

Summary

The use of herbal medicines to treat depression, anxiety and sleeping disorders is a tendency that has increased over the past decades. Valerian (*Valeriana officinalis* L., Caprifoliaceae), St. John's wort (*Hypericum perforatum* L., Hypericaceae) and California poppy (*Eschscholzia californica*, Cham., Papaveraceae) are herbal medicines that are commonly used for the management of these disorders. They contain pharmacologically relevant compounds such as valerenic acid (valerian), hyperforin and hypericin (St. John's wort), and californidine, escholtzine and protopine (California poppy). To date, the intestinal permeability of these herbal compounds has been poorly investigated. In addition, the reciprocal interactions between these compounds and the human gut microbiota have not been explored; in particular, their possible biotransformation by the gut microbiome, or a possible impact of the exposure of these herbal compounds or extracts on the microbial metabolism of short-chain fatty acids (SCFAs) and on the bacterial viability. In light of the growing number of studies describing the biotransformation of oral compounds (drugs, dietary compounds, or phytochemicals) by the gut microbiome, or the emerging evidence that gut microbial metabolites such as SCFAs play a significant role in the modulation of the central nervous system (CNS) via the microbiota-gut-brain axis, an assessment of these gut microbiota interactions is necessary. Finally, considering herbal medicines, unlike for valerian and St. John's wort, only very few studies have determined the contents of pharmacologically active constituents in commercial preparations of California poppy (californidine, escholtzine and protopine), making it challenging to estimate the levels that can be anticipated in patients.

Firstly, the intestinal permeability of herbal compounds valerenic acid, hyperforin, hypericin, californidine, escholtzine and protopine was studied, with filter-grown Caco-2 cell monolayers as a model of the human small intestinal epithelium. The model was validated with markers of low-to-moderately and highly permeable compounds, atenolol and propranolol, respectively. The transport of all compounds was assessed in both directions, from apical to basolateral and vice versa.

Thereafter, the gut microbiota interactions between herbal extracts and compounds were evaluated with short-term batch fermentation experiments (24 h) using an *in vitro* gut microbiota, the Polyfermentor Intestinal Model (PolyFermS). Experiments were conducted with effluents from two PolyFermS, each one generated from a different healthy fecal donor. The validity of both PolyFermS was confirmed by stable gut microbiota composition and steady metabolic activity (production of SCFAs), hallmarks of a healthy gut microbiome. Batch fermentation experiments allowed, on the one hand, the assessment of a microbiota-mediated biotransformation of herbal compounds, and on the other hand, the measurement of microbial metabolic activity (SCFAs production) and bacterial viability in the presence of herbal compounds and extracts. SCFAs were quantified by HPLC coupled with a refractive index detector and total viable and dead bacterial cells were determined by flow cytometry.

Furthermore, the contents of californidine, escholtzine and protopine were determined in eight commercial preparations of California poppy, sold as phytomedicines or food supplements. The preparations consisted of dry herbal powders, dry extracts or fluid extracts of flowering aerial parts of California poppy.

For each herbal compound, a sensitive and selective UHPLC-MS/MS method was developed and validated for the analysis of Caco-2 cells, gut microbiota and California poppy samples.

Valerenic acid, hyperforin, escholtzine and protopine were highly absorbed in the Caco-2 cell model. A carrier-mediated process was possibly involved in the transport of valerenic acid (uptake), escholtzine (efflux) and protopine (efflux), whereas hyperforin was likely transported by passive diffusion. In addition, the low recovery values (13 – 69%) obtained for valerenic acid, escholtzine and protopine suggest that the compounds might be metabolized in the Caco-2 cells. In turn, hypericin and californidine showed a low-to-moderate absorption, possibly with passive diffusion as transport process for hypericin and active transport for californidine (efflux). These data indicate that hypericin and californidine have the potential to be found at relevant concentrations in the colon segment, where the gut microbiome is the densest.

All the herbal compounds showed a high stability in the batch fermentation experiments, suggesting that they are not biotransformed by the human gut microbiome. These results support that the disposition of these herbal compounds is not influenced by the gut microbiome. Furthermore, the exposure of herbal extracts and compounds did not markedly impact the bacterial metabolism of SCFAs or the bacterial viability. This suggests that valerian, St. John's wort or California poppy, at the tested concentrations, may not exert an indirect effect on the CNS via modulation of bacterial SCFAs implicated in microbiota-gut-brain axis signaling, at least not after a short-term exposure (24 h). Given the high inter-individual variabilities between human gut microbiota and short-term experiments setup, these findings need to be confirmed with a larger number of microbiota and with continuous fermentation models to further evaluate the possible impact on microbiota metabolic activity and bacterial viability, over a prolonged exposure.

Alkaloid contents differed strongly between the commercial products of California poppy, ranging from 0.13 – 2.55 mg/g for californidine, 0.05 – 0.63 mg/g for escholtzine and 0.008 – 0.200 mg/g for protopine. These marked variations are likely due, at least in part, to differing extraction procedures. Based on these data and the dosage recommended by manufacturers, maximum daily doses for the three alkaloids were calculated to range from 0.16 to 2.97, 0.10 to 1.11, and 0.02 to 0.31 mg/day, respectively. Thus, for patients using different California poppy preparations, significant variations in the daily intake of californidine, escholtzine and protopine, have to be expected.

Zusammenfassung

Die Verwendung pflanzlicher Arzneimittel zur Behandlung von Depressionen, Angstzuständen und Schlafstörungen zeigt eine zunehmende Tendenz in den letzten Jahrzehnten. Baldrian (*Valeriana officinalis* L., Caprifoliaceae), Johanniskraut (*Hypericum perforatum* L., Hypericaceae) und Kalifornischer Mohn (*Eschscholzia californica*, Cham., Papaveraceae) sind pflanzliche Arzneimittel, die häufig zur Behandlung der oben genannten Krankheiten eingesetzt werden. Sie enthalten pharmakologisch relevante Verbindungen wie Valerensäure (Baldrian), Hyperforin und Hypericin (Johanniskraut) sowie Californidin, Escholtzin und Protopin (Kalifornischer Mohn). Bisher wurde die intestinale Permeabilität dieser pflanzlichen Verbindungen jedoch nur unzureichend untersucht. Ebenfalls wurden Wechselwirkungen zwischen den Stoffen und der menschlichen Darmflora nicht erforscht, insbesondere ihre mögliche Biotransformation durch das Darmmikrobiom sowie mögliche Auswirkungen auf den mikrobiellen Stoffwechsel kurzkettiger Fettsäuren (SCFAs) und die bakterielle Lebensfähigkeit durch die Exposition gegenüber den pflanzlichen Verbindungen oder Extrakten. Angesichts der zunehmenden Anzahl Studien, die die Biotransformation oraler Substanzen (Arzneimittel, Nahrungsbestandteile oder sekundäre Pflanzenstoffe) durch das Darmmikrobiom beschreiben und der sich abzeichnenden Hinweise darauf, dass Stoffwechselprodukte des Darmmikrobioms wie SCFAs eine wichtige Rolle spielen bei der Modulation des zentralen Nervensystems durch die Mikrobiota-Darm-Hirn-Achse, ist eine Aufarbeitung dieser Interaktionen mit dem Darmmikrobiom notwendig. Bezüglich pflanzlicher Arzneimittel sind im Unterschied zu Baldrian und dem Johanniskraut nur sehr wenige Studien zum Gehalt an pharmakologisch wirksamen Bestandteilen in kommerziellen Präparaten von Kalifornischem Mohn (Californidin, Escholtzin und Protopin) publiziert, weshalb es schwierig ist die zu erwartenden Spiegel in Patienten abzuschätzen.

Zunächst wurde die intestinale Permeabilität der pflanzlichen Verbindungen Valerensäure, Hyperforin, Hypericin, Californidin, Escholtzin und Protopin untersucht, wobei als Modell für das menschliche Dünndarmepithel filtrierte Caco-2-Zellmonoschichten verwendet wurden. Das Modell wurde mit Markern für gering bis mittelmäßig und hoch durchlässige Verbindungen, Atenolol bzw. Propranolol validiert. Der Transport aller Verbindungen wurde jeweils in beide Richtungen untersucht, von apikal nach basolateral und umgekehrt.

Anschließend wurden die Wechselwirkungen zwischen den pflanzlichen Extrakten und den Verbindungen mit der Darmmikrobiota in Kurzzeit-Batch-Fermentierungsexperimenten (24 Stunden) untersucht unter Verwendung einer In-vitro-Darmmikrobiota, dem Polyfermentor Intestinal Model (PolyfermS). Die Experimente wurden mit den künstlichen Mikrobiota von zwei PolyfermS durchgeführt, die jeweils von zwei unterschiedlichen gesunden Fäkalspender stammten. Die Validität beider PolyfermS wurde durch die stabile Zusammensetzung der Darmmikrobiota und der gleichbleibenden Stoffwechselaktivität (Produktion von SCFAs) bestätigt, beide Faktoren sind Kennzeichen für ein gesundes Darmmikrobiom. Die Batch-Fermentationsexperimente ermöglichten

zum einen die Beurteilung der durch Mikrobiota bedingten Biotransformation der pflanzlichen Verbindung und zum anderen die Messung der mikrobiellen metabolischen Aktivität (SCFAs Produktion) und der bakteriellen Lebensfähigkeit unter Anwesenheit der pflanzlichen Verbindungen und Extrakten. Die SCFAs wurde über einen HPLC quantifiziert, welche an einen Brechungsindexdetektor gekoppelt war. Die Gesamtzahl lebendiger und toter Bakterienzellen wurde mittels Durchflusszytometrie bestimmt.

Des Weiteren wurde der Gehalt an Californidin, Escholtzin und Protopin in acht kommerziellen Präparaten aus Kalifornischem Mohn bestimmt. Alle Präparate werden als Phytopharmaka oder Nahrungsergänzungsmittel verkauft. Bei den Zubereitungen handelte es sich um getrocknete Pflanzenpulver, Trockenextrakte oder Flüssigextrakte der blühenden oberirdischen Teile des Kalifornischen Mohns.

Für jede pflanzliche Verbindung wurde eine sensitive sowie selektive UHPLC-MS/MS-Methode entwickelt und validiert, welche für die Analyse der Caco-2-Zellen, dem Darmmikrobiota und der Kalifornischen Mohnproben verwendet wurde.

Valerensäure, Hyperforin, Escholtzin und Protopin wurden im Caco-2-Zellmodell stark absorbiert. Die Absorption von Valerensäure (Aufnahme), Escholtzin (Efflux) und Protopin (Efflux) erfolgte möglicherweise durch einen Carrier-vermittelten Transportprozess, wogegen Hyperforin wahrscheinlich durch passive Diffusion transportiert wurde. Zudem deutet die niedrige Wiederfindungsrate (13 - 69 %) von Valerensäure, Escholtzin und Protopin darauf hin, dass die Verbindungen in den Caco-2-Zellen womöglich metabolisiert wurden. Hypericin und Californidin wiederum zeigten eine geringe bis mittelmässige Absorption, möglicherweise durch die passive Diffusion als Transportprozess für Hypericin und den aktiven Transport für Californidin (Efflux). Diese Daten zeigen auf, dass Hypericin und Californidin das Potenzial haben in relevanten Konzentrationen im Dickdarmsegment gefunden zu werden, wo das Darmmikrobiom am dichtesten ist.

Alle pflanzlichen Verbindungen zeigten eine hohe Stabilität in den Batch-Fermentierungsexperimenten, was darauf hindeutet, dass sie nicht durch das menschliche Darmmikrobiom biotransformiert werden. Diese Ergebnisse unterstützen, dass die Verfügbarkeit dieser pflanzlichen Stoffe nicht durch das Darmmikrobiom beeinflusst wird. Zudem hatte die Exposition gegenüber pflanzlichen Extrakten und Stoffen keinen nennenswerten Einfluss auf den bakteriellen Metabolismus von SCFAs sowie die bakterielle Lebensfähigkeit. Dies lässt vermuten, dass Baldrian, Johanniskraut oder Kalifornischer Mohn in den getesteten Konzentrationen keine indirekte Wirkung auf das zentrale Nervensystem ausübt über die Modulation von bakteriellen SCFAs, die in die Mikrobiota-Darm-Hirn-Achse-Signalisierung involviert sind, zumindest nicht nach einer kurzzeitigen Exposition (24 Stunden). Angesichts der hohen interindividuellen Variabilität zwischen der menschlichen Darmmikrobiota und dem Aufbau der Kurzzeit-Experimente müssen diese Ergebnisse mit einer größeren Anzahl von Mikrobiota sowie kontinuierlichen Fermentationsmodellen bestätigt werden, um die möglichen Auswirkungen auf die

metabolische Aktivität der Mikrobiota und die bakterielle Lebensfähigkeit über eine längere Exposition aufzuzeigen.

Der Gehalt an Alkaloiden in den kommerziellen Präparaten des Kalifornischen Mohns unterschied sich stark und reichte von 0,13 - 2,55 mg/g für Californidin, 0,05 - 0,63 mg/g für Escholtzin und 0,008 - 0,200 mg/g für Protopin. Diese deutlichen Unterschiede lassen sich, zumindest teilweise, womöglich auf die unterschiedlichen Extraktionsverfahren zurückführen. Basierend auf diesen Daten und der von den Herstellern empfohlenen Dosierungen wurden für die drei Alkaloide Tageshöchst Dosen von 0,16 bis 2,97, 0,10 bis 1,11 bzw. 0,02 bis 0,31 mg/Tag berechnet. Bei Patienten mit unterschiedlichen Präparaten aus Kalifornischem Mohn ist folglich mit erheblichen Schwankungen bei der täglichen Einnahme von Californidin, Escholtzin und Protopin zu rechnen.

1 Aim of the work

Phytopharmaceuticals such as valerian, St. John's wort or California poppy are widely used to treat depressive, anxiety and sleeping disorders. Currently, little is known regarding the intestinal absorption of pharmacologically relevant constituents in these herbal drugs. Moreover, possible interactions of herbal extracts or herbal constituents with the human gut microbiota have not been investigated up to now.

The first aim of this work was to evaluate the possibilities for the pharmacologically relevant constituents valerenic acid (from valerian), hyperforin and hypericin (from St. John's wort), californidine, escholtzine and protopine (from California poppy), to be found at relevant concentrations inside the colon segment of the gastrointestinal (GI) tract, which hosts the most diverse and densest microbiota. Therefore, for each herbal compound, an assessment of the intestinal transport properties was conducted with the Caco-2 cell model.

The second aim was to explore the reciprocal interactions between the human gut microbiome and these herbal compounds and extracts; i.e., on the one hand, an evaluation of the potential for the gut microbiome to metabolize the herbal compounds, and on the other hand, an assessment of the impact of herbal compounds and extracts exposure on the metabolic activity (SCFAs production) and bacterial viability of the gut microbiome. Hence, batch fermentation experiments with herbal compounds and extracts were performed with two different PolyFermS systems.

Another objective of this work was to estimate the levels of californidine, escholtzine and protopine that can be expected in patients that use products containing California poppy. Thus, the contents of alkaloids californidine, escholtzine and protopine were determined in eight commercial products of California poppy.

2 Introduction

2.1 The intestinal absorption of xenobiotics

Oral ingestion is a common route for the entry in the human body of synthetic, phyto- or food chemicals (referred as xenobiotics, compounds or drugs in this work). When administered orally, the disposition of xenobiotics can be divided into four main steps: Absorption, distribution, metabolism, and excretion (ADME). The absorption phase corresponds to the entry of xenobiotics in the systemic circulation of the body. This phase mostly occurs in the GI tract, at the physical and physiological barrier segregating the human body from external environment, the intestinal barrier [1]. Distribution is the phase in which xenobiotics, once absorbed, may be distributed to the peripheral tissues via the bloodstream. The metabolism phase corresponds to the metabolism (also referred as biotransformation) of xenobiotics, occurring in the intestinal barrier and in the liver. Finally, the excretion is the step in which xenobiotics and their metabolites are cleared from the body. Excretion processes are mostly ensured by both kidneys and liver [2].

The intestinal absorption is critical in the bioavailability of orally ingested xenobiotics. Bioavailability refers to the portion of a xenobiotic that enters the systemic circulation of the body and reaches the site of action unchanged [3]. It is established that solubility in the physiological fluids, permeability across biologic membranes and pre-systemic metabolism (first-pass metabolism) of xenobiotics are major contributors of their bioavailability [3,4]. In early drug discovery programs, these properties are evaluated using various *in silico* or *in vitro* systems [3]. Due to its relative similarity to the human intestinal barrier, the use of the human colon carcinoma (Caco-2) cell monolayers has become an integral part of early drug discovery pipelines to investigate permeability properties of new chemical entities [3]. This system has also become useful to investigate permeability properties of phytochemical compounds.

In this chapter, the structural and functional aspects of the human GI tract, intestinal barriers, mechanisms of permeation and intestinal metabolism are presented in the context of intestinal absorption of xenobiotics. Moreover, a focus is made on the Caco-2 cell model as a system to screen intestinal permeability properties of xenobiotics.

2.1.1 The gastrointestinal tract

Upon oral ingestion, xenobiotics transit through the GI tract, and may permeate across the gastrointestinal mucosa. An estimate of 90% of compounds absorption is thought to occur in the small intestine [5]. With its nine meters length, the GI tract has a considerable absorptive surface of about 250 – 400 m² [6]. It can be divided in three main absorptive segments such as the stomach, the small intestine and the large intestine (colon) (Figure 1A). The GI tract is composed of distinct tissue layers: the mucosa, submucosa, muscularis propria and serosa (Figure 1B). The cellular structure of the mucosa differs between the GI segments, whereas the other layers are similar throughout the GI tract. Each segment possesses additional specific properties including morphology, length, absorptive area, surrounding pH, fluid composition, transit time, mucus thickness, transporters expression, permeability, metabolic enzymes activity, and resident microbiota [6,7].

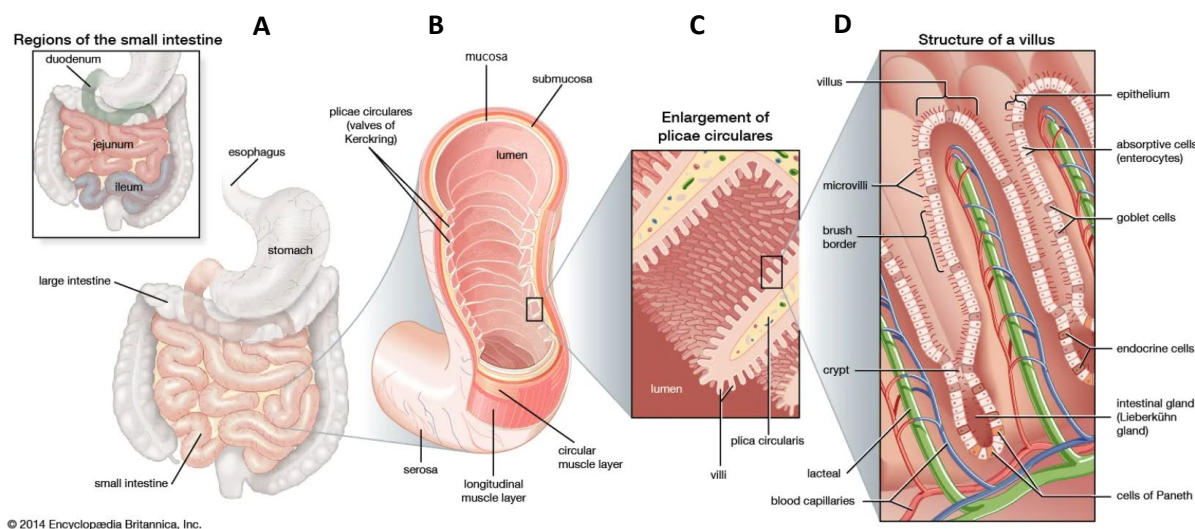


Figure 1. Structure of the small intestine [8]. The small intestine connects the stomach to the colon (A). The serosa, muscularis propria and submucosa constitute the baseline of the GI tract structure, whereas the mucosa is specific of each segment of the GI tract (B). The structural anatomy of the small intestine mucosa in plicae circulares, villi (C), and microvilli maximize the intestinal absorptive area (D).

Stomach

Following oral ingestion and transit throughout oesophagus, xenobiotics may reach the stomach where they become exposed to an environment combining mechanical forces, enzymatic degradation and acidic pH (pH 1.5 – 2) [6,9]. This environment together with a particularly thick mucus layer, a large capacity, and a relative short transit time (0 - 2 h) contribute to limit the absorption of xenobiotics in this segment [6]. The mucosa of the stomach has a morphology in vertical tubular indentations and has a high secretory activity [10]. Pepsinogen and hydrochloric acid represent the main secretions that allow the digestion and breakdown of foreign compounds [10].

Small intestine

Following gastric residence, xenobiotics may reach the small intestine, the compartment where the majority of xenobiotics are absorbed [5]. It is estimated that from approximately 9 L of fluid reaching the small intestine daily, about 90% is absorbed in the small intestine, 8% downstream in the colon, and 2% is excreted through feces [11]. The high absorption capacities of the small intestine are mainly due to its size (6 m in length and 2.5 – 3.0 cm in diameter) and to the morphology of its mucosa in circular folds (plicae circulares), in villi and microvilli (Figure 1BCD). Thin mucus layer, transit time (2 – 6 h) and motility are additional factors that contribute to the important absorption capacities of the small intestine [6]. Unlike the stomach, the local pH in the small intestine is around 6 – 7.4, which allow the absorption of larger range of compounds [9].

The small intestine can be compartmented in three substructures such as the duodenum, jejunum, and ileum. The hepatopancreatic duct arrives into the duodenum and allows the arrival of bile and pancreatic juice. The bile is a mixture secreted by the liver mostly composed of water, bile salts, and phospholipids which ensures the emulsion of lipids in the small intestine. Pancreatic juice consists of water, salts, sodium bicarbonate, and several digestive enzymes. Sodium bicarbonate contributes to increase the luminal pH which results in activating pH-sensitive digestive enzymes in the small intestine, whereas pancreatic enzymes mostly ensures the digestion of sugars, proteins, and fats [12,13].

Colon

Xenobiotics which are not absorbed in the small intestine may reach the colon. The tubular colon can be divided into four segments; ascending, transverse, descending and sigmoid colon. It has a large volume (1.5 m in length and 6.0 – 7.5 cm in diameter), a transit time of approximately 51 h [14] and a luminal pH ranging from 6 to 6.7 [9,14]. Its main roles include the transport of water and electrolyte, the formation of feces and the fermentation of dietary fiber. The latter is ensured by the set of commensal microorganisms populating the colon, the microbiota. The microbiota is present all over the GI tract but in a higher extend in the colon, and account for most of the fermentation activity. This process can contribute to up to 15% of total energy requirements of humans [15].

2.1.2 The mucosa of the intestines

The intestinal mucosa is a physical and biochemical barrier between the external milieu and the human body. The main components of the intestinal mucosa are an outer mucus layer, a middle single layer of intestinal epithelial cells (the intestinal epithelium) and an inner layer of loose connective tissue (the lamina propria) which provide support and defense to the intestinal epithelium and where immune cells such as T cells, B cells, macrophages and dendritic cells (DCs) ensure an immunological defense role [10,16]. While these three building blocks constitute the elemental basis of the intestinal mucosa, certain differences such as the mucus layer formation or the morphology of the mucosa can be observed between the small intestine and the large intestine segments [16].

Intestinal mucus layer

The mucus layer is the first line of the intestinal barrier. Its primary role is to prevent infiltration across the intestinal barrier of microorganisms, microbial by-products, digestive enzymes and acids, xenobiotics and toxins [17]. Intestinal mucus mainly comprises branched glycoproteins (mucins) forming a gel-like sieve structure which act as a lubricant for luminal contents and as a protective coat against luminal bacteria and antigenic substances [16]. Immune regulators including antimicrobial peptides (AMPs), secretory immunoglobulin A (sIgA) and trefoil factor 3 (TFF3) molecules are released into the mucus to maintain the immunological balance of the microbiota. While the main biological components of the mucus are similar throughout the gut, some structural differences can be found between the small intestine and the colon (Figure 2) [17].

In the small intestine, the mucus layer is single and discontinuous which enable the absorptive function and luminal release of digestive enzymes from the epithelial cells [17] (Figure 2).

In the colon the mucus layer is divided into two layers; an outer layer that is loose and allows the proliferation of long-term commensal bacteria, the gut microbiota that is essential in the colon, and an inner layer largely devoid of bacteria (Figure 2) [16,18]. Whether these layers are adherent to the epithelium or the luminal content is under debate [17].

Intestinal epithelia

The mucosa of the small intestine has a morphology in numerous subfolds, constituting the villi and intestinal crypts (intestinal glands) (Figure 1D, Figure 2), that are vascularized by a dense blood capillary and lymphatic network supplying the epithelial cells (Figure 1D). The epithelial cells are connected together by 3 main junctional complexes: desmosomes, adherens junctions and tight junctions [16,19]. An estimate of 80% of the intestinal epithelial cells are enterocytes, mainly specialized in nutrient uptake [11]. Enterocytes are polarized, with a brush border (microvilli) at the luminal side, which enlarge the

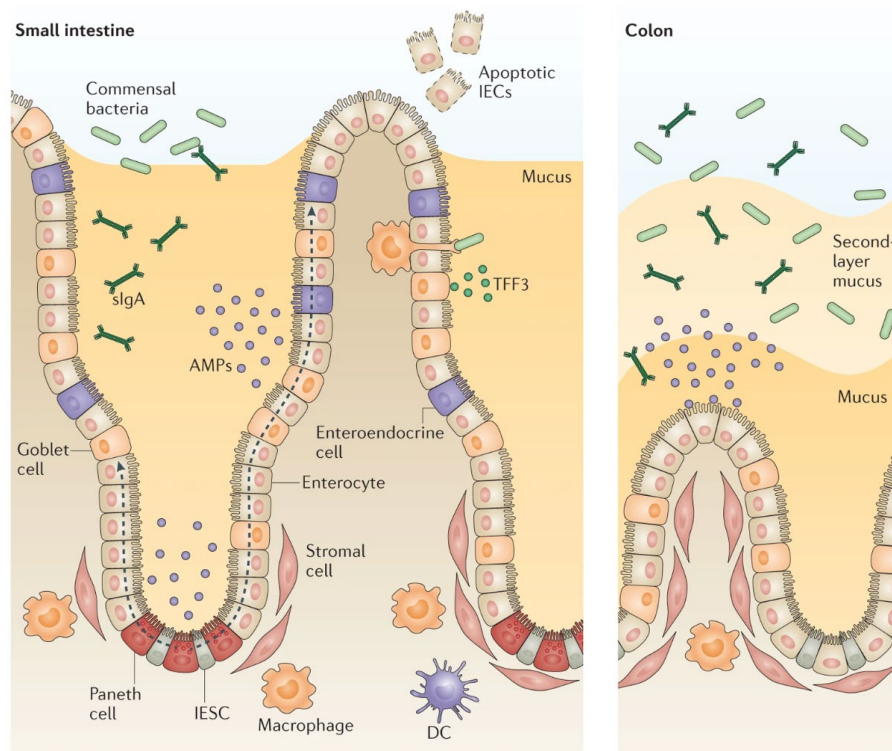


Figure 2. Mucosa of the small and large intestine [20]. IECs, intestinal epithelial cells. IESC, intestinal epithelial stem cells. DC, dendritic cells. AMPs, antimicrobial peptides. sIgA, Secretory immunoglobulin A. TFF3, trefoil factor 3

absorptive area of the small intestine [11]. The intestinal epithelium is also constituted by secretory cells including goblet cells that secrete the mucus (mucins) acting as a protective coat and lubricant, Paneth cells (immune cells) and enteroendocrine cells (mostly secreting gastrointestinal hormones). Paneth cells are found at the intestinal crypts whereas the other mature epithelial cells are localized at the villi [11].

The mucosa of the colon has a flat structure interspersed with crypts (Figure 2). A single layer of epithelial cells (as in the small intestine, connected together by similar adherent proteins) is contiguous to the lamina propria. The colon epithelial cells consist of colonocytes which have a comparable structural and absorptive role as enterocytes in the small intestine, mucus-producing goblet cells that represent around 25% of epithelial cells and enteroendocrine cells. The colon epithelium is devoid of Paneth cells [21,22].

2.1.3 Permeation mechanisms of xenobiotics

Orally ingested xenobiotics must cross several biological barriers and plasma membranes before becoming bioavailable. First, xenobiotics must traverse the intestinal epithelium to reach the lamina propria wherein they transit until they reach the fenestrated blood capillaries of the endothelium, allowing their entrance into the systemic circulation [23,24]. The disposition of xenobiotics involves the crossing of additional membranes including membranes of liver and kidney tissues [25].

Mechanisms of transcellular membrane permeation are generally allowed by two types of processes; transcellular passive diffusion and carrier-mediated transport (Figure 3). Paracellular crossing between cells is another route (Figure 3), which is ensured under passive diffusion process [26]. Whether the transport of xenobiotics is passive or active depends on the type of cell, and the physicochemical properties and structural characteristics of xenobiotics [25].

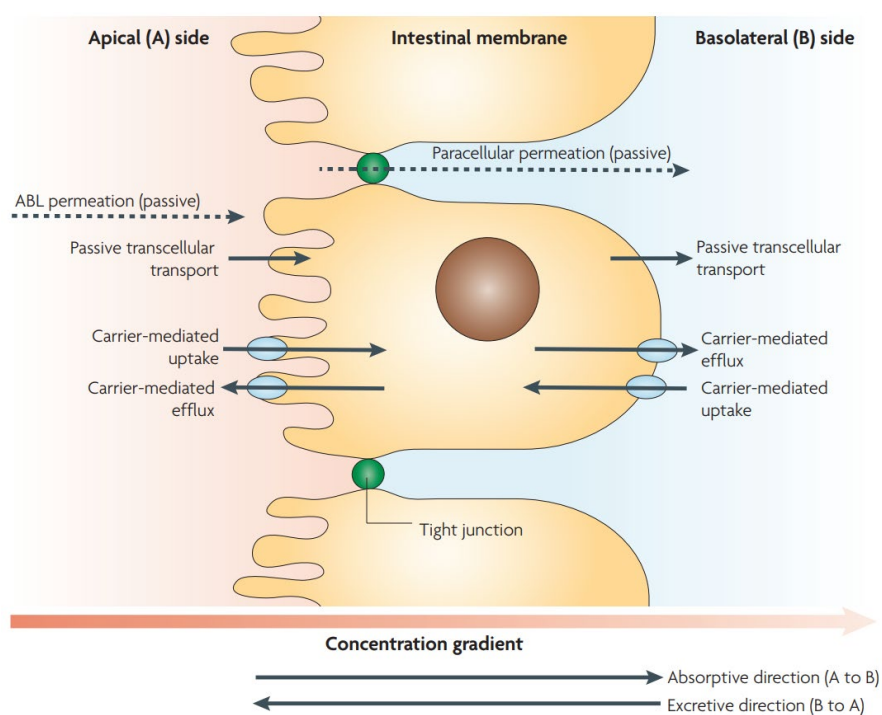


Figure 3. Transport mechanisms allowing permeation of xenobiotics across the intestinal epithelium [26]. The apical side corresponds to the luminal compartment whereas basolateral side corresponds to the lamina propria compartment.

Plasma membrane

A transcellular transport corresponds to the crossing of the plasma membrane. The plasma membrane of cells is a dynamic and selective barrier to endogenous or exogenous substances. It is mainly composed of amphiphilic phospholipids and other lipids such as cholesterol and glycosphingolipids which form a lipid bilayer (Figure 4). It is further structured by globular integral proteins and glycoproteins which are intercalated into the lipid bilayer (Figure 4). Additional intercalated transporter proteins allow the transport of endogenous and exogenous substances [25,27].

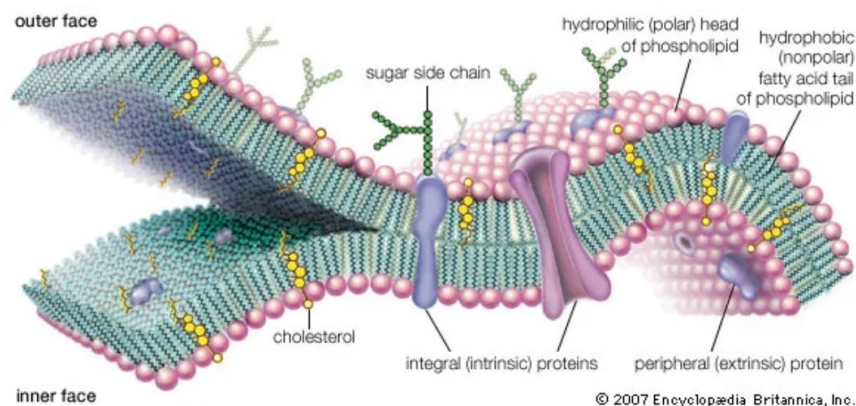


Figure 4. Structure of the bilayer membrane of cells [28].

Transcellular passive diffusion

Transcellular passive diffusion can be defined as a mass transport of a compound, driven by a concentration gradient, from one side of a cellular membrane to the other, throughout a portion of the lipid bilayer [26]. As passive diffusion occurs in a portion of a membrane devoid of specific binding sites, it is usually not saturable, cannot be inhibited and is not affected by the stereochemistry of compounds. Compounds diffusing across lipid bilayer tend to be uncharged, desolvated, hydrophobic and with a relative low molecular weight [26].

Paracellular passive diffusion

Paracellular diffusion corresponds to the transport of compounds between adjacent cells and is regulated by the tight junctions. Two paracellular pathways can be distinguished in normal physiological conditions, the pore pathway and the leak pathway [29]. The pore pathway is driven by channels of pore-forming claudin proteins (structural proteins of the tight junctions). This pathway is charge-selective and size-selective. In the GI tract, this pathway allows the transfer of cations [29]. The leak pathway allows the crossing of macromolecules (about 20-fold larger molecules in comparison to the pore pathway). This pathway is size selective but not charge selective and has a low capacity flux [23]. Although the leak pathway is also driven by tight junctions, its functional anatomy is still poorly understood [23]. A third pathway, the unrestricted pathway which is characterized by the diffusion of material at sites of epithelial damage, is described in advanced disease conditions. This pathway is independent of tight junctions, non-selective and with high capacities [29,30].

Active transport and transporter proteins

Unlike passive diffusion that is regulated by lipid components of plasma membrane, active transport of some endogenous or foreign molecules is mediated by transmembrane transporter proteins. Generally, this biological process requires adenosine triphosphate (ATP) hydrolysis, or ion or concentration gradients [31]. Membrane protein transporters can be divided into two superfamilies: ATP-binding cassette transporters (ABCs) and solute carriers (SLCs). In the GI tract, the highest expression levels of transporter proteins are found in the jejunum and the ileum [32]. ABC transporters consist of efflux transporters which require ATP hydrolysis to transfer compounds from the internal to the external cellular compartment [25]. In turn, SLC membrane proteins primarily (but not exclusively) consist of uptake transporters. SLC membrane proteins rely on either electrochemical gradient or ion gradient to transport substrates [33]. More than 400 membrane transporters have been identified, from which a dozen is considered as clinically relevant [34,35] (Figure 5).

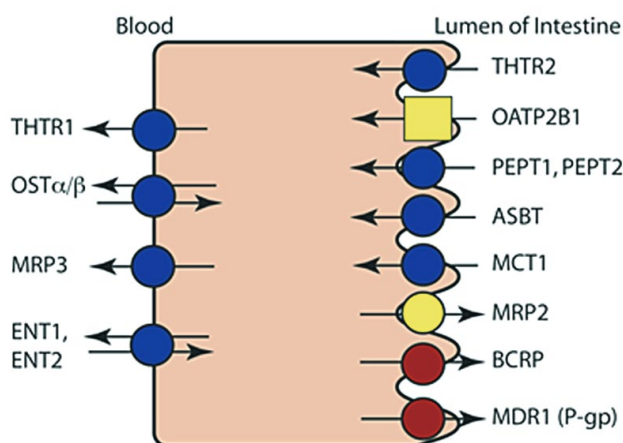


Figure 5. Clinically relevant intestinal transporters in the disposition of xenobiotics [35]. ABC transporters P-glycoprotein (Pg-p), breast cancer resistance protein (BCRP), multidrug resistance protein (MRP)2 are expressed apically and MRP3 is expressed at the basolateral side. SLC transporters thiamine transporters (THTR)2, organic anion transporting polypeptide OATP2B1, peptide transporter (PEPT)1, PEPT2, apical sodium-dependent bile acid transporter (ASBT) and monocarboxylate transporter 1 (MCT1) are expressed apically whereas THTR1, organic solute transporter (OST) α/β , MRP3, equilibrative nucleoside transporter (ENT)1 and ENT2 are expressed at the basolateral side.

Activity of intestinal transporters can affect the disposition of xenobiotics, including intestinal absorption, pharmacokinetics and drug-drug interactions (as well as herb-drug interactions or food-drug interactions) [36,37]. Pg-p, MRP2, or BCRP were described as limiting intestinal absorption of some synthetic drugs, by pumping them back into the lumen [37]. In turn, other synthetic drugs were shown (in few cases) to be substrate of uptake transporters such as PEPT1 and OATP2B1, contributing to improve their absorption [37,38]. Concomitant administration of synthetic and herbal drugs or food may affect the transport of some xenobiotics through inhibition or induction of intestinal transporters. A well-known example is the up-regulation of Pg-p by St. John's wort which results in decreased systemic exposure of the co-administered drug [37,38]. Similar to these interactions, the genetic polymorphisms

of intestinal transporters may lead to variations in the concentrations of xenobiotics which are substrates of these transporters [39]. Recommendations in evaluating impacts of transporters on intestinal absorption, drug-drug or food-drug interactions were made by the International Transporter Consortium (ITC). Accordingly, intestinal transport via Pg-p, BCRP, MRP2 and OATP2B1 should be evaluated in the drug development phase [35].

2.1.4 Intestinal metabolism of xenobiotics

Intestinal metabolism is another factor that may decrease the bioavailability of orally ingested compounds [40]. In addition, this metabolism can result in reduced or completely inactivated biological activities of the parent compound [41]. Intestinal metabolism occurs either in the gut lumen or in the gut wall [42]. In the gut lumen, xenobiotic metabolism is mostly driven by the gut microbiota [43]. A description of microbiota-mediated metabolism of exogenous compounds is provided in section 2.2.3. In the enterocyte, metabolism can take place via mostly two reaction pathways, phase I or phase II metabolism. Phase I metabolism refers to oxidation, reduction and hydrolysis reactions whereas phase II metabolism is characterized by conjugation reactions, comprising glucuronidation, sulfoconjugation or glutathione *S*-conjugation [41].

Intestinal phase I metabolism is mostly ensured by enzymes from the cytochrome P450 (CYP) superfamily, from which CYP3A subfamily enzymes are the most relevant [44]. The subtype CYP3A4 is the most involved in xenobiotic metabolism [2,44]. High levels of CYP3A are found in the tip of the intestinal villi, in the small intestine [45]. Regional differences are observed throughout the GI tract, with higher CYP3A levels detected in the duodenum and the jejunum in comparison to the ileum or the colon [41]. Intestinal phase II metabolism is mediated by various conjugation enzymes wherein uridine diphospho-glucuronosyltransferases (UGTs) and sulphotransferases (SULTs) act as main contributors [40,42]. Intestinal phase II metabolism is thought to mostly occur in the colon [41].

Finally, as observed for some transporter proteins, interactions (drug-drug, herb-drug or food-drug) of co-administered compounds with intestinal enzymes may affect the disposition of xenobiotics [46].

2.1.5 The Caco-2 cell model

The Caco-2 cell model is the most popular *in vitro* system used to study intestinal absorption of xenobiotics [47]. The principle is to grow Caco-2 cells on a semipermeable membrane, which after 21 days will form a monolayer of enterocyte-like cells connected by means of tight junctions [48]. The semipermeable membrane separates two compartments (also named chambers) filled with culture medium, the apical compartment (modelling the lumen) and the basolateral compartment (modelling the lamina propria) (Figure 6). This system is appropriate for running permeability experiments.

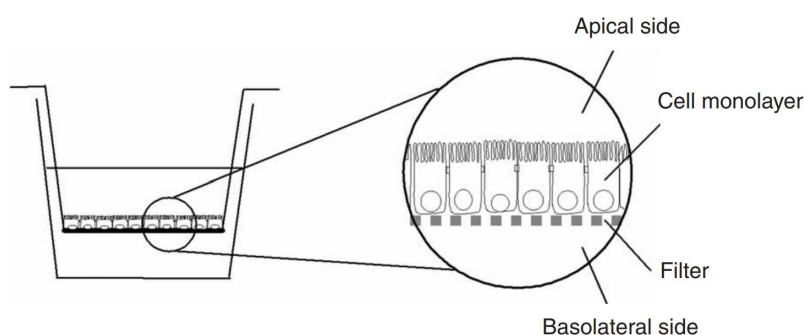


Figure 6. Scheme of the Caco-2 cell model [48].

2.1.5.1 Origin

Origin of the Caco-2 cell line

In the 1970s, cancer development and effects of cell therapy were important focus areas in cellular and molecular biology research. Gastrointestinal tumors were used to isolate epithelial cell lines. An objective was to obtain cell lines of specialized cells found in the small intestinal epithelium (for instance enterocytes, goblet cells or Paneth cells). While the addition of synthetic or biological factors in the medium partly differentiated several cell lines, one of them, the *Cancer coli-2* (Caco-2) had the unique feature of spontaneously differentiating, when reaching confluence, into enterocyte-like cells [49]. In 1977, Fogh et al. established the Caco-2 cell line from a human colorectal adenocarcinoma [50,51]. Later in early 1980s, Pinto et al. showed that differentiated Caco-2 cells had a morphology and biology close to small intestinal enterocytes, including a polarized shape with microvilli on the apical side and expression of apical intestinal enzymes [52]. Moreover, Pinto described that differentiated Caco-2 cells were connected by means of tight junctions [52].

Origin of the Caco-2 cell model

The resembling features of Caco-2 cells with enterocytes inspired Hidalgo et al. to create a cell-based model of the human intestinal mucosa [53]. In 1989, Hidalgo et al. published a seminal paper

characterizing morphological and biochemical properties of Caco-2 cell monolayers grown on semipermeable polycarbonate membranes (also named filters) [54]. Hidalgo et al. are credited as the first to grow Caco-2 cell monolayers on semipermeable filters to perform drug permeability experiments [54,55].

Application for drug permeability screening

In 1990, Artursson compared the permeability properties of five beta-blocking agents using filter-grown Caco-2 cell monolayers with permeability data from rat ileum, and could show comparable transport rates [56]. Later in 1991, Artursson and Karlsson showed good correlation between oral absorption in humans and permeability across Caco-2 cell monolayers of 20 drugs (structurally different), designating the Caco-2 cell model as a promising *in vitro* system to study intestinal drug absorption [57]. Today, the Caco-2 cell model is still the most employed *in vitro* system to study compound permeability in drug discovery.

2.1.5.2 Structural and functional features of differentiated Caco-2 cells

Differentiated Caco-2 cells express a wide range of proteins that are characteristic of differentiated intestinal cells [58]. This includes membrane proteins expressed at the brush border membrane, such as villins which ensure a structural support role, and enzymes, including hydrolases. Intercellular proteins including adherens junction proteins, tight junction proteins and integrins are additionally marker proteins [58]. Among these intercellular proteins, some barrier-forming claudins are found to be upregulated in Caco-2 monolayers, with a comparable expression pattern found in the colon. This may explain why Caco-2 monolayers have a higher transepithelial electrical resistance in comparison to the small intestinal epithelium, resulting in a reduced paracellular flux in Caco-2 monolayers [58–60].

Differentiated Caco-2 cells express a wide range of protein transporters which are relevant in drug disposition processes [58,61]. Of the twelve protein transporters of clinical importance (according to the ITC) present in the intestinal epithelium, nine are expressed in Caco-2 cells. This includes P-gp, BCRP, MRP2 and OATP2B1 which are considered to be the most important in drug disposition processes [35,58]. While the expression pattern of most transporters in Caco-2 cells is in agreement with intestinal epithelial cells, OATP2B1 is found at significantly higher levels in Caco-2 cells (expressed 20 to 60-fold higher) [58,62].

While phase I enzymes are poorly expressed in differentiated Caco-2 cells, phase II enzymes including UGTs, SULTs, and glutathione-S-transferases (GSTs) can be found at significant levels [48,58]. Lack of significant expression levels of phase I enzymes is a noticeable difference between Caco-2 monolayers and the small intestinal epithelium.

2.1.5.3 Permeability experiments

The Caco-2 cell model (Figure 6) is a convenient system to study the permeability of orally ingested compounds.

Apparent permeability coefficient

A typical permeability assay in the absorptive direction consists of applying a test compound in the apical chamber and measuring its flux across the Caco-2 monolayer, over a defined time period (usually 1 h) with sample collections from the basolateral chamber (usually every 15 minutes) [48]. From this experiment, a curve of the cumulated fraction transported of the test compound can be plotted and used to determine the apparent permeability coefficient (P_{app}) by means of the following equation [48,63]:

$$P_{app} = \left(\frac{dQ}{dt}\right) \left(\frac{1}{AC_0}\right)$$

Where dQ/dt is the steady-state flux ($\mu\text{M/s}$), A the surface area of the filter (cm^2), and C_0 the initial concentration in the donor compartment (μM).

The P_{app} in the absorptive direction (from apical to basolateral, P_{appAB}) reflects the permeability properties of a compound. Typically, a P_{appAB} value higher than 1×10^{-6} cm/s defines a highly permeable compound whereas a P_{appAB} value lower than 1×10^{-6} cm/s is characteristic of a poor-to-moderately permeable compound [48,56,64].

Efflux ratio and active transport

In order to investigate the involvement of transporter proteins in compound transfer, an additional permeability experiment in the opposite direction (the secretory direction, from basolateral to apical) can be carried out. The obtained P_{app} value (P_{appBA}) can be used to calculate the efflux ratio (ER), as follows [48]:

$$ER = \frac{P_{appBA}}{P_{appAB}}$$

If the value is higher than 2, the compound most probably permeates according to an efflux process; whereas if the value is lower than 0.5, the transfer is most probably enabled via an uptake process. If P_{appAB} and P_{appBA} values are the same, the compound most probably permeates via passive diffusion [48]. Permeability experiments with co-incubation of test compound with specific inhibitors of transporter proteins can be performed to study active transport mechanisms [48].

Experimental considerations

To approach the physiological conditions of the human small intestine, and because the activity of some transporter proteins such as PEPT1 or OATP2B1 is dependent on a proton gradient, acidic conditions in the apical chamber (pH 6.5) and neutral conditions in the basolateral chamber (pH 7.4) should be applied [48]. In addition, the concentration of test compounds should not exceed the micromolar range to prevent saturation of protein transporters [48]. Finally, for test compounds which pose problems of solubility, precipitation or adsorption to experimental material, the addition of bovine serum albumin (BSA) may be necessary [48,65]. This approach is particularly relevant to study the permeability of highly lipophilic phytochemicals.

Relevance to human *in vivo* situation

As previously discussed in section 2.1.5.2., the Caco-2 cell model does not perfectly mimic the entire properties of the human small intestine. Despite this, good correlations are found between P_{app} values obtained from Caco-2 experiments and fraction absorbed in human studies [57,66]. The strongest correlations are obtained for compounds transported via passive transcellular diffusion [49,66].

2.1.6 Other models to predict permeability of xenobiotics

In support of or independent to transport experiments with Caco-2 monolayers, other models can be used to predict the intestinal permeability of xenobiotics. These models consist of rule-based approaches [67,68], physicochemical assays [67,69] or biological models [70,71].

2.1.6.1 Nonbiological models

Rule-based approaches

A popular approach used to predict permeability of drugs is the rule of five, introduced by Lipinski et al. in 1997 [67]. This rule states that a compound with favorable permeation properties, a “drug-like” compound, should comply with a molecular weight (MW) lower than 500 Da, a calculated logP (clogP) lower than five, a maximum of five hydrogen bond donors, and a maximum of ten hydrogen bond acceptor [67]. The rule of five can only be applied to compounds that are passively absorbed. While this approach has influenced pharmaceutical scientists, a significant number of marketed drugs do not entirely comply to the rule of five, with particular deviations noticed for the MW and the hydrogen bond acceptor status [72]. To predict lipophilicity of ionizable compounds, the clogD is more suitable than the clogP; as the clogP reflects lipophilicity of neutral compounds only [68]. Other parameters have been introduced, such as polar surface area, sum of rotatable bonds, number or fraction of sp³ or number of aromatic rings [66,69]. Some of these parameters can be provided by computational models (e.g., ACD/Percepta platform) with calculations based on chemical structures. While these *in silico* approaches appear rapid and cost-effective, they should still be considered as “qualitative” and only as a preliminary readout of compound permeability [73].

Physicochemical assays

The parallel artificial membrane permeability assay (PAMPA) is a well-known physicochemical assay that consists of assessing test compound flux across an artificial membrane (typically hexadecane membrane). This model has proven its efficiency by being implemented in early drug discovery programs [74]. Additional biomimetic models have been developed, including vesicle-based permeation assay or Permeapad® [70]. While physicochemical assays enable cost-effective and high throughput screenings, these can only provide information on transcellular passive diffusion, due to the absence of biological structures such as tight junctions or transporter proteins [70].

2.1.6.2 Biological models

Cell-based models

Monoculture of immortalized cell lines cultivated on filters have been employed to mimic the intestinal epithelium *in vitro*. While the human derived Caco-2 cell line remains the most popular (section 2.1.5), other human derived cell lines have proven to be relevant [70,71]. An example is the TC7 which originates from late-passage Caco-2 cells, that offers the advantage of expressing CYP enzymes, and can be used to screen compounds transported by passive diffusion [70]. Non-human cell lines can also be employed. The Madin-Darby canine kidney (MDCK) cell line is very popular in pharmaceutical discovery programs. Good correlations with permeability data in humans or from Caco-2 experiments are described, in particular for compounds transferred via transcellular passive diffusion [75,76]. Additionally, transfected MDCK cell lines such as MDCK-Pg-p (overexpressing Pg-p) or MDCK-BCRP (overexpressing BCRP) allows to further understand carrier-mediated transport mechanisms. Moreover, an advantage of MDCK cells is the short culturing time (3 – 4 days) [71]. Another relevant non-human cell line is the 2/4/A1 cell line (originating from rat intestine) which enables the study of paracellular transport [77].

Dual co-culture models can be used to overcome some limitations faced with monoculture models [70]. An example is the Caco-2/HT29-MTX combination, that is used to simulate mucus secretion, as differentiated HT29-MTX (originating from human colon adenocarcinoma) have the same structural and functional features as goblet cells [71].

Despite their complexity and sometimes high cost, other *in vitro* models have been developed such as triple-culture models, 3D cell models, membrane vesicles, or microfluidics-based systems [70,71]. This area of research is particularly active, and major advances have been achieved in the development of these techniques, particularly regarding 3D cell and microfluidics-based models. It is nevertheless still early to decide if these models will be systematically applied in early drug discovery programs [78,79].

Ex vivo models

Ex vivo models including diffusion chamber systems (e.g., Ussing chamber), intestinal rings and slices or everted intestinal sacs, consist in using intestinal tissues (typically using rat intestinal tissue) to mimic the intestinal barrier. These models offer the possibility to work with the entire mucosa and its preserved functions, such as, the epithelium with mucus layer, expression of transporter proteins and enzymes, and blood and nerve supply [70,75]. While these techniques enable better simulation of the intestinal epithelium over *in vitro* models, they are often expensive and difficult to handle due to short-term tissue integrity [70].

2.2 The gut microbiota interactions with xenobiotics

The gut microbiota (or gut microbiome) is a set of microorganisms populating the GI tract. The gut microbiota ensures important functions in human physiology including the regulation of host immunity, the modulation of the intestinal barrier, the protection against pathogenic microorganisms, and the fermentation of dietary fiber into short-chain fatty acids (SCFAs) to provide energy to the host [80].

In addition to interacting with endogenous molecules, the gut microbiota can interact with orally ingested xenobiotics. These xenobiotic-gut microbiota interactions can lead to biotransformation of xenobiotics, with possible impact on their disposition, bioactivity and toxicity [81,82]. Another mode of interaction is the impact of xenobiotic on the production of bacterial metabolites including SCFAs [81]. There are further known modes of interactions, namely bacterial growth promotion or inhibition by xenobiotics, xenobiotic accumulation by bacteria or impact on virome and virulence [81].

After a presentation of the gut microbiota composition and main functions, this chapter focuses around microbiota-mediated metabolism of xenobiotics and the impact of their exposure on the production of bacterial metabolites. Moreover, the artificial microbiota Polyfermentor Intestinal Model (PolyFermS) model to study microbiota interactions with xenobiotics is presented.

2.2.1 Gut microbiota composition

It is estimated that the human gut microbiome is composed of $10^{13} - 10^{14}$ microorganisms, which for the majority comprise anaerobic bacteria, but also viruses, archaea, fungi and protozoa [80,83,84]. Gut bacteria can be divided into more than 1000 species, mostly belonging to five bacterial phyla, namely Firmicutes and Bacteroidetes (the two most prominent which represent more than 90% of total bacterial species), Actinobacteria, Proteobacteria and Verrucomicrobia [84,85]. Along the GI tract, regional differences in bacterial content and species can be observed, with increasing concentration from the stomach to the colon (Figure 7). The stomach, the small intestine and the colon contain, $10^2 - 10^3$, $10^3 - 10^7$, and $10^9 - 10^{12}$ of microbial cells per mL, respectively (Figure 7) [86]. These longitudinal variations can be explained by fluctuating environments such as transit time, bile content, oxygen concentration, local pH, and mucus layer formation along the GI tract [87].

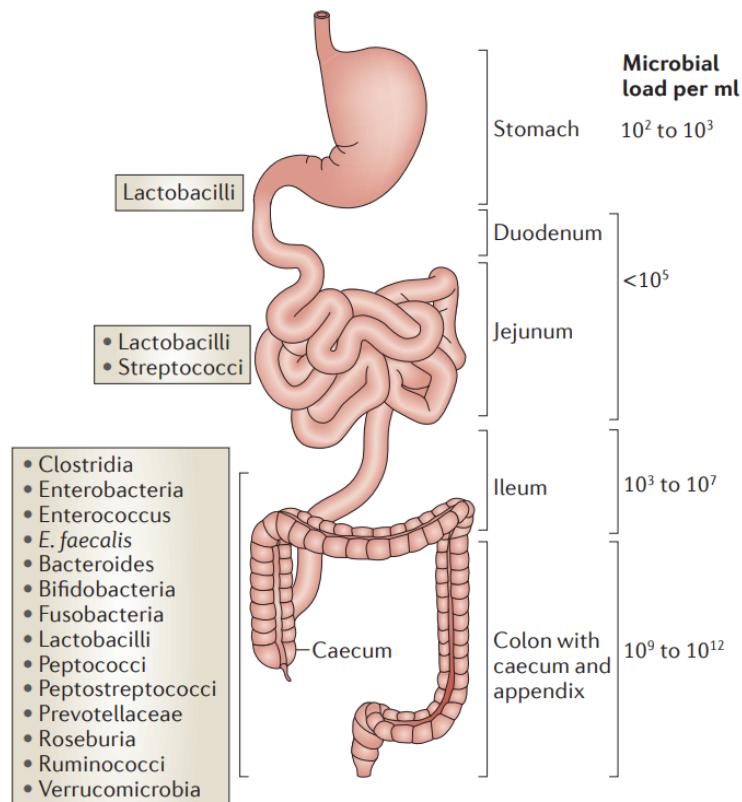


Figure 7. Main represented genera and microbial content along the human GI tract [86].

In addition, there are important interindividual variations in the composition of the gut microbiota, characterized by differences in number of species and their relative abundances [80,88]. These variations have been attributed to multiple factors including diet habits, lifestyle, age, gender, host-genetic, health-status and medication [88]. Out of 14 widely shared genera, *Bacteriodes*, *Ruminococcaceae* and *Prevotella* were described as the genera exhibiting the most significant variations in abundance, and therefore can be used as identifiers of different ‘enterotypes’ [88]. However, despite important variations

in composition, gut microbiota are considered as largely functionally equivalent [89]. The gut microbiota is relatively stable over time, following natural fluctuations with age, but it can vary upon various factors such as stress, antibiotics use, diet, xenobiotics exposure and more [90].

2.2.2 Functions of the gut microbiota

With 3.3 million microbial genes (around 150 times more than the human genome), the human gut microbiome has important functional capacities [83,84]. A major function of the gut microbiome is its considerable metabolic capacity, which is considered equal to that of the liver [91]. End-products of microbial metabolization include SCFAs, which mainly serve as substrates to provide energy to the host and cover up to 10% of human caloric energy requirement [92]. Besides their role in serving as energy substrates, SCFAs can also act as signaling molecules and regulate numerous biological processes including neuroimmunoendocrine function via the interconnected gut-brain axis [92]. Other functions ascribed to the gut microbiome include, synthesis of essential vitamins, epithelial and mucosal homeostasis, development of the immune system or regulation of pathogen colonization [80].

Metabolism of SCFAs

The major function of the gut microbiota is the fermentation of dietary fibers, namely resistant starch, non-starch polysaccharides and oligosaccharides, that promotes microbial growth and activity [93]. Fermentation is ensured by carbohydrate-active enzymes expressed in bacteria and mainly takes place in the proximal colon [80]. End products of these microbial conversions are gases (H_2 , CO_2 and CH_4) and SCFAs. SCFAs can act as substrates for energy metabolism and anabolic processes, or as signaling molecules [94,95]. SCFAs are volatile monocarboxylic acids with a hydrocarbon chain length of 1 to 6 carbon atoms, from which acetate, propionate and butyrate are the most abundant (90%) and with an estimated molar ratio of 3:1:1 [80,94]. While acetate is produced by most anaerobic bacteria, propionate and butyrate are mostly generated by distinct bacteria subsets, namely Bacteroidetes and Firmicutes, respectively [80]. The microbial synthesis of acetate, propionate and butyrate follow different biochemical pathways (Figure 8). When colonic concentrations of dietary fibers are depleted, in the distal colon, endogenous or dietary proteins can be used as substrates to produce SCFAs via proteolytic fermentation. Some products of proteolytic fermentation including aromatic compounds, polyamines, hydrogen sulfide (H_2S) or ammonia were shown to be potentially toxic for the host [96,97].

The produced SCFAs are largely absorbed (about 95%) in colonocytes, and are for the most part used locally as substrates to cover energy requirements (60-70%) of the colonic epithelium [98,99]. SCFAs, and in particular butyrate, regulate additional functions in the gut epithelium, including intestinal epithelial turnover and homeostasis, and the gut barrier integrity [94,100]. SCFAs can also transit via the portal vein to the liver and be further distributed in the periphery to affect peripheral tissues and cells [80,94]. There is a concentration gradient fall in SCFA levels from the lumen to the periphery, with selective uptake of butyrate at the colonic epithelium, propionate at the liver and acetate in the periphery [100]. The significance of this gradient is currently not known [100]. Peripheral concentrations of acetate, propionate and butyrate reach 19-160, 1-13 and 1-12 $\mu\text{mol/L}$, respectively [92]. SCFAs also act as signaling molecules (at colonic level and in periphery) in additional processes such as lipid and

glucose metabolism, energy intake, immune and inflammatory response or central nervous system (CNS) related functions [80,94,100].

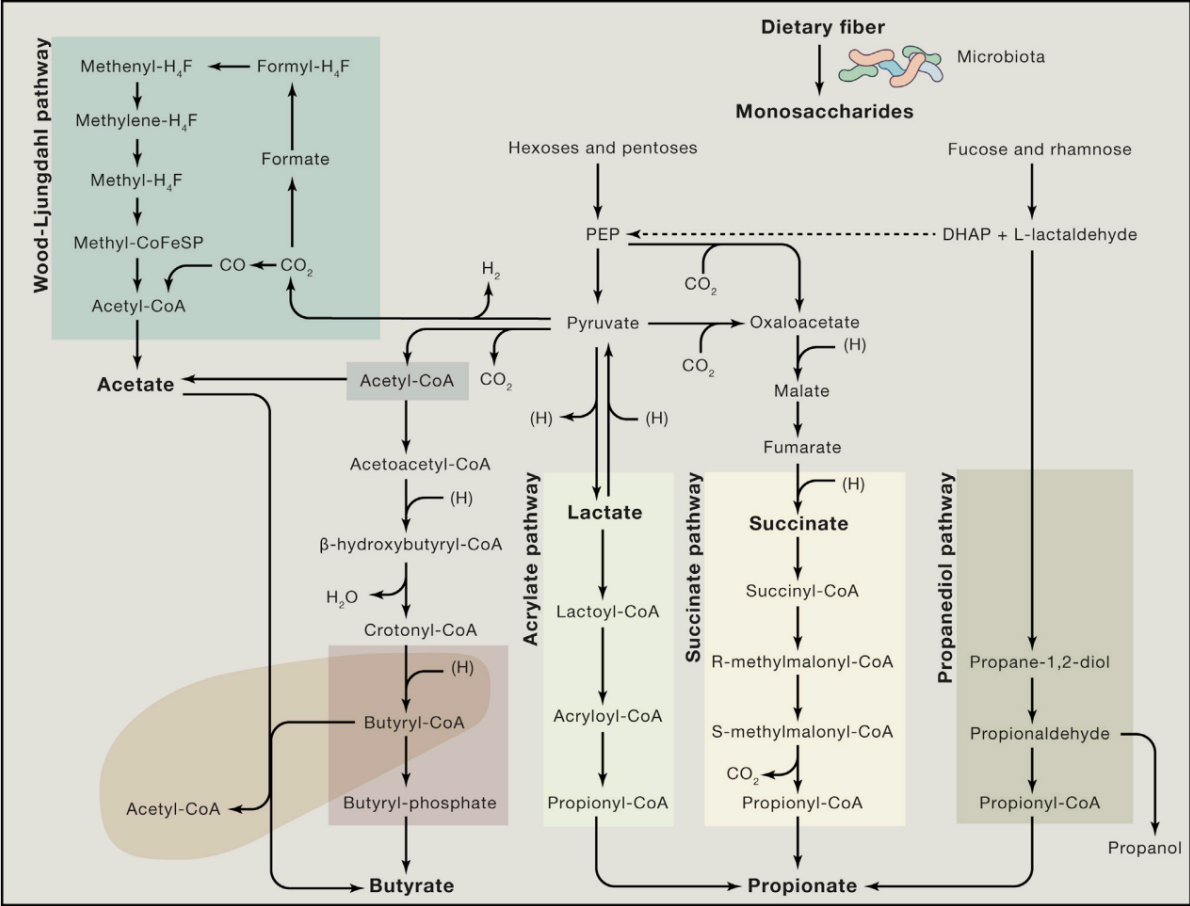


Figure 8. Overview of biochemical pathways of acetate, propionate and butyrate [94]. While acetate can be produced according to the Wood-Ljungdahl pathway, propionate and butyrate formation follows distinct molecular pathways. Propionate can be produced following three pathways, namely the acrylate, succinate and propanediol pathways. Butyrate is produced via glycolysis from acetoacetyl-coenzyme A (CoA). PEP: phosphoenolpyruvate, DHAP: dihydroxyacetonephosphate.

SCFAs and the microbiota-gut-brain axis

There is emerging evidence that gut-derived metabolites including SCFAs play a pivotal role in CNS functions via the microbiota-gut-brain axis [92,101,102]. The term microbiota-gut-brain axis is employed to describe the bidirectional signaling processes between the gut microbiota, the GI tract and the CNS [101]. While the brain affects gut function through the hypothalamic-pituitary-adrenal axis and the autonomic nervous system, the gut acts on the CNS through microbiota-derived metabolites and products, neuroactive compounds, and gut hormones that reach the brain via several routes including the enteric nervous system, vagus nerve, immune system or circulatory system [103]. SCFAs are thought to be implicated in the modulation of mechanisms of the microbiota-gut-brain axis, via the immune pathway, endocrine, vagal pathways and additional humoral pathways (Figure 9). These pathways can subsequently induce CNS-mediated behavioral or mental state responses including appetite, stress, mood, anxiety and depression [101]. Although SCFAs can cross the blood-brain-barrier, it is thought that they do not affect CNS functions through uptake in the brain, due to their low systemic exposure levels [101].

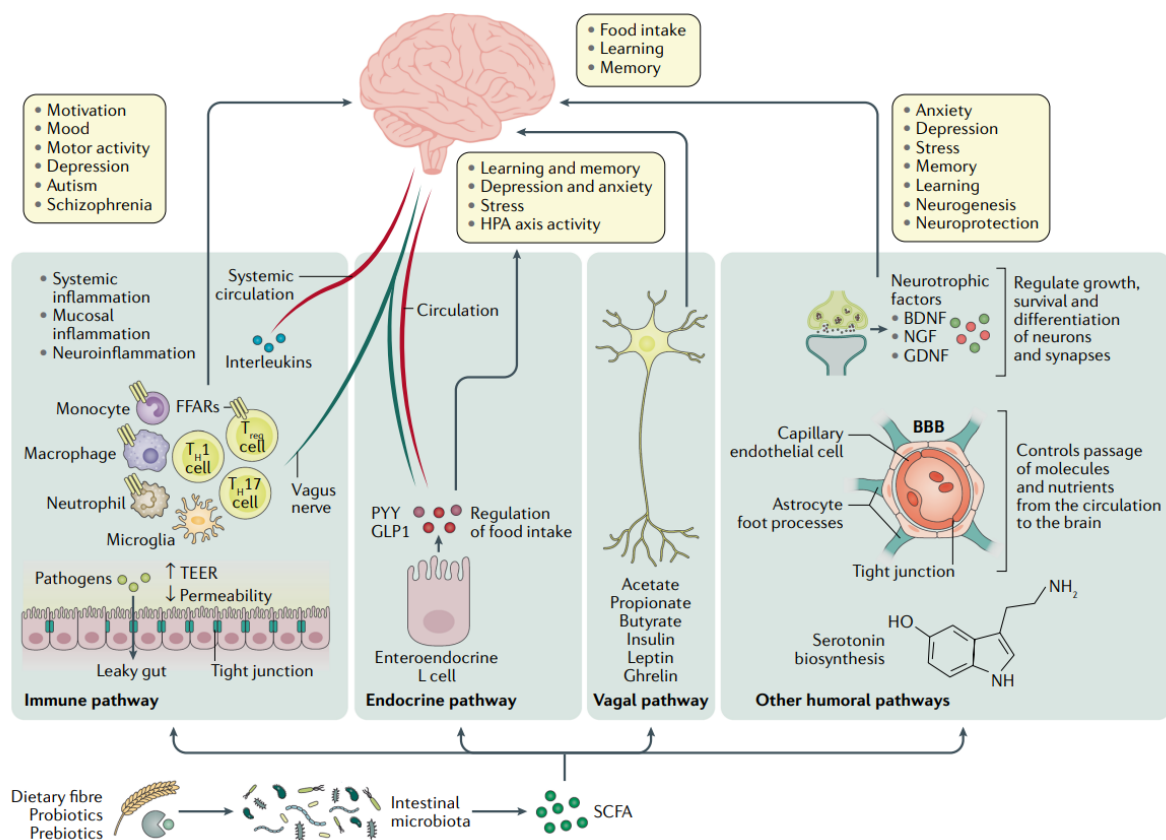


Figure 9. Microbiota-gut-brain axis pathways wherein SCFAs might be implicated [101].

PYY, peptide YY. GLP1, glucagon-like-peptide 1. BDNF, brain-derived neurotrophic factor. NGF, nerve growth factor. GDNF, glial cell line-derived neurotrophic factor. BBB, blood-brain-barrier. FFARs: Free fatty acid receptors.

In mice, supplementation in SCFAs improved emotional processing and behavior including depressive, anxiety and stress-related disorders [104]. Supplementation of SCFAs in other pre-clinical studies have shown a pivotal role of SCFAs in colonic and overall health [105]. Thus, in addition to being relevant markers for metabolic activity of the gut microbiota, SCFAs are also applicable markers of the host health.

2.2.3 Microbiota-mediated biotransformation of xenobiotics

Besides the ability to metabolize a wide range of endogenous compounds, the gut microbiota can also biotransform (metabolize, convert or breakdown) orally ingested xenobiotics [106]. These microbiota-mediated biotransformations mostly take place in the colon, where the gut microbiota is the densest [106]. Oral xenobiotics can come into contact with colonic gut microbiota via multiple routes. Poorly absorbed xenobiotics can pass through the small intestine to reach the colon. In contrast, highly absorbed xenobiotics may enter the circulatory system, be metabolized (generally in the liver) and excreted via the biliary duct back into the lumen, where xenobiotic-microbiota interactions can take place [107]. In the gut lumen, they can possibly be reabsorbed in the GI tract through a process called enterohepatic circulation [107].

Mechanisms of gut microbial biotransformation of xenobiotics and their consequences

Gut microbiota-mediated biotransformation of xenobiotics is enabled by bacterial enzymes. Bacterial enzymes that are linked to xenobiotic metabolism include hydrolases, oxidoreductases, lyases, and transferases, and are widely distributed among gut bacteria species [107]. It is thought that there are the most prevalent protein families in the gut microbiota and that many xenobiotic transformations may be enabled by different phylogenetic groups of bacteria [107]. Reduction, oxidation, hydroxylation, hydrolysis, deglycosylation, deacetylation and conjugation represent the main microbial enzymatic reactions [107,108]. Reduction and hydrolysis have been the most often observed enzymatic reactions in microbial metabolism of xenobiotics [109]. It may be because of the energetic demands of the gut microbiome, with xenobiotic reductive reactions that foster anaerobic respiration and xenobiotic hydrolysis reactions that directly provide substrates to the gut microbiome [109]. The commonality of these chemical transformations suggest that the gut microbiome is composed of core microbial species or gene families that can impact a wide range of small molecules [109].

The microbial breakdown of xenobiotics can have consequences in their bioavailability, or their pharmacological properties. Three main processes have been characterized, namely activation, inactivation and toxicity (formation of toxic compounds) by the gut microbiota (Figure 10) [109]. Gut microbiota activation is defined by a microbial conversion of an inactive therapeutic (prodrug) into an agent that exerts therapeutic effects. A prominent example is the microbial conversion of sulfonamide antibiotic prontosil (by reduction of its azo bond) into the active compound, sulfanilamide (Figure 10) [109]. Another example is the reduction of the inflammatory bowel disease prodrug sulfasalazine into the active agent 5-aminosalicylic acid (Figure 10). In contrast, gut microbiota inactivation corresponds to the conversion by gut bacteria of an active therapeutic agent into an inactive metabolite. This can result in a significant decrease in concentration of active drug leading to subtherapeutic dosing. The cardiac glycoside digoxin is a typical example, wherein microbial conversion into dihydrodigoxin reduces levels of digoxin, resulting in reduction or suppression of the therapeutic effect (Figure 10)

[109]. Gut microbiota biotransformation of xenobiotic can lead to the formation of toxic compounds (Figure 10) [109]. An interesting but complex case is the anticancer drug irinotecan (inactive prodrug) [107]. Irinotecan is activated by host enzymes into the therapeutic agent SN-38; SN-38 is converted into inactive glucuronide conjugates in the liver, that are then transported back to the intestine via the hepatobiliary route. Once in the gut lumen, microbial β -glucuronidases convert the glucuronide conjugates back into the active SN-38, that exhibits toxicity towards the gut epithelium and exacerbates diarrhea. A similar mechanism involving enterohepatic circulation and hepatic glucuronidation is described for nonsteroidal anti-inflammatory drugs (NSAIDs), resulting in damages to the gut mucosa [109]. For some of these drugs, strategies have been employed to tackle their microbial conversion [106]. As a general strategy, broad-spectrum antibiotics appeared to be efficient but deleterious to the gut microbiota. More targeted approaches with agents inhibiting microbial enzymes (for instance microbial β -glucuronidase) offer more convenient alternatives [109].

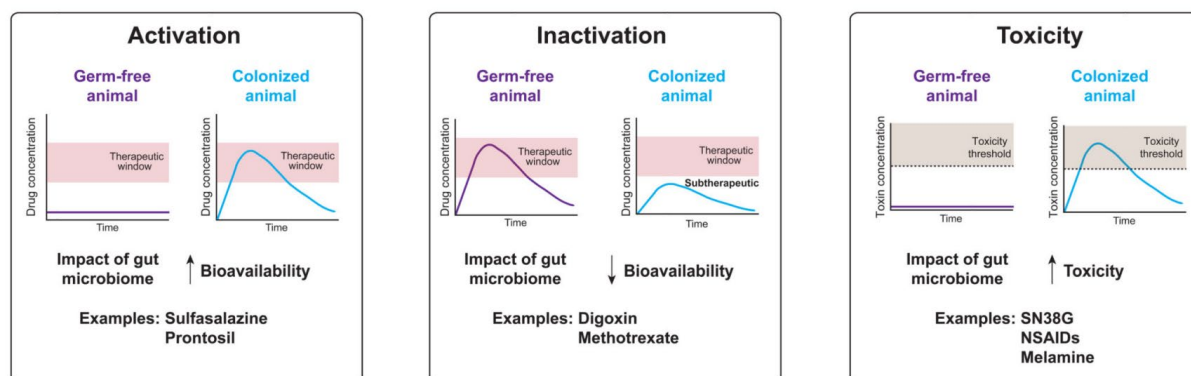


Figure 10. Pharmacological consequences of xenobiotic metabolism by the gut microbiome [109]. Understanding the mechanisms of xenobiotic activation, inactivation or toxicity by the gut microbiome has been enabled by comparing their drug disposition in normal versus germ-free animals (animals grown without exposure to any microorganisms). SN38G, glucuronide conjugate of the anticancer drug SN38. NSAIDs, nonsteroidal anti-inflammatory drugs.

Microbial metabolism of drugs and phytochemicals

Investigations of xenobiotic metabolism by gut microbiota have mainly focused on oral drugs [107,109]. Currently, 55 drugs have been shown via *in vitro* and/or *in vivo* studies to undergo microbiota-mediated metabolism; with 23 compounds (42%) of these medicines corresponding to natural products, natural product derivatives or analogues of endogenous compounds [109,110]. Due to the vast genetic diversity of the gut microbiota, and the lack of any systematic analyses of microbial metabolism of drugs, this number is likely to be underestimated [109]. Recent screening studies revealed that the potential for oral drugs to undergo gut microbiota metabolism is significant. A study showed that out of 271 oral drugs (non-antibiotic) from different pharmacological classes, 176 drugs (65%) were metabolized by at least one strain out of 76 human representative gut bacterial strains [111]. Another recent study found that

out of 438 drugs from various pharmacological classes, 13% were metabolized by microbial communities isolated from human feces [112].

In contrast to drugs, the gut microbial conversion of bioactive phytochemicals from herbal medicines has been less investigated [107]. It was shown that the cyanogenic glycoside amygdalin (found in almonds and fruit pits), which was used primarily as an anticancer agent in the 1960s, was hydrolyzed by gut bacteria into mandelonitrile, a compound that spontaneously breaks down to yield benzaldehyde and toxic cyanide [107]. Berberine, a plant-derived benzylisoquinoline alkaloid, was found to be metabolized (reduction reaction) by the gut microbiota into dehydroberberine, that showed a higher intestinal absorption in comparison to berberine [113]. Another example is the gut microbial conversion of poorly absorbed ginsenosides (steroid glycoside occurring in ginseng) into different deglycosylated metabolites that can enter the blood circulation and affects CYP3A4 activity [107,114].

Phytochemicals originating from dietary plants have also been found to undergo gut microbiota-mediated metabolism. Often, microbial conversion of diet-derived phytochemicals results in the release of metabolites with health promoting effects [110]. An example is the microbial conversion of ellagitannins (from in pomegranates, walnuts and berries) into poorly absorbed ellagic acid, that is further converted into well absorbed urolithins, metabolites exerting health beneficial effects [115]. Similarly, the formation of health promoting and bioavailable compounds by microbiota transformation was reported for other polyphenolic compounds including flavonoids (catechins and gallate esters from tea), isoflavones (from soy) or lignans (from flaxseed and sesame seeds) [107,110].

2.2.4 Impact of xenobiotics on gut bacterial metabolism

A healthy gut microbiota produces SCFAs, but also ensures the *de novo* synthesis of a range of essential compounds that the host is not able to produce, such as vitamins (including vitamin B12, folate, vitamin K, riboflavin, biotin, nicotinic acid, pantothenic acid, pyridoxine and thiamine), choline, purines and phenolic compounds [80,116]. The gut microbiome also converts bile acids into secondary bile acids [80]. The metabolism or *de novo* synthesis of this set of molecules is pivotal in human health [80]. To date, only a few studies have focused on the mechanisms underlying the modulation of the bacterial metabolism induced by the exposure of orally ingested xenobiotics [81].

An example is the anti-diabetic metformin that was shown to alter bacterial synthesis of folate and methionine [117,118], and additionally to modify central bacterial pathways such as downregulation of glycolysis, upregulation of tricarboxylic cycle and arginine degradation [81]. The latter pathways can be linked to the fermentative metabolism of SCFAs [98]. Another drug, the antidepressant duloxetine was found to bioaccumulate in different gut bacterial species and alter several bacterial pathways, including purine, pyrimidine and amino acids biosynthesis as well as amino acid metabolism [119].

In regards to phytochemicals, the alkaloid trigonelline (present in coffee) induced shifts in the metabolism of choline in isolated *Citrobacter freundii*, resulting in a reduced production of the pro-atherosclerotic compound trimethyl-amine N-oxide [81]. Another alkaloid present in several plants from the Chinese Pharmacopeia, berberine, was shown to increase the production of SCFAs partly through upregulation of enzymes involved in SCFA biosynthetic pathways [118].

2.2.5 The *in vitro* PolyFermS model, an artificial gut microbiota

Understanding gut microbial interactions with xenobiotics was partly enabled by the development of artificial gut microbiota systems. A convenient system is the fermentation model PolyFermS, that allows stable and reproducible cultivation of colonic microbial communities derived from a single human fecal donor [120]. The PolyFermS is a chemostat model, consisting of interconnected bioreactors supplied continuously with fresh nutritive medium and in which effluent (containing microorganisms and metabolic products) is evacuated at the same rate to maintain a constant volume [121].

Overview of the PolyFermS model

The PolyFermS can be established from fresh feces from a single human donor, which is the gold standard to ensure maximum viability and fitness of bacterial species, in comparison to cryopreserved fecal microbiota [121]. Fecal material is immobilized in gel beads (1 to 2 mm diameter mainly composed of gellan and xanthan gums), a process performed under anaerobic conditions. Gel beads offer a suitable and stable environment for the long-term growth of anaerobe bacterial consortia that reflect communities found in the feces of the human donor (both in diversity and abundance) [120,122]. The fresh fecal beads are then transferred into an inoculum reactor (IR) and mixed with a culture medium that simulates the conditions of a human adult chyme [120,123]. The continuous fermentation system is established when connecting the IR to the other control and test reactors as depicted in Figure 11. The system is continuously provided with nutritive medium, CO₂ and the pH is automatically adjusted with NaOH. To ensure the validity of the system, monitoring the gut microbiota composition and metabolic activity (production of SCFAs) can be performed at relevant time points over the course of running of the system (Figure 11). A PolyFermS system can be run from a few weeks to four months [121].

Chemostat and batch fermentation experiments

The PolyFermS can be used either for chemostat experiments or as a starting point for batch fermentation experiments. Chemostat experiments are convenient to study community dynamics, cross-feeding mechanisms or treatment responses on the gut microbiome, with a long-term perspective (typically from weeks to months) [121]. For these experiments, the setup consists of applying experimental features in the test reactors and use of a control reactor as reference microbiota. A strength of chemostat experiments is that microbiota renewal, anaerobic, pH and mixing efficiency can be kept constant over the course of the experiment, ensuring system's stability [121]. However, chemostat experiments come with various drawbacks including labor-intensive, low-throughput, complex infrastructure and high costs [121].

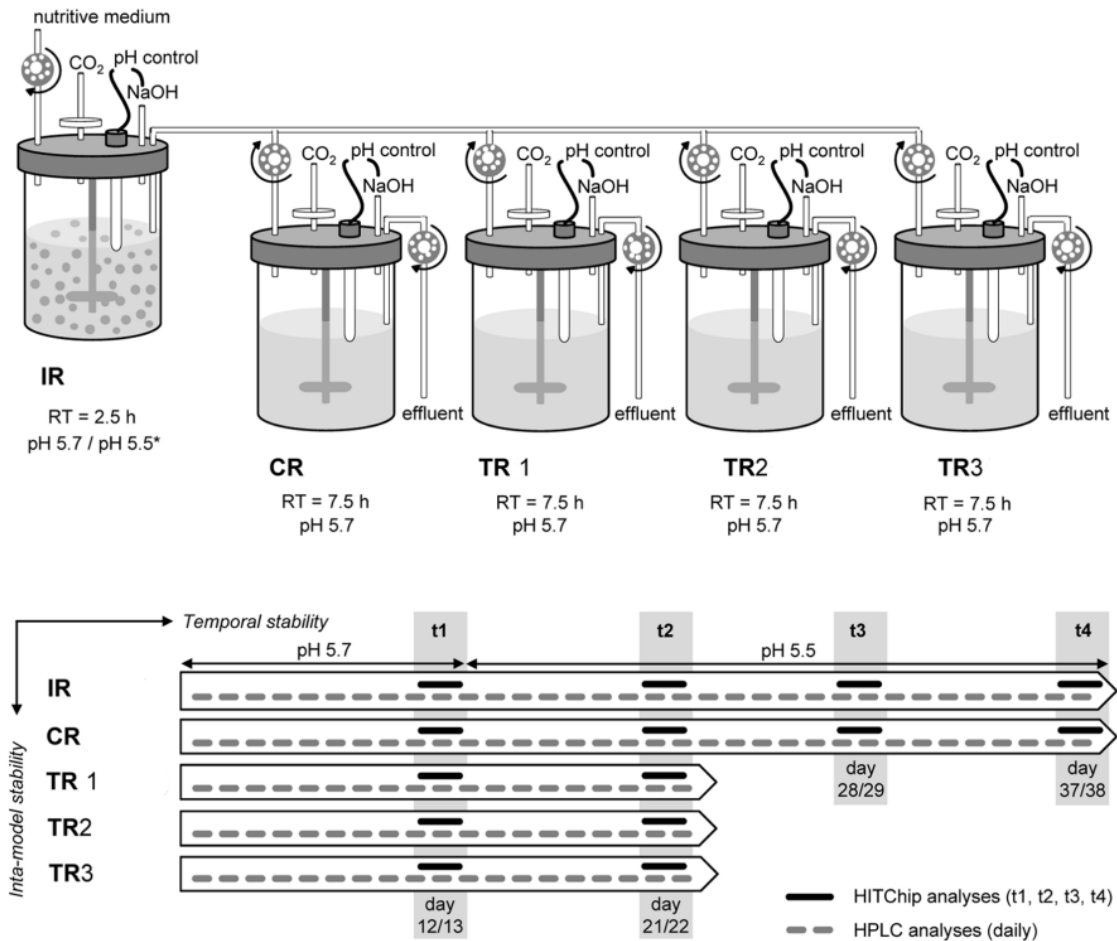


Figure 11. Principle of the Polyfermentor Intestinal model (PolyFermS)

The inoculum reactor (IR) continuously provides to control (CR) and test reactors (TR), effluents composed of 30% of fecal beads from a single human fecal donor. The system is operated under strict anaerobic conditions, and maintained at the same pH. Herein, pH of 5.7 corresponds to conditions found in the proximal colon. Metabolic activity or community structure of the artificial microbiota can be controlled daily or at selected time points (t1, t2, t3 and t4), respectively. Adapted from [120]. RT, retention time. HITChip, Human Intestinal Tract Chip.

Alternatively, artificial microbiota from a test reactor can be used to perform batch experiments, which are easy to operate, with a simplified setup and a high throughput potential [121]. Batch experiments consist of incubating viable microbiota with appropriate nutritive medium in a closed anaerobic environment, for a fixed and short period of time (typically 24 – 48 h) [121]. Batch experiments can be performed with varying conditions (inoculation level, nutritional medium, scale) and require multiple replicates. For static batch experiments in closed-tubes, the strict anaerobic Hungate technology enables to monitor SCFAs production and microbial kinetics changes in response to a treatment [121]. A drawback of batch experiments is that they cannot reflect long-term gut microbiota dynamics upon treatment in comparison to continuous chemostat experiments [121].

The use of the PolyFermS for chemostat or batch experiments has some limitations; the main being the absence of host-related factors such as metabolic and water absorption or intestinal cells [120]. Also, PolyFermS systems lack a simulation of upper parts of the GI tract, in which test compounds can already undergo a pre-treatment (degradation or absorption) [121].

2.2.6 Other *in vitro* fermentation models of the human gut microbiome

Other *in vitro* models established from human stools can be used to study the gut microbiome [124]. Some of these models are chemostat models that can simulate several segments of the GI tract. For instance, the reading model can simulate proximal, transverse and distal compartments in three connected reactors [124]. Some other systems like the TIM-2, SHIME®, or SIMGI, can mimic additional segments of the GI tract such as the stomach and the small intestine [121,124]. Additional models are more adapted to high throughput settings such as small-scale reactors. An example is the highly automated mini-bio *in vitro* model which remotely controls various factors in up to 32 bioreactors mounted in parallel [124,125].

To reduce the complexity of the *in vitro* fermentation models generated from fecal suspension, which are characterized by a high microbial diversity and abundance, models with defined consortia of gut bacteria can be used. The SIHUMIx (Simplified Human Intestinal Microbiota), a consortium of eight representative gut bacterial strains is a relevant example. While these models enable a simplified setup and readout, the stability of microbial communities is challenged over long-time handling [124].

2.3 Investigated herbal drugs and phytochemicals

Herbal medicines have been employed by humans for tens of thousands of years to treat or relieve numerous of disorders [126]. The assumed oldest trace of medicinal plants was found from 60'000 years old Neanderthal tombs in Iraq and the earliest systematic medical text (mentioning around 800 medicinal plants), the Egyptian *Papyrus Ebers*, was dated to 1'500 BC [126]. Plants have been indeed the primary therapeutic agents since the dawn of time for humans. Despite the development of modern science and evidence-based medicinal approaches, which largely rely nowadays on pharmacological treatments with single molecules, herbal medicines continue to be widely employed around the world [126]. Interestingly, the use of herbal medicines has increased over the last decades [127]. This includes herbal medicines used to treat anxiety, mild-depression or sleeping disorders. In 2019, 12.5% of the worldwide population was living with a mental disorder, with anxiety and depression as the most common [128]. Plant products used to ease these disorders include valerian (*Valeriana officinalis* L., Caprifoliaceae), St. John's wort (*Hypericum perforatum* L., Hypericaceae) or California poppy (*Echscholzia californica*, Cham., Papaveraceae).

In this chapter, the three herbal medicines and their pharmacologically relevant phytochemicals will be presented. Thereafter, current data on the disposition of these phytochemicals will be provided, with a focus on aspects related to their intestinal absorption.

2.3.1 Valerian

Valerian is a perennial herbaceous plant native to Europe and Asia [129]. Preparations of valerian roots have probably been used since the ancient Greeks and Romans as a remedy for urinary tract, menstrual cramps and liver diseases [129]. Currently, valerian is commonly used to treat nervous states or sleeping disorders and was listed in 2017 among the top 20 most sold herbal medicines in the USA [130]. The hydroalcoholic extract of valerian is qualified for well-established use by the European Medicine Agency (EMA) for “the relief of mild nervous tension and sleeping disorders” [129]. *In vitro* and *in vivo* data support that valerian extracts allosterically modulate GABA_A receptor [131]. The sesquiterpene valerenic acid is considered as the main contributor of this GABAergic activity (Figure 12) [131].

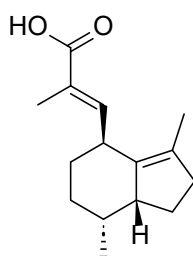


Figure 12. Chemical structure of valerenic acid

Disposition of valerenic acid upon ingestion of valerian has been explored in a pharmacokinetic study in rats, which found an absolute bioavailability of 34%, with a very short mean t_{\max} of 5 mins [132]. In contrast, data from pharmacokinetics in volunteers, showed a higher mean t_{\max} of 1.7 h [133].

2.3.2 St John's wort

St. John's wort is a perennial herbaceous plant, largely diffused in Europe, Northern Africa, Asia and North America [134]. St. John's wort has been used since antiquity as a diuretic, wound-healing and antimalarial agent [135]. Over the past 30 years, its use in the treatment of depressive disorders has gained popularity [135]. In 2017, St. John's wort was ranked among the top 20 most sold herbal drugs in the USA [130]. Various meta-analysis evaluating St. John's wort in the management of mild to moderate depression, noticed a superior effect of St. John's wort therapy over placebo, and no significant difference with antidepressant therapy [134]. Currently, St. John's wort is qualified for well-established use in the treatment of mild to moderate depressive disorders [134]. As reported in several *in vitro* and *in vivo* studies, St. John's wort's mechanism of action include the modulation of neurotransmitters in the brain either by regulating their re-uptake from the synaptic cleft or by direct binding to neurotransmitter transporters [136]. While the whole plant extract is considered as the active ingredient, the phloroglucinol hyperforin and naphthodianthrone hypericin are seen as important contributors of the antidepressant-like effects (Figure 13) [136].

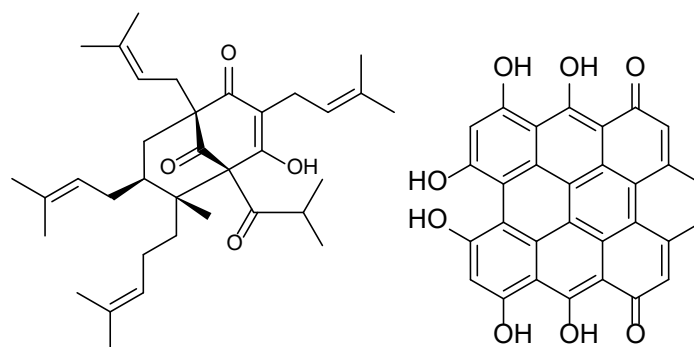


Figure 13. Chemical structure of hyperforin (left) and hypericin (right).

Few studies have investigated intestinal absorption properties of hyperforin and hypericin. Pharmacokinetics studies in volunteers showed that upon ingestion of St. John's wort, both compounds were bioavailable with varying pharmacokinetic parameters. Hyperforin levels reached maximum plasma concentration in 4.4 h (t_{max}), with a relatively short lag-time (time for an oral compound to reach the systemic circulation) of 1.3 h whereas hypericin was characterized by a higher t_{max} (8.1 h) and a longer lag-time (2.3 h) [137]. These data suggest that hyperforin bioavailability is higher than hypericin. Another pharmacokinetic study with two healthy volunteers also reported for hypericin a high lag-time (1.9 h) and an absolute bioavailability of 14% [138]. In addition, data with the Caco-2 cell model indicated that the intestinal permeability of hypericin was low, and with high compound binding to cellular surface [139–141].

2.3.3 California poppy

California poppy is an annual plant native from Western North America, that has been traditionally used as a sedative, hypnotic, and analgesic by Native American populations [142]. Currently, California poppy is mostly used to treat anxiety or sleeping disorders [142]. Several *in vitro* and *in vivo* studies have shown that California poppy extracts have analgesic and sleep-inducing properties [142]. These extracts are thought to exert these effects through modulation of the GABA_A receptor activity, modulation of catecholamine metabolism or serotonin receptor binding [143–145]. California poppy alkaloids such as californidine, escholtzine and protopine are thought to be among the main contributors (Figure 14) [142]. Although data on commercial products of California poppy are lacking, it is known that californidine, escholtzine and protopine alkaloids are the most abundant in flowering aerial parts of California poppy [146,147].

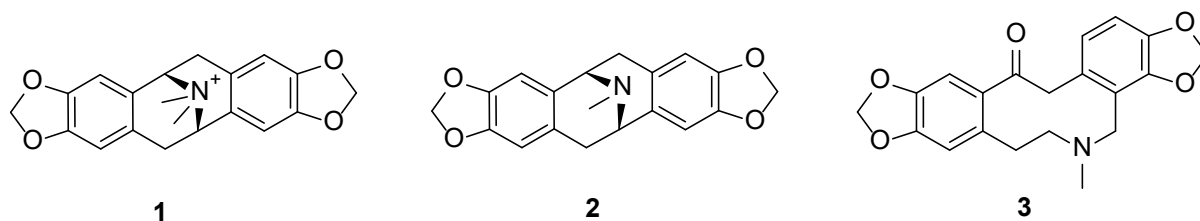


Figure 14. Chemical structure of californidine (1), escholtzine (2), and protopine (3).

Apart from protopine, the disposition of these alkaloids has not been studied. A pharmacokinetic study on rats found an absolute bioavailability of 26% for protopine, with a t_{\max} of 2.7 h [148]. Intestinal permeability properties of the three alkaloids, have not been investigated up to now.

3 Results and discussion

3.1 Intestinal permeability and gut microbiota interactions of pharmacologically active compounds in valerian and St. John's wort

Antoine Chauveau, Andrea Treyer, Annelies Geirnaert, Lea Bircher, Angela Babst, Vanessa Fabienne Abegg, Ana Paula Simões-Wüst, Christophe Lacroix, Olivier Potterat, Matthias Hamburger

Biomedicine & Pharmacotherapy, 2023, 162, 114652

doi: 10.1016/j.biopha.2023.114652

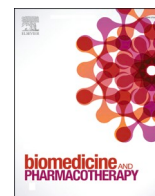
Abstract

Phytomedicines such as valerian and St. John's wort are widely used for the treatment of sleeping disorders, anxiety and mild depression. They are perceived as safe alternatives to synthetic drugs, but limited information is available on the intestinal absorption and interaction with human intestinal microbiota of pharmacologically relevant constituents valerenic acid in valerian, and hyperforin and hypericin in St. John's wort. The intestinal permeability of these compounds and the antidepressant and anxiolytic drugs citalopram and diazepam was investigated in the Caco-2 cell model with bidirectional transport experiments. In addition, interaction of compounds and herbal extracts with intestinal microbiota was evaluated in artificial human gut microbiota. Microbiota-mediated metabolism of compounds was assessed, and bacterial viability and short-chain fatty acids (SCFA) production were measured in the presence of compounds or herbal extracts. Valerenic acid and hyperforin were highly permeable in Caco-2 cell monolayers. Hypericin showed low-to-moderate permeability. An active transport process was potentially involved in the transfer of valerenic acid. Hyperforin and hypericin were mainly transported through passive transcellular diffusion. All compounds were not metabolized over 24 h in the artificial gut microbiota. Microbial SCFA production and bacterial viability was not substantially impaired nor promoted by exposure to the compounds or herbal extracts.

The supporting information is available in the appendix (pages 93 – 100), or at:

<https://doi.org/10.1016/j.biopha.2023.114652>

My contribution to this work: Caco-2 cell culture; permeability experiments; sample extraction and analysis (UHPLC/MS-MS) of Caco-2 and microbiota samples; UHPLC/MS-MS method development and validation for compounds hyperforin, diazepam, atenolol and propranolol; writing of the manuscript draft and preparation of figures and tables.



Intestinal permeability and gut microbiota interactions of pharmacologically active compounds in valerian and St. John's wort

Antoine Chauveau^a, Andrea Treyer^a, Annelies Geirnaert^b, Lea Bircher^b, Angela Babst^b, Vanessa Fabienne Abegg^a, Ana Paula Simões-Wüst^c, Christophe Lacroix^b, Olivier Potterat^{a,*}, Matthias Hamburger^{a,*}

^a Division of Pharmaceutical Biology, Department of Pharmaceutical Sciences, University of Basel, Basel, Switzerland

^b Laboratory of Food Biotechnology, Institute of Food, Nutrition and Health, Department of Health Science and Technology, ETH Zurich, Zurich, Switzerland

^c Department of Obstetrics, University Hospital Zurich, University of Zurich, Zurich, Switzerland

ARTICLE INFO

Keywords:

Valerianic acid
Hyperforin
Hypericin
Caco-2 cells
Gut microbiota
Short-chain fatty acids

ABSTRACT

Phytomedicines such as valerian and St. John's wort are widely used for the treatment of sleeping disorders, anxiety and mild depression. They are perceived as safe alternatives to synthetic drugs, but limited information is available on the intestinal absorption and interaction with human intestinal microbiota of pharmacologically relevant constituents valerianic acid in valerian, and hyperforin and hypericin in St. John's wort. The intestinal permeability of these compounds and the antidepressant and anxiolytic drugs citalopram and diazepam was investigated in the Caco-2 cell model with bidirectional transport experiments. In addition, interaction of compounds and herbal extracts with intestinal microbiota was evaluated in artificial human gut microbiota. Microbiota-mediated metabolism of compounds was assessed, and bacterial viability and short-chain fatty acids (SCFA) production were measured in the presence of compounds or herbal extracts. Valerianic acid and hyperforin were highly permeable in Caco-2 cell monolayers. Hypericin showed low-to-moderate permeability. An active transport process was potentially involved in the transfer of valerianic acid. Hyperforin and hypericin were mainly transported through passive transcellular diffusion. All compounds were not metabolized over 24 h in the artificial gut microbiota. Microbial SCFA production and bacterial viability was not substantially impaired nor promoted by exposure to the compounds or herbal extracts.

1. Introduction

Phytomedicines containing extracts of herbal drugs such as valerian (*Valeriana officinalis* L., Caprifoliaceae) and St. John's wort (*Hypericum perforatum* L., Hypericaceae) are widely used, also during pregnancy, for the treatment of sleeping disorders, anxiety and mild depression, and are perceived as safe alternatives to synthetic drugs [1]. These herbal drugs have been well studied from a pharmacological perspective, but little is known regarding the intestinal absorption of important constituents in these drugs. Furthermore, possible interactions of extracts and constituents with the human microbiota have not been investigated up to now.

Extracts of valerian are widely used to treat mild nervous tension, anxiety or sleep disorders, and their use is considered by European Medicines Agency (EMA) as well established [2]. Valerianic acid (Fig. 1)

is a pharmacologically relevant constituent acting through a positive allosteric modulation of γ -aminobutyric acid (GABA) receptors [2]. The use of St. John's wort extracts for the treatment of mild to moderate depression is also considered by the EMA as well established [3]. Several compounds in the extract are believed to contribute to the antidepressant-like effects, including flavonoids, hyperforin and hypericin (Fig. 1) [3]. In various in vitro and in vivo models for depression these constituents were shown to act on neurotransmitters in the brain, via regulation of their re-uptake from the synaptic cleft, or by direct binding to neurotransmitter transporters [3].

The treatment of more severe cases of anxiety, depression and sleep disorders nevertheless relies on synthetic drugs such as diazepam and citalopram (Fig. 1). Diazepam is a benzodiazepine that has anxiolytic, sedative and muscle-relaxant effects via a positive allosteric modulation

* Correspondence to: Division of Pharmaceutical Biology, Department of Pharmaceutical Sciences, University of Basel, Klingelbergstrasse 50, 4056 Basel, Switzerland.

E-mail addresses: olivier.potterat@unibas.ch (O. Potterat), matthias.hamburger@unibas.ch (M. Hamburger).

<https://doi.org/10.1016/j.bioph.2023.114652>

Received 15 February 2023; Received in revised form 31 March 2023; Accepted 31 March 2023

Available online 5 April 2023

0753-3322/© 2023 The Authors. Published by Elsevier Masson SAS. This is an open access article under the CC BY license (<http://creativecommons.org/licenses/by/4.0/>).

of γ -aminobutyric acid type A (GABA_A) receptors [4]. Citalopram is an antidepressant that exerts serotonergic activity via an inhibition of neuronal reuptake of serotonin [5].

Numerous studies explored the pharmacological properties of valerenic acid, hyperforin and hypericin, but little is known about their intestinal absorption, transcellular transport and cellular uptake [2,3], even though a good understanding of these processes is important for optimal treatment with valerian and St. John's wort preparations. No data have been published up to now on the intestinal uptake of valerenic acid and hyperforin, and only limited data is available on the intestinal permeability of hypericin and citalopram [6–8]. Furthermore, nothing is known regarding a possible biotransformation of valerenic acid, hyperforin, hypericin, citalopram, and diazepam by the gut microbiota, and the impact of these compounds and of valerian and St. John's wort on the integrity of human microbiota also has not been investigated up to now. The latter aspect is of particular interest in the context of stress-related mental conditions, given the bidirectional crosstalk between the gut microbiome and the central nervous system via the gut-brain axis [9].

In vitro human gut microbiota models inoculated with fecal microbiota and mimicking the physicochemical conditions of the gut are powerful tools to evaluate the xenobiotic-microbiota interactions [10, 11]. We previously showed that the artificial microbiota produced with the PolyFermS model inoculated with immobilized fecal microbiota is a reproducible source of large amounts of inocula for high throughput testing and comparison of different treatment conditions, including xenobiotic degradation with the same microbiota background [10,12]. A particular advantage of using the latter is that the amount of inoculum is not limiting and high inoculation ratios (e.g. 80 %) can be used to accurately measure the bioconversion activity of the microbiota without the confounding factor of the microbial growth [10,11,13]. Thus, the biotransformation of xenobiotics can be investigated in this model, as well as the possible impact of xenobiotics on the viability of the artificial colon microbiota and on their SCFAs metabolism. SCFAs serve as an energy source for intestinal cells, as signaling molecules, modulators of lipid metabolism, and as regulators of the intestinal immunity [14].

Also, they have been associated with health benefits in numerous diseases, such as inflammatory bowel disease, colon cancer, and diabetes [14].

In this study, the bidirectional transport of valerenic acid, hyperforin, hypericin, citalopram, and diazepam in the Caco-2 cell model, their biotransformation by artificial gut microbiota, and their impact on bacterial viability of microbiota and SCFAs metabolism during short term batch fermentation was studied. The effect of valerian and St. John's wort extracts on the microbiota were also examined.

2. Materials and methods

2.1. Cell lines, chemicals and biochemicals

The Caco-2 cell line was kindly provided by Prof. Per Artursson, Uppsala University, Sweden [15]. Dulbecco's Modified Eagle's Medium (DMEM, with high glucose, L-glutamine, phenol red, without sodium pyruvate), Dulbecco's phosphate-buffered saline (DPBS, without calcium/magnesium, without phenol red), fetal bovine serum (FBS), MEM non-essential amino acids solution (NEAA, without L-glutamine), penicillin-streptomycin (PEST, 10,000 U/mL), trypsin (2.5 %, without phenol red), were purchased from Gibco (Paisley, UK). Hank's balanced salt solution (HBSS, without phenol red), 4-(2-hydroxyethyl)piperazine-1-ethanesulfonic acid (HEPES), 4-morpholineethanesulfonic acid monohydrate (MES), sodium bicarbonate (NaHCO₃), bovine serum albumin (BSA), dimethyl sulfoxide (DMSO), cellobiose, soluble potato starch, amylase, meat extract, mucin from porcine stomach type II, arabinogalactan from larch wood, Tween 80, hemin, NaHCO₃, KCl, MgSO₄, CaCl₂·2H₂O, MnCl₂, FeSO₄·7H₂O, ZnSO₄·7H₂O, 4-aminobenzoic acid (PABA), nicotinic acid, biotine, folic acid, cyanocobalamin, thiamine, riboflavin, phyloquinone, menadione, and pantothenate were purchased from Sigma-Aldrich (Saint-Louis, MO, USA). Xylan from oat spelts, and bacto tryptone were from Chemie Brunschwig AG (Basel, Switzerland). Inulin was provided by Cosucra (Warcoing, Belgium), and yeast extract by Lesaffre (Marcq-en-Barœul, France). Bile salts were purchased from Thermo Fischer Diagnostics (Pratteln, Switzerland).

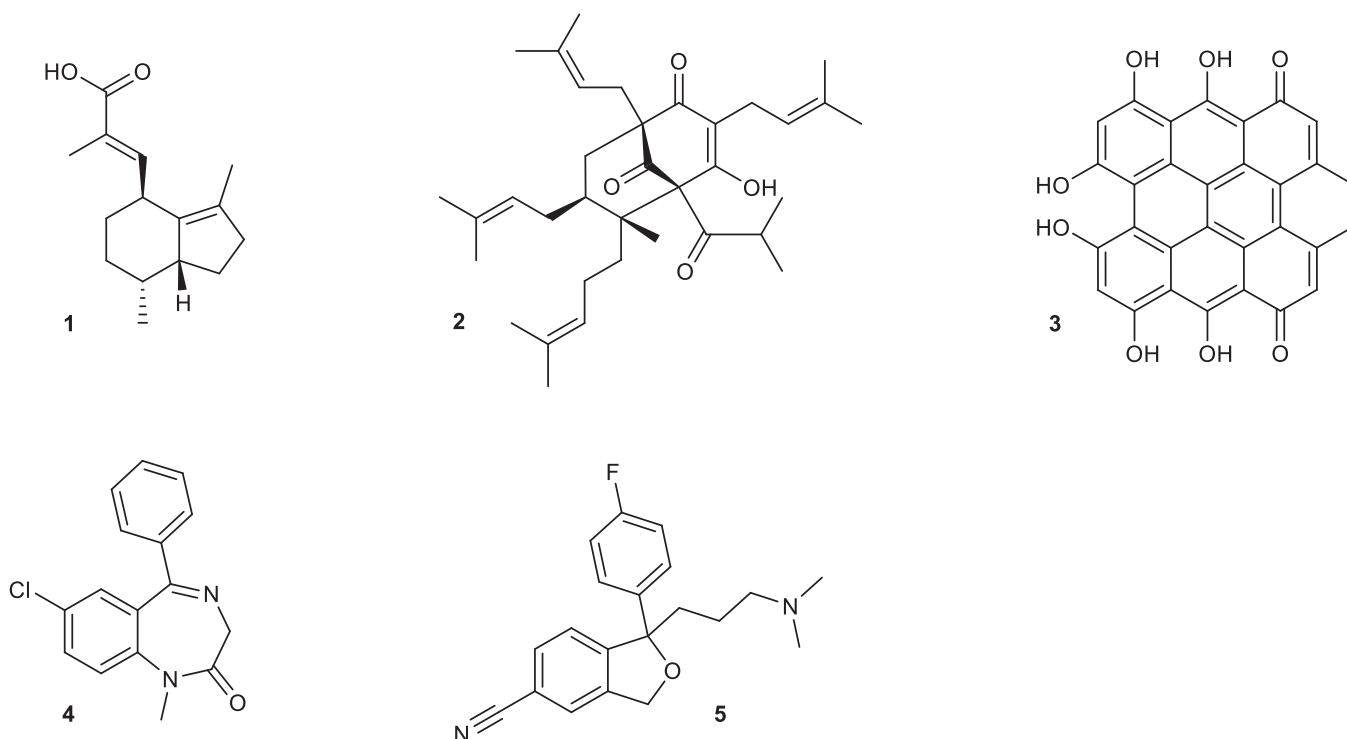


Fig. 1. Chemical structures of valerenic acid (1), hyperforin (2), hypericin (3), diazepam (4) and citalopram (5).

KH₂PO₄, NaCl, pyridoxine-HCl (Vit. B6), folic acid and menadione were obtained from VWR International (Dietikon, Switzerland). Ethylenediaminetetraacetic acid (EDTA, 0.2 % in PBS, without calcium/magnesium) was purchased from MP biomedical (Santa Ana, CA, USA). Culture flasks (75 cm²), bottle top filters (pore size 0.22 μm), 12-well Costar® plates, 12-well Transwell® plates (with inserts of 12 mm diameter and a polycarbonate membrane with pores of 0.4 μm), were purchased from Corning Incorporated (Corning, NY, USA). Sodium fluorescein salt, atenolol, propranolol HCl, verapamil HCl, hyperforin dicyclohexylammonium salt (DCHA), and digoxin were purchased from Sigma-Aldrich (Saint-Louis, MO, USA). Diazepam and diazepam-D₅ were purchased from Lipomed (Arlesheim, Switzerland). Citalopram hydrobromide (HBr) was obtained from Acros Organics (Geel, Belgium) and citalopram-D₄ HBr from CDN isotopes (Pointe-Claire, QC, Canada). Warfarin was purchased from Toronto Research Chemicals (Toronto, ON, Canada). Hypericin was obtained from Carbosynth (Compton, UK), and valerenic acid was purchased from Extrasynthese (Genay, France) and Phytolab (Vestenbergsgreuth, Germany). Acetonitrile (MeCN) and acetone were from Supelco (Bellefonte, PA, USA). Methanol (MeOH), isopropyl alcohol and ethanol (EtOH) were obtained from Macron Fine Chemicals (Radnor, PA, USA). *n*-Butanol (BuOH) and ethyl acetate (EtOAc) were purchased from Scharlau (Sentmenat, Spain). All solvents were of UHPLC grade. HPLC grade water was obtained from a Milli-Q integral water purification system Millipore Merck (Darmstadt, Germany). Materials for flow cytometry were purchased from Beckman Coulter International (Nyon, Switzerland), except for stains SYBR Green I and propidium iodide which were from Life Technologies Europe (Zug, Switzerland).

2.2. Plant material and extraction

Plant material was of Ph. Eur. grade. *Hypericum perforatum* and *Valeriana officinalis* (lot numbers 180,084, 192,140, respectively) were purchased from Dixa (St. Gallen, Switzerland). Voucher specimens (No 1029, 1166, respectively) have been deposited at the Division of Pharmaceutical Biology, University of Basel. 2 g of powdered plant material was extracted with 70 % EtOH by pressurized liquid extraction in a Dionex ASE 200 Accelerated Solvent Extractor (Sunnyvale, CA, USA). Three extraction cycles of 5 min were performed at a temperature of 70 °C and a pressure of 120 bar. The herbal extracts were previously characterized [16].

2.3. Caco-2 cell model and permeability experiments

2.3.1. Cell culture

Cells were grown in 75 cm² culture flasks using DMEM (supplemented with 10 % FBS, 1 % NEAA, 1 % PEST) in a humidified atmosphere (95 %) consisting of 10 % CO₂, at a temperature of 37 °C. When confluence of 90–95 % was reached, cells were subcultured by dissociation with trypsin solution (0.25 % trypsin, 0.2 % EDTA). To prepare monolayers for permeability experiments, cells were seeded at a density of 4.5×10^5 cells/cm² and cultivated on Transwell® inserts over 22–28 days. During the culturing of cells on inserts, medium volumes at apical and basolateral chambers were set at 0.5 and 1.5 mL. The medium on both chambers was changed three times a week. The seeding on inserts was performed with cells corresponding to passage number 94–108.

2.3.2. Permeability experiments

Permeability across Caco-2 monolayers was studied in the both directions, from apical to basolateral (AB), and from basolateral to apical (BA). To approach physiological conditions found in the human small intestine, transport buffers were adjusted to pH 6.5 in the apical chamber (10 mM MES, 4.2 mM NaHCO₃ in HBSS) and to pH 7.4 in the basolateral chamber (25 mM HEPES, 4.2 mM NaHCO₃ in HBSS). Prior to use, buffers were sterilized through filtration (0.22 μm pore filter) and

stored in autoclaved bottles. Before starting the experiments, cell monolayers were washed with pre-warmed buffer HBSS/HEPES pH 7.4. Volumes at apical and basolateral chambers were set at 0.4 and 1.2 mL respectively. All permeability experiments were performed with DMSO as co-solvent (1 %, v/v) to improve solubility of study compounds. In experiments with hyperforin and hypericin, buffers were supplemented with BSA (10 %) to further improve solubility. Experiments were performed at a final concentration of 10 μM in the donor chamber, over 60 min with 15 min sampling time intervals. For hyperforin and hypericin, the experiment duration was extended to 120 min, with 15 min sampling time intervals from 0 to 60 min, and 30 min sampling time intervals from 60 min to 120 min. Hyperforin and hypericin solutions were protected from any light source during handling. Sampling volume was 0.6 mL or 0.2 mL from the basolateral chamber or apical chamber, respectively. After each sampling from the receiver chamber the volume was replaced by the same volume of transport buffer. All experiments were done under mild agitation (450 rpm at 37 °C) on an orbital shaker (QInstruments, Jena, Germany) [15]. At the end of the experiments, sampling (0.2 or 0.6 mL in apical or basolateral chambers, respectively) from the donor chamber was performed, to determine the mass balance. Sink conditions of the receiver chamber were maintained over the course of all permeability experiments [15]. Permeability experiments were performed in triplicate. Collected samples were precipitated with MeCN and stored at –80 °C until UHPLC-MS/MS analysis. Cumulative fraction curves for each experiment of all compounds are shown in Figs. S1–S7.

2.3.3. Cell lysis

Following permeability experiments, cell monolayers were washed quickly with buffer HBSS/HEPES pH 7.4 and lysed with MeCN for 30 min. Cell lysis experiments were performed in duplicate. Samples were stored at –80 °C until UHPLC-MS/MS analysis.

2.3.4. Control of Caco-2 cell monolayer integrity

To control their integrity, transepithelial electrical resistance (TEER) of Caco-2 cell monolayers was measured with an EVOMX (WPI, Sarasota, FL, USA) before and after permeability experiments. Only monolayers with TEER values > 200 Ω cm² were used (Table S1). To further control the integrity of monolayers, the transport of the paracellular leakage marker fluorescein was assessed at the end of the experiments (Table S1). Following washing of monolayers, fluorescein was added to the apical chamber at a final concentration of 1 mg/mL before incubation in an orbital shaker (450 rpm, 37 °C) for 1 h. Fluorescein was quantified by fluorescence spectrophotometry (λ_{ex} 485 nm, λ_{em} 535 nm) with a Chromeleon microplate reader (HIDEX, Turku, Finland), and a passage of < 1 % of fluorescein per hour used as an indicator of monolayer integrity [17]. As an additional control atenolol and propranolol were included as references for low-to-moderately and highly permeable drugs, respectively.

2.3.5. Experiments with cell-free inserts

Control experiments with cell-free inserts were performed to assess the passage of the compounds in absence of cells. As for the permeability experiments, study compounds were added to the donor chamber and incubated for 1 h (2 h for hypericin and hyperforin) at 37 °C under shaking (450 rpm). At the end of the experiment, aliquots were withdrawn from donor and receiver chambers, and stored at –80 °C until analysed by UHPLC-MS/MS.

2.3.6. Determination of apparent permeability coefficients and efflux ratio

Apparent permeability coefficients (P_{app}) were calculated according to equations described by Hubatsch et al. [15]. The apparent permeability coefficients (P_{app}), expressed in cm s⁻¹, were calculated according to the following equation:

$$P_{app} = \left(\frac{dQ}{dt} \right) \left(\frac{1}{AC_0} \right) \quad (1)$$

where dQ/dt is the steady-state flux ($\mu\text{M s}^{-1}$), A the surface area of the filter (cm^2), and C_0 the initial concentration in the donor chamber (μM).

The lowered donor concentration after each sampling was taken into account, and recalculated by subtracting the cumulative fraction transported (FA_{cum}) to the receiver chamber, at each time interval. Details on the FA_{cum} equation are presented in the [Supporting information Eq. \(A.1\)](#).

P_{app} values in apical to basolateral (P_{appAB}) and P_{app} values in basolateral to apical direction (P_{appBA}) were calculated to determine the efflux ratio (ER) as follows:

$$ER = \frac{P_{appBA}}{P_{appAB}} \quad (2)$$

2.3.7. Determination of recoveries

Recovery considering A and B chambers (Re_{AB}) was calculated according to the following equation [15] as:

$$Re_{AB}(\%) = \left(C_{D(fin)}V_D + C_{R(fin)}V_{R(fin)} + \sum (C_{S(t)}V_{S(t)}) \right) 100 / (C_{D(0)}V_{D(0)}) \quad (3)$$

whereby $C_{D(0)}$ and $C_{D(fin)}$ are the initial or final concentration in the donor chamber, and $C_{R(0)}$ and $C_{R(fin)}$ the respective concentration on the receiver side. $C_{S(t)}$ represents the respective concentrations of samples withdrawn at different time points t , and V_D , V_R and V_S are the respective volumes.

Recovery considering A, B and cell fraction (Re_{ABC}) was calculated to evaluate the accumulation or binding of study compounds to the cells. Re_{ABC} was calculated according to the following equation:

$$Re_{ABC}(\%) = Re_{AB} + A_{cells}100/A_{D(0)} \quad (4)$$

whereby A_{cells} represents the amount in the cell fraction, and $A_{D(0)}$ the initial amount in the donor chamber.

2.4. In vitro gut microbiota experiments

2.4.1. In vitro PolyFermS model microbiota

The artificial human gut microbiota used in this study were derived from two independent stable PolyFermS bioreactor systems that were both inoculated with immobilized fecal microbiota. The PolyFermS system is designed and operated to mimic the proximal colon conditions and allows to continuously cultivate the proximal colon microbiota akin to donor profile [18,19]. The fecal samples for initiating the PolyFermS system were donated by two healthy female individuals (female, age 25–35) with Western-style diet who did not receive any antibiotics or probiotics for at least 3 months before donation. The Ethics Committee of ETH Zürich exempted this study from review because the sample collection procedure has not been performed under conditions of intervention. Informed written consent was obtained from fecal donors. The PolyFermS system was operated as described before in Poeker et al. [18]. The bioreactor containing the immobilized donor microbiota served as inoculum reactor for parallel second-stage reactors that were connected to the bead reactor with a peristaltic pump and operated at identical conditions. The second stage microbiota reactors were continuously supplied with 5 % (v/v) IR microbiota effluent and 95 % (v/v) sterile and anaerobic Macfarlane-based nutritive medium [18]. After a period of 6–8 days the second stage bioreactor microbiota stabilized and showed a similar fermentation metabolite profile as the inoculum reactor (data not shown). For each anaerobic batch experiment the artificial human colon microbiota from a single stabilized second stage bioreactor were completely harvested under anaerobic conditions (10 % CO_2 , 5 % H_2 and 85 % N_2) in an anaerobic tent (Coy

Laboratories, MA, USA).

2.4.2. Anaerobic batch fermentation experiments with herbal and synthetic compounds

PolyFermS microbiota were incubated with herbal and synthetic control compounds to monitor the colon microbial biotransformation potential and impact on fermentation metabolites and bacterial viability. The incubation mixture consisted of fresh and metabolically highly active PolyFermS colon microbiota effluent supplemented with nutritive medium (MacFarlane medium) at a ratio of 7:3, and adjusted to pH 6.5. The high microbiota to medium ratio was chosen to enable the evaluation of the microbial biotransformation of the compounds and impact of the compounds on microbial viability under limited growth. The nutritive medium was based on the Macfarlane medium for the cultivation of human colon microbiota [20] and contained (in g/L): cellobiose (1); oat xylan (1); larch wood arabinogalactan (1); inulin (0.5); soluble potato starch (1); amylase (3); meat extract (1.5); mucin (4); tryptone (5); yeast extract (4.5); bile salts (0.4); KH_2PO_4 (3); NaHCO_3 (9); NaCl (4.5); KCl (4.5); MgSO_4 (0.61); $\text{CaCl}_2 \cdot 2\text{H}_2\text{O}$ (0.1); $\text{MnCl}_2 \cdot 4\text{H}_2\text{O}$ (0.2); $\text{FeSO}_4 \cdot 7\text{H}_2\text{O}$ (0.005); Tween 80 (1 mL); hemin (0.00005). A sterile-filtered vitamin solution [21] was added to autoclaved and cooled down nutritive medium prior to use. The final concentration of vitamins in nutritive medium ($\mu\text{g/L}$) were: pyridoxine-HCl (Vit. B6) (100); 4-aminobenzoic acid (PABA) (50); nicotinic acid (Vit. B3) (50); biotine (20); folic acid (20); cyanocobalamin (5); thiamine (50); riboflavin (50); phylloquinone (0,075); menadione (10); pantothenate (100). Single compounds or plant extracts were added to 10 mL microbiota mixture, at a final concentration of 30 $\mu\text{g/mL}$ or 500 $\mu\text{g/mL}$, respectively. Microbiota-nutrient-compound mixtures were prepared under anaerobic conditions and filled into sterile serum flasks that were closed with sterile butyl rubber septa. Incubations were performed in the dark, at 37 °C, and shaking (100 rpm) for 24 h, and under strict anaerobic conditions. 1 mL sample was withdrawn before (T0h) and after 24 h (T24h) of incubation and stored at – 80 °C until extraction and UHPLC-MS/MS analysis. All the compounds were dissolved in DMSO to improve their solubility, but DMSO may inhibit microbial activity. Therefore, the impact of different levels of DMSO (0.25 %, 0.50 %, 0.75 % or 1.00 % (v/v)) on microbiota fermentation was assessed in a preliminary experiment. Based on this, the final DMSO content was set to 0.2 % or 0.5 % (v/v), for single compounds or plant extracts, respectively, because at these concentrations, DMSO showed low impact on SCFA production compared to DMSO-free incubations (Fig. S8). Moreover, for each experiment DMSO controls with 0 %, 0.2 % and 0.5 % DMSO were included. A 1 mL sample of microbial content was collected at the end of the experiment and SCFAs were quantified by HPLC with a refractive index (RI) detector. Moreover, to evaluate the impact of herbal compounds or extracts exposure on microbial metabolism, SCFAs quantification was performed for all incubation experiments. All incubation experiments were performed in triplicate with two artificial microbiota generated from two different healthy female adults. Additionally, study compounds were incubated under same conditions with microbial-free (sterilization through 0.20 μm filter) incubation mixture to assess degradation in abiotic conditions.

2.4.3. Fermentation metabolite quantification

The metabolites acetate, propionate, butyrate, isobutyrate, lactate, succinate, valerate, and isovalerate were quantified in collected fermentation samples. Therefore, an aliquot of 1 mL was centrifuged (13'000 cfm for 10 min at 4 °C) and the supernatant then filtered using an 0.2 μm nylon filter. The samples were analyzed by HPLC (LaChrom, Merck-Hitachi, Germany, or Accela, Thermo Fisher Scientific, Reinach, Switzerland) equipped with a Security Guard Cartridge Carbo-H (4 × 3.0 mm) and a Rezex ROA-Organic Acid H+ (300 × 7.8 mm) column (Phenomenex, Basel, Switzerland) and a refractive index detector (Thermo Fisher Scientific). The injection volume was 20 μL (Accela HPLC) or 40 μL (LaChrom HPLC). The mobile phase used was 10 mM

H₂SO₄ with a flow rate of 0.4 mL/min at 40 °C for 60 min per sample under isocratic conditions. The metabolites were quantified by external calibration.

2.4.4. Bacterial viability

Bacterial flow cytometry was used to determine the total viable and dead bacterial cell counts of microbiota incubated with control and test compounds. The assay is based on a bacterial cell staining with a live/dead staining that consists of two DNA-binding fluorescent stains: SYBR® Green I and propidium iodide (PI). The former penetrates all cells and results in a green fluorescence, the latter penetrates only cells with a damaged cell membrane resulting in red fluorescence. The amount of cells with intact (viable) and damaged (dead) membrane were determined in each sample with a flow cytometer (Cytomics FC 500, Beckman Coulter) equipped with a blue (488 nm) laser and bandpass filters on the FL-1 (525 nm) and FL-3 (620 nm SP) detectors for detection of green and red fluorescent cells, respectively. The method was based on previously validated protocols [22]. In short, freshly taken samples were diluted thousand-fold in sterile filtered (0.2 µm pore-size) reduced phosphate buffer solution. Incubation in the dark for 20 min was done with 30 µL of diluted sample mixed with 267 µL sterile filtered PBS and 3 µL of SYBRGreen I-propidium iodide solution (end concentration: 1 × SYBR® Green I and propidium iodide 4 µM). After incubation, 30 µL Flow-Count™ Fluorospheres beads with known concentration and different fluorescent color (FL-5 detector) were added to allow for absolute cell quantification. Data was acquired with CXP software and analyzed with Kaluza Analysis software (Beckman Coulter). Forward, side scatter and fluorescence plots were manually inspected for all stained samples and unstained controls. Cell concentrations were determined by gating on the FL-1 versus FL-3 plots to count the events corresponding to the SYBR® Green (viable) and SYBR® Green+PI (dead) labelled cells and by counting the events corresponding to the Flow-Count™ Fluorospheres counting beads. The collected cell concentrations were exported to Microsoft Excel and converted to cell count/mL, taking into account the sample dilution factor.

2.4.5. Microbiota sample extractions

Microbiota samples were thawed and directly processed by sequential liquid-liquid extractions with EtOAc and *n*-BuOH. Aliquots of 1 mL were extracted with 1 mL EtOAc and centrifuged (3000 rpm, 20 °C, 10 min). Then, the supernatant was collected and the residue further extracted with 1 mL EtOAc, followed by 1 mL *n*-BuOH. The extracts were combined, evaporated to dryness using a rotary evaporator (Buchi, Flawil, Switzerland) and stored at – 80 °C until analysis by UHPLC-MS/MS.

2.5. UHPLC-MS/MS analysis

2.5.1. Instrumentation and chromatographic conditions

Caco-2 and microbiota samples were analyzed by ultrahigh performance liquid chromatography (UHPLC) coupled to electrospray ionization (ESI) tandem mass spectrometry (MS/MS) in multiple reaction monitoring (MRM) mode and with the use of an internal standard (IS).

Valerenic acid, hypericin (both with IS digoxin) and citalopram (with IS citalopram-D₄) were analyzed on an Acquity UPLC® system (consisting of a binary solvent manager, a sample manager and a column heater) coupled to TQD triple quadrupole mass spectrometer (all Waters Corp., Milford, CT, USA). MS parameters for MRM methods were first optimized using the Waters Intellistart software and subsequently further optimized manually. The MS parameters are presented in Table S2. Hyperforin (with IS warfarin), diazepam (with IS diazepam-D₅), atenolol and propranolol (with IS verapamil), were analyzed on a 1290 Infinity UHPLC system (consisting of a binary pump G4220A, an autosampler G4226A and a thermostated column compartment G1316C) coupled to a 6460 triple quadrupole mass spectrometer (all Agilent, Waldbronn, Germany). MS parameters (MRM transitions, cone voltage and collision energy) for MRM methods were optimized using

the Agilent MassHunter program Optimizer (Table S3).

UHPLC parameters of all study compounds, such as gradient, flow rate, run time, eluents, column, injection volume, column temperature and autosampler temperature are presented in Table S4.

2.5.2. Sample preparation prior to UHPLC-MS/MS of Caco-2 samples

2.5.2.1. Sample preparation of valerenic acid, hypericin, diazepam and citalopram. To 200 µL of analyte in a mixture of HBSS and MeCN (1:1) were added 100 µL of methanol (containing the IS), 200 µL of 6 % BSA in water, and 800 µL of ice cold MeCN. The samples were mixed for 10 min at room temperature on an Eppendorf Thermomixer (1400 rpm) and finally centrifuged at 10 °C for 30 min at 3500 rpm (Centrifuge 5810 R, Eppendorf, Hamburg, Germany). An aliquot of 700 µL supernatant was collected and transferred into a 96-deepwell plate (96-DPW, Biotage, Uppsala, Sweden), and dried under nitrogen gas flow (Evaporex EVX-96, Apricot Designs, Covina, CA, USA). For valerenic acid and hypericin, samples were redissolved with 200 µL of a mixture of A (water with 0.1 % NH₄OH, pH 10.7) and B (MeCN mixed with A at a ratio 9:1) at a ratio 1:1. For diazepam, samples were redissolved with 200 µL of a mixture of water and MeCN (65:35), both containing 0.1 % of formic acid, or with 200 µL DMSO in case of citalopram. All samples were mixed for 30 min on an Eppendorf MixMate shaker prior to UHPLC-MS/MS analysis.

2.5.2.2. Sample preparation of hyperforin. To 60 µL of analyte in a mixture of HBSS and 10 % BSA in water (1:1) were added 180 µL of ice cold methanol containing the IS. The samples were mixed for 10 min at room temperature on an Eppendorf Thermomixer (1400 rpm), and then centrifuged at 10 °C for 20 min at 3500 rpm (Centrifuge 5810R). An aliquot of 100 µL supernatant was collected and transferred into an HPLC vial.

2.5.2.3. Sample preparation of atenolol and propranolol. To 200 µL of analyte in a mixture of HBSS and MeCN (1:1) were added 100 µL of 6 % BSA in water and 900 µL of ice cold MeCN (containing the IS). The samples were mixed for 10 min at room temperature on an Eppendorf Thermomixer (1400 rpm), and finally centrifuged at 10 °C for 30 min at 3500 rpm (Centrifuge 5810R). An aliquot of 800 µL supernatant was collected (300 µL for propranolol), transferred into a 96-deepwell plate (96-DPW, Biotage) and dried under nitrogen gas flow (Evaporex EVX-96). Samples were redissolved with 100 µL (atenolol) or 200 µL (propranolol) of a mixture of water and MeCN (65:35), both containing 0.1 % of formic acid, followed by 30 min of shaking on an Eppendorf MixMate.

2.5.3. Sample preparation of microbiota samples

Microbiota samples were extracted as described in Section 2.4.5. Microbiota dry samples obtained at T0h and T24h were reconstituted with DMSO (containing the corresponding internal standard) and analysed by UHPLC-MS/MS. Chromatographic and MS/MS conditions were as for Caco-2 sample analysis.

2.5.4. UHPLC-MS/MS quantification methods and acceptance criteria

UHPLC-MS/MS methods for absolute quantification of study compounds in Caco-2 samples consisted in the injection of 2 sets of 7 calibrator samples validated with 2 sets of 3 quality control (QC) samples from the low, middle and high level of the calibration curve. Calibrators, QC and Caco-2 samples were processed with the same sample preparation protocol, and prepared fresh before UHPLC-MS/MS analysis. To be accepted, a bioanalytical run was required to have a coefficient of determination (R²) higher than 0.96, with at least 75 % of all calibrators valid. Additionally, for the lower limit of quantification (LLOQ) and upper limit of quantification (ULOQ), only one value could be excluded. Furthermore, between bioanalytical runs, the imprecision (CV%) had to

be lower than 15 % (20 % at the LLOQ), and the inaccuracy (RE%) had to be within ± 15 % (± 20 % at the LLOQ). The above mentioned criteria were in accord with requirements of the US Food and Drug Administration (FDA) and the European Medicines Agency (EMA) for bioanalytical methods [23,24]. Calibration range was from 2 to 1000 ng/mL for valerianic acid, and from 2.5 to 250 ng/mL for hyperforin. Hypericin, diazepam and citalopram were analysed over the range 10–1000 ng/mL. The calibration range for propranolol and atenolol was from 10 to 2000 ng/mL. For very low concentrated samples of atenolol, an additional UHPLC-MS/MS method was developed in a lower range of 0.05–10 ng/mL. Calibration curves are provided as Figs. S9–S16, and curve parameters, calibrator and QC samples in Tables S5–S20. Additionally, carry-over values were determined to not exceed 20 % for the analyte, and 5 % for the internal standard (Table S21).

2.6. Data acquisition and statistical analysis

UHPLC-MS/MS data were acquired and processed using Agilent MassHunter version 10.0, or Waters MassLynx V4.1 software. Statistical analysis was performed and graphs drawn with GraphPad Prism 9.3.1.

3. Results and discussion

3.1. Permeability studies

In Caco-2 cell monolayer systems, atenolol and propranolol are widely used as representative markers of low-to-moderately and highly permeable compounds, whereby P_{appAB} values < 3.5 ($\times 10^{-6}$ cm/s) indicate low-to-moderately permeable, and values > 3.5 ($\times 10^{-6}$ cm/s) highly permeable compounds [25]. In the present study, atenolol mean P_{appAB} was 0.11×10^{-6} cm/s, and mean P_{appBA} was 0.14×10^{-6} cm/s, with a corresponding ER < 2 (Table 1). Propranolol mean P_{appAB} was 53.4×10^{-6} cm/s, and mean P_{appBA} was 121×10^{-6} cm/s, with a corresponding ER of 2.3 (Table 1). Thus, calculated P_{app} and ER values of the two compounds were in accordance with previously published data [26,27] and confirmed the validity of the experimental setup.

Diazepam and citalopram are frequently prescribed anxiolytic and antidepressant drugs and were included in our study as synthetic reference drugs. Diazepam showed a mean P_{appAB} of 180×10^{-6} cm/s (Table 1) and thus was classified as a highly permeable compound. The P_{appBA} was 168×10^{-6} cm/s and the calculated ER was 0.9 (< 2). This suggests that diazepam was undergoing a passive transport across the Caco-2 monolayer (Table 1). Our findings were in accord with previously published data [28]. The mean P_{appAB} of citalopram was 47.8×10^{-6} cm/s (Table 1), the mean P_{appBA} 133×10^{-6} cm/s, and the ER was 2.8 (Table 1). In AB direction, the Re_{AB} was 37.8 %, and Re_{ABC} was 56.9 % (Table 1). In BA direction, the Re_{AB} was 33.5 %, and Re_{ABC} was 41.7 % (Table 1). The calculated ER of 2.8 suggested a possible efflux transport [15]. In a previous study [7], an ER of 0.7 was determined for citalopram, suggesting a passive transport. However, these

experiments were conducted with transport buffers at pH 7.4 in both chambers. In contrast, we used buffers with pH 6.5 in the apical chamber and with pH 7.4 in the basolateral compartment to mimic the physiological pH in the small intestine and the circulation. Calculated physicochemical properties of citalopram (Table S22) indicated that at pH 6.5 a higher fraction of citalopram would be found in charged form, which in turn would decrease its permeability [27]. An efflux of citalopram at the intestinal epithelium may be involved, given that in vitro and in vivo studies in mice have shown that citalopram was a P-glycoprotein (P-gp) substrate at the blood-brain-barrier [29]. Transport studies in Caco-2 cells with carrier-protein inhibitors will be needed to clarify this point. The low recoveries of 56.9 % and 41.7 % (Table 1) suggested that citalopram may be metabolized. Caco-2 cells express low levels of phase I metabolizing enzymes, while phase II enzymes such as UDP-glucuronosyltransferases (UGTs), sulfotransferases (SULTs) and glutathione S-transferases (GSTs) are highly expressed [30]. Hepatic phase II metabolism of citalopram has not been reported, but glucuronide conjugates have been detected in human urine samples, thereby supporting a possible extrahepatic glucuronidation of the drug [31]. Additional experiments will be required to understand a possible metabolism of citalopram at the intestinal level.

The mean P_{appAB} for valerianic acid was 199×10^{-6} cm/s, the mean P_{appBA} was 60.4×10^{-6} cm/s, and the calculated ER was 0.3 (Table 1). Re_{AB} and Re_{ABC} were 34.1 % and 42.7 % in AB direction, and 63.2 % and 69.2 % in BA direction, respectively (Table 1). The P_{appAB} value of 199×10^{-6} cm/s classified valerianic acid as a highly permeable compound. This was in accordance with previously published pharmacokinetic data in rats and in volunteers [32]. The ER value of 0.3 suggested that an active transport could be involved in the transfer (Table 1) [15]. In isolated perfused rat livers, the biliary excretion of valerianic acid is mediated by the multidrug resistance-associated protein (MRP) 2, a transporter expressed in the canalicular membrane of hepatocytes [33]. In Caco-2 cells, MRP2 (located apically) is among the most highly expressed ATP-binding cassette transporters [30]. An active uptake process of valerianic acid needs to be corroborated by experiments utilizing specific carrier-protein inhibitors. The calculated recovery suggests a possible metabolization of valerianic acid in Caco-2 cells. This is supported by data from isolated perfused rat livers, where several glucuronides of valerianic acid, hydroxyvalerianic acid, and dehydrohydroxyvalerianic acid were found [33], and similar findings with pooled human liver microsomes (Manuscript in preparation).

The mean P_{appAB} of hyperforin was 4.76×10^{-6} cm/s, the mean P_{appBA} 6.38×10^{-6} cm/s, and the calculated ER was 1.3 (Table 1). In AB and BA directions, hyperforin Re_{AB} was 52.5 % and 79.0 %, respectively. In both direction, no hyperforin was found in the cell fraction (values below LOQ). The P_{appAB} indicated that hyperforin was highly permeable (Table 1). This finding was in accordance with published pharmacokinetic data obtained in volunteers treated with St. John's wort extract [34]. The ER value suggested a passive transport of hyperforin (Table 1). The low recovery at first pointed at a possible

Table 1

Permeability data from Caco-2 transwell experiments. Data are presented as mean \pm S.D. (n = 3).

Compounds	AB direction			BA direction			ER ^c
	P_{appAB} ($\times 10^{-6}$ cm/s)	Re_{AB} ^a (%)	Re_{ABC} ^b (%)	P_{appBA} ($\times 10^{-6}$ cm/s)	Re_{AB} ^a (%)	Re_{ABC} ^b (%)	
Valerianic acid	199 \pm 27	34.1 \pm 13.1	42.7	60.4 \pm 2.0	63.2 \pm 8.3	69.2	0.3
Hyperforin	4.76 \pm 0.21	52.5 \pm 17.3	52.5	6.38 \pm 0.18	79.0 \pm 13.0	79.0	1.3
Hypericin	0.48 \pm 0.05	78.1 \pm 5.4	83.4	0.39 \pm 0.03	118 \pm 3	120	1.2
Diazepam	180 \pm 5	121 \pm 3	126	168 \pm 12	46.3 \pm 30.9	51.5	0.9
Citalopram	47.8 \pm 3.3	37.8 \pm 4.4	56.9	133 \pm 3	33.5 \pm 17.4	41.7	2.8
Atenolol	0.11 \pm 0.03	88.7 \pm 6.3	92.8	0.14 \pm 0.02	118 \pm 22	118	1.3
Propranolol	53.4 \pm 5.3	39.5 \pm 1.1	58.1	121 \pm 4	61.8 \pm 5.2	69.8	2.3

^a Recovery considering apical and basolateral compartments.

^b Recovery considering apical and basolateral compartments, and cell fraction.

^c Efflux ratio.

metabolization of hyperforin in Caco-2 cells. However, control experiments in both AB and BA directions with cell-free inserts indicated a low passage of the compound (Fig. S17). Indeed, the high lipophilicity of hyperforin ($\text{clogD}_{\text{pH}6.5}$ and $\text{clogD}_{\text{pH}7.4}$ of 8.2 and 7.4, respectively, Table S22) renders the compound prone to non-specific adsorption on the polymer surface of the inserts. A possible metabolism of hyperforin in Caco-2 cells requires further studies.

The mean P_{appAB} of hypericin was 0.48×10^{-6} cm/s, the mean P_{appBA} was 0.39×10^{-6} cm/s (Table 1), and the calculated ER was of 0.8. Re_{AB} values in AB direction and BA direction were of 78.1 %, and of 118 %, respectively (Table 1). Re_{ABC} values in AB direction and BA direction were of 83.4 %, and of 120 %, respectively (Table 1). The P_{appAB} classified hypericin as a low-to-moderately permeable compound. The ER value suggested that hypericin underwent a passive transport. This was in accordance with previously published permeability studies with Caco-2 monolayers [6,8]. Various studies in healthy volunteers ingesting St. John's wort extract reported a slow increase and decrease of the hypericin plasma concentrations, and long mean lag-time [34]. Together with our data, this suggests that only a portion of hypericin is absorbed in the small intestine upon oral administration of St. John's wort extract. The remainder could reach the colon where interactions with the gut microbiota may occur.

The results of permeability studies with the Caco-2 model should be interpreted in the context of the following limitations. When recovery values (Re_{AB}) are below 80 %, the calculated P_{app} values are thought to be slightly underestimated and should, therefore, be considered only as a qualitative readout [15]. This was the case with propranolol, citalopram, valerenic acid and hyperforin. In transwell experiments with lipophilic compounds, BSA is used in the transport media to increase solubility and limit non-specific adsorption to surfaces [15]. Hyperforin and hypericin are known to strongly bind to plasma proteins [35,36]. In

preliminary experiments with cell-free inserts, an acceptable equilibrium between apical and basolateral compartments was reached with the two compounds only in the presence of 10 % BSA (Fig. S17). While such high BSA concentrations allow for higher recovery on the one side, they lead to an underestimation of P_{app} values on the other [15].

3.2. Stability of compounds during in vitro gut microbiota fermentation

Valerenic acid, hyperforin, hypericin, diazepam and citalopram were incubated with fresh and metabolically active artificial human colon microbiota from the PolyFermS model supplemented with 30 % nutritive medium to assess the microbial biotransformation capacity under conditions of limited growth. The two studied microbiota originated from two different healthy adult female fecal donors. The compounds were stable in abiotic incubation (microbe-free PolyFermS effluent with 30% nutritive medium buffered at pH 6.5) over 24 h (Fig. 2). No marked differences were found between abiotic and microbiota incubations, suggesting that no microbiota-mediated transformation of the compounds occurred.

Upon ingestion, drugs transit through the gastrointestinal tract and are absorbed in the small intestine. The permeability experiments in the Caco-2 model suggested that hyperforin, diazepam and citalopram are well absorbed in the small intestine. Assuming that a very limited fraction could still bypass the intestinal absorption, our results suggest that no biotransformation mediated by the microbiota is to be expected. Hypericin was classified as being low-to-moderately permeable and, hence, could potentially be found at relevant concentrations in the human colon. Our results indicate that no biotransformation of hypericin is to be expected in the colon. Valerenic acid, in contrast, was highly permeable in the Caco-2 model. However, in vivo data in rats suggest that valerenic acid undergoes enterohepatic circulation.

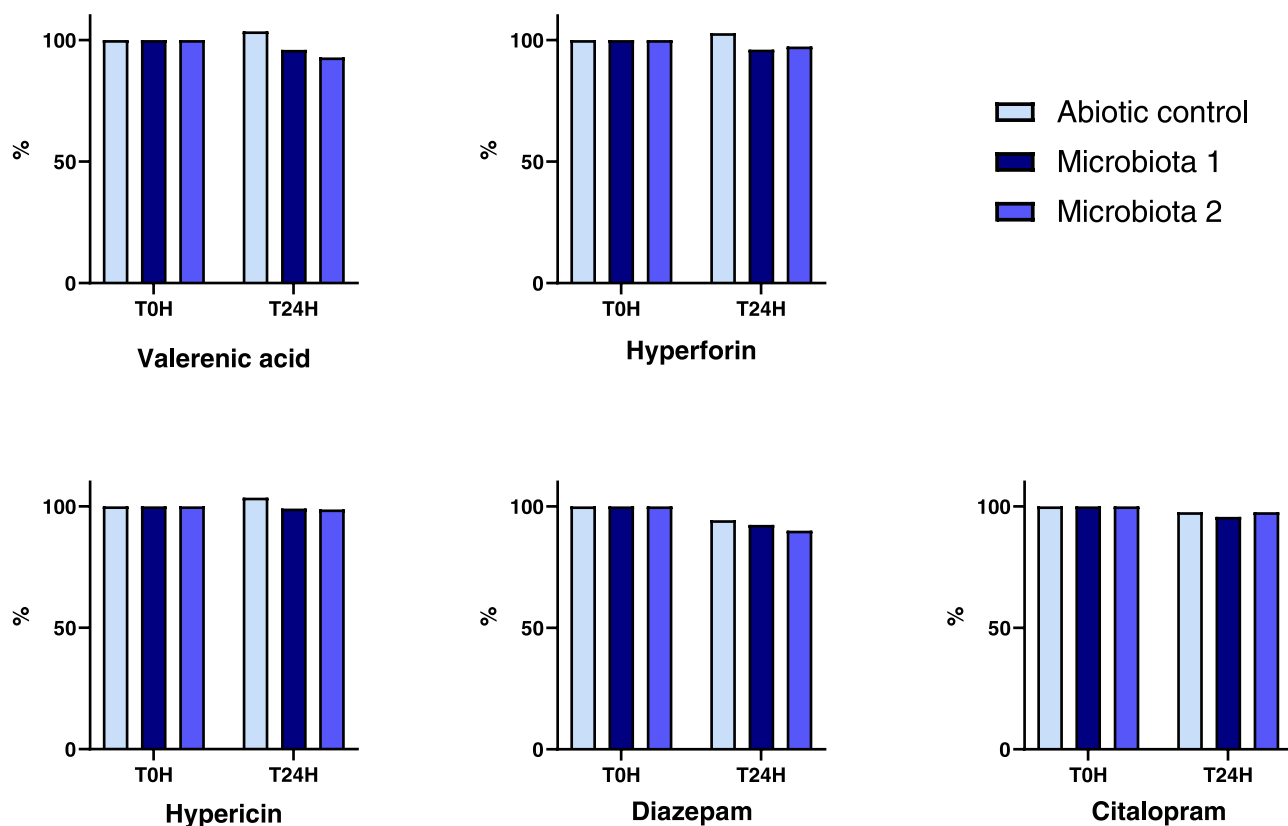


Fig. 2. Stability of compounds after 24 h incubation in inactivated PolyFermS microbiota, and in viable PolyFermS microbiota of donors 1 and 2 supplemented with 30 % nutritive medium. All incubations contained 20 μL DMSO. Mean concentration values ($n = 2$) are normalized to 100 %. The two replicate values are presented in Table S23.

Glucuronidation and biliary excretion of the compound has been reported [33], and the pharmacokinetic profile corresponded to that typically observed in enterohepatic recycling [32]. Whether enterohepatic circulation also occurs in humans deserves further investigations.

3.3. Impact of compounds or plant extracts exposure on microbiota activity and viability

Upon fermentation of undigested polysaccharides, healthy microbiota produce SCFA, with acetate, propionate and butyrate as main compounds [18,37]. The fermentation metabolic capacity of the tested microbiota during incubation was confirmed by the comparable SCFA

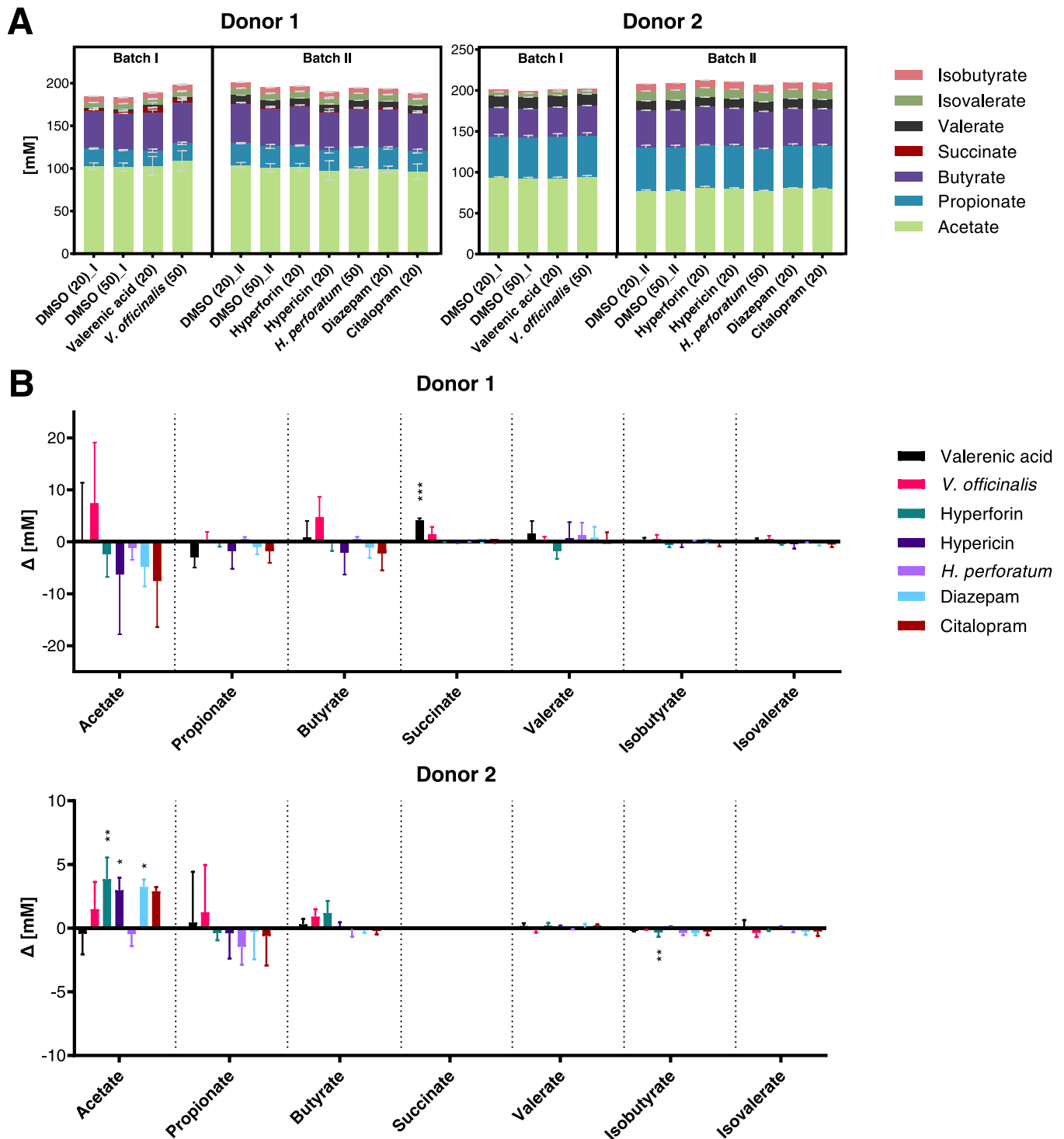


Fig. 3. (A) Fermentation metabolite concentrations after 24 h incubation of PolyFermS microbiota of donors 1 and 2, respectively. Incubations were supplemented with 30 % nutritive medium and DMSO, with or without test compounds or herbal extracts. Two independent experiments (batch I and batch II) were performed for each microbiota. Averages \pm stdev (n = 3). (B) Delta of fermentation metabolite concentration in compound versus DMSO control fermentation after 24 h. Averages \pm stdev (n = 3). Asterisks indicate significant differences in average metabolite concentration between compound fermentation and respective DMSO control analyzed by one-way ANOVA.

production in control samples with and without DMSO (Fig. S18). Microbiota of donor 1 was characterized as butyrogenic (producing more butyrate) while microbiota of donor 2 was characterized as propiogenic (producing more propionate). They represented therefore two distinct but prevalent human adult colon microbiota types (Fig. 3). In both microbiota, neither compounds nor herbal extracts significantly impacted the total SCFA levels (Fig. 3A). Acetate, propionate and butyrate were the most abundant SCFA, with higher levels of butyrate for the microbiota from donor 1, and higher levels of propionate for the microbiota from donor 2 (Fig. 3A). In the microbiota from donor 1, succinate production markedly increased in presence of valerianic acid when compared to the control incubation (Fig. 3B). In the microbiota from donor 2, acetate production slightly increased in presence of hyperforin, hypericin and diazepam when compared to the control incubation (Fig. 3B). However, the average increase in acetate concentration with hyperforin, hypericin and diazepam (3.8, 3.0 and 3.2 mM) was low compared to the average acetate concentration (81, 80.1 and 80.4 mM). Amounts of isobutyrate slightly decreased (-0.34 mM) in the presence of hyperforin (Fig. 3B). Hence the exposure of compounds or extracts had an overall minimal impact on SCFA production in both microbiota.

To assess the impact of compounds and extracts on bacterial viability during exposure, the total concentration of viable and dead bacteria in the microbiota were quantified after 24 h of incubation with live/dead flow cytometry. Compared to the respective controls, no antimicrobial effect was observed in both PolyFermS microbiota for valerian and St. John's wort extracts, and for valerianic acid, hyperforin, hypericin, diazepam and citalopram (Fig. 4). For a few compounds and extracts (hyperforin, hypericin, citalopram in the microbiota 1, and valerian extract, valerianic acid, and hyperforin in the microbiota 2) there was an increased level of bacteria compared to the control, which may indicate that they promoted growth.

Our findings suggest that exposure of valerianic acid, hyperforin, hypericin, diazepam, citalopram, and valerian and St. John's wort extracts does not affect the balance of microbial SCFAs metabolism and has minimal impact on bacterial viability at the tested concentrations (30 $\mu\text{g}/\text{mL}$ for compounds, and 500 $\mu\text{g}/\text{mL}$ for herbal extracts). One cannot, however, exclude that higher concentrations in the batch fermentation assays would affect viability and SCFA production. Batch experiments mimic a single intake and are suited for assessing the biotransformation capacity, but not the effects of long-term exposure for which continuous fermentation experiments are required. Considering the maximum recommended daily oral intake of valerian or St. John's wort extracts (1800 mg and 1000 mg, respectively) [2,38], the

concentration of test compounds in commercial valerian and St. John's wort extracts [39,40], an average volume of 200 mL of the proximal colon [41], assuming stability of compounds and lacking absorption in the upper compartments of the gastrointestinal tract, and a colonic retention time of 8 h [18,42] resulting in 600 mL proximal colon suspension per day, the calculated concentrations of valerianic acid, hyperforin and hypericin in the colon would be in the range of 0.03–21, 0.3–27, and 1.3–3.5 $\mu\text{g}/\text{mL}$, respectively. Based on daily prescribed doses [4,5], calculated colonic concentrations of diazepam and citalopram would be in the range of 3.3–17 and 17–67 $\mu\text{g}/\text{mL}$, respectively. Thus, the test concentrations used in our study were within theoretical colonic concentrations assuming homogenous dispersion of the ingested compound in the proximal colon, except for citalopram where they were up to 2.2-fold lower. However, citalopram is well absorbed in the small intestine and thus does not reach the colon. As for the valerian and St. John's wort extracts, intake of the maximum recommended daily dose would lead to colonic concentrations of 3 or 1.7 mg/mL, respectively, assuming that no absorption occurs in the small intestine. This would correspond to concentrations that are 3–6-fold higher than those used in our microbiota fermentations.

4. Conclusions

The intestinal permeability of valerianic acid, hyperforin, hypericin, diazepam and citalopram was evaluated with the Caco-2 cell model. Calculated P_{app} values showed that valerianic acid, hyperforin, diazepam and citalopram were highly permeable, while hypericin was in the range of low-to-moderately permeable compounds. Calculated efflux ratios indicated a passive transport of hyperforin, hypericin and diazepam. In contrast, valerianic acid and citalopram were likely transported via a carrier-mediated process, and also possibly metabolized. Inhibition studies need to be conducted with relevant transporters to investigate whether the observed fluxes are pH dependent or due to carrier-mediated transport. Additionally, identification of potential metabolites is needed.

Biotransformation of valerianic acid, hyperforin, hypericin, diazepam and citalopram was assessed with PolyFermS microbiota from two different healthy female fecal donors. Herbal and synthetic compounds were stable, suggesting that there is probably no biotransformation taking place in the human colon.

Using the same model, the impact of compounds, and valerian and St. John's wort extracts on microbial SCFAs production and bacterial viability was investigated. Compounds and extracts neither significantly modulated SCFA production of microbiota nor impaired bacterial

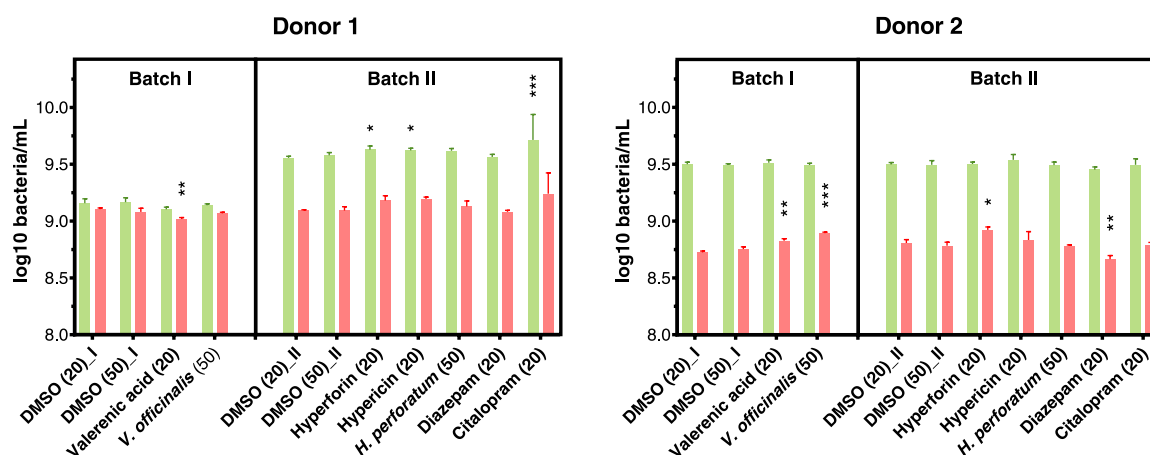


Fig. 4. Concentration of viable (green) and dead (red) bacteria after 24 h incubation in PolyfermS microbiota of donors 1 or 2. Microbiota were supplemented with 30 % nutritive medium and DMSO, with or without single compounds or herbal extracts. Two independent experiments (batch I and batch II) were performed for each microbiota. Averages on $\log_{10} \pm \text{stdev}$ ($n = 3$). Asterisks indicate significant differences in average \log_{10} bacterial concentration between compound fermentation and respective DMSO control fermentation analyzed by one-way ANOVA.

viability. They may thus not exert an indirect effect, at least in short-term exposure, on the central nervous system by modulating bacterial signaling via the gut-brain axis. However, considering the important interindividual variability of gut microbiota, studies with a larger number of individual PolyFermS microbiota, continuous fermentations, and/or validation in human studies are warranted.

CRedit authorship contribution statement

Antoine Chauveau: Conceptualization, Methodology, Validation, Investigation, Writing – original draft. **Andrea Treyer:** Conceptualization, Methodology, Validation, Investigation, Writing – review & editing, Supervision. **Annelies Geirnaert:** Conceptualization, Methodology, Validation, Investigation, Writing – review & editing, Supervision. **Lea Bircher:** Investigation. **Angela Babst:** Investigation. **Vanessa Fabienne Abegg:** Investigation. **Ana Paula Simões-Wüst:** Conceptualization, Project administration, Funding acquisition. **Christophe Lacroix:** Conceptualization, Methodology, Validation, Supervision, Project administration, Funding acquisition. **Olivier Potterat:** Conceptualization, Methodology, Validation, Formal analysis, Resources, Writing – review & editing, Supervision, Project administration, Funding acquisition. **Matthias Hamburger:** Conceptualization, Methodology, Validation, Formal analysis, Resources, Writing – review & editing, Supervision, Project administration, Funding acquisition.

Declaration of Competing Interest

The authors declare no competing interests.

Data Availability

Data will be made available on request.

Acknowledgments

This work was supported by the Swiss National Science Foundation [CRSII5_177260; Herbal Safety in Pregnancy]. We would like to acknowledge Alfonso Die, Laboratory of Food Technology, ETH Zurich, for HPLC-RI analysis.

Appendix A. Supporting information

Supplementary data associated with this article can be found in the online version at doi:10.1016/j.biopha.2023.114652.

References

- G. Gantner, D. Spiess, E. Randecker, K.C. Quack Lötscher, A.P. Simões-Wüst, Use of herbal medicines for the treatment of mild mental disorders and/or symptoms during pregnancy: a cross-sectional survey, *Front. Pharm.* 12 (2021), 729724, <https://doi.org/10.3389/fphar.2021.729724>.
- EMA/HMPC, Final European Union herbal monograph on *Valeriana officinalis* L., radix, 2016. (<https://www.ema.europa.eu/en/medicines/herbal/valeriana-radi-x>), (Accessed 12 September 2022).
- M. Schmidt, V. Butterweck, The mechanisms of action of St. John's wort: an update, *Wien. Med. Wochenschr.* 165 (2015) 229–235, <https://doi.org/10.1007/s10354-015-0372-7>.
- FDA, Valium brand of diazepam tablets, 2016. (https://www.accessdata.fda.gov/drugsatfda_docs/label/2016/013263s094lbl.pdf), (Accessed 27 September 2022).
- FDA, Celexa (citalopram hydrobromide) tablets, 2017. (https://www.accessdata.fda.gov/drugsatfda_docs/label/2017/020822s047lbl.pdf), (Accessed 27 September 2022).
- K. Forsch, B. Siewert, J. Drewe, G. Fricker, L. Disch, Sustained release for St. John's wort: a rational idea? *J. Bioequiv. Availab.* 09 (2017) 565–576, <https://doi.org/10.4172/jbb.1000363>.
- E. Sevin, L. Dehouck, A. Fabulas-da Costa, R. Cecchelli, M.P. Dehouck, S. Lundquist, M. Culot, Accelerated Caco-2 cell permeability model for drug discovery, *J. Pharm. Toxicol. Methods* 68 (2013) 334–339, <https://doi.org/10.1016/j.vascn.2013.07.004>.
- S. Verjee, D. Brügger, H. Abdel-Aziz, V. Butterweck, Permeation characteristics of hypericin across Caco-2 monolayers in the absence or presence of quercitrin – a mass balance study, *Planta Med.* 81 (2015) 1111–1120, <https://doi.org/10.1055/s-0035-1546034>.
- G. Clarke, K.V. Sandhu, B.T. Griffin, T.G. Dinan, J.F. Cryan, N.P. Hyland, Gut reactions: breaking down xenobiotic-microbiome interactions, *Pharm. Rev.* 71 (2019) 198–224, <https://doi.org/10.1124/pr.118.015768>.
- A. Ramirez García, J. Zhang, A. Greppi, F. Constancias, E. Wortmann, M. Wandres, K. Hurley, A. Pascual-García, H.-J. Ruscheweyh, S.J. Sturla, C. Lacroix, C. Schwab, Impact of manipulation of glycerol/diol dehydratase activity on intestinal microbiota ecology and metabolism, *Environ. Microbiol.* 23 (2021) 1765–1779, <https://doi.org/10.1111/1462-2920.15431>.
- J. Isenring, L. Bircher, A. Geirnaert, C. Lacroix, In vitro human gut microbiota fermentation models: opportunities, challenges, and pitfalls, *Microbiome Res. Rep.* 2 (2023) 2, <https://doi.org/10.20517/mrr.2022.15>.
- T. Demuth, V. Edwards, L. Bircher, C. Lacroix, L. Nyström, A. Geirnaert, In vitro colon fermentation of soluble arabinoxylan is modified through milling and extrusion, *Front. Nutr.* 8 (2021), 707763, <https://doi.org/10.3389/fnut.2021.707763>.
- M.I. Fekry, C. Engels, J. Zhang, C. Schwab, C. Lacroix, S.J. Sturla, C. Chassard, The strict anaerobic gut microbe *Eubacterium hallii* transforms the carcinogenic dietary heterocyclic amine 2-amino-1-methyl-6-phenylimidazo[4,5-b]pyridine (PhIP), *Environ. Microbiol. Rep.* 8 (2016) 201–209, <https://doi.org/10.1111/1758-2229.12369>.
- R.N. Carmody, P.J. Turnbaugh, Host-microbial interactions in the metabolism of therapeutic and diet-derived xenobiotics, *J. Clin. Invest.* 124 (2014) 4173–4181, <https://doi.org/10.1172/JCI72335>.
- I. Hubatsch, E.G.E. Ragnarsson, P. Artursson, Determination of drug permeability and prediction of drug absorption in Caco-2 monolayers, *Nat. Protoc.* 2 (2007) 2111–2119, <https://doi.org/10.1038/nprot.2007.303>.
- D. Spiess, M. Winker, A. Chauveau, V.F. Abegg, O. Potterat, M. Hamburger, C. Gründemann, A.P. Simões-Wüst, Medicinal plants for the treatment of mental diseases in pregnancy: an in vitro safety assessment, *Planta Med.* 88 (2021) 1036–1046, <https://doi.org/10.1055/a-1628-8132>.
- K. Cattoor, M. Bracke, D. Deforce, D. De Keukeleire, A. Heyerick, Transport of hop bitter acids across intestinal Caco-2 cell monolayers, *J. Agric. Food Chem.* 58 (2010) 4132–4140, <https://doi.org/10.1021/jf904079h>.
- S.A. Poeker, A. Geirnaert, L. Berchtold, A. Greppi, L. Krych, R.E. Steinert, T. de Wouters, C. Lacroix, Understanding the prebiotic potential of different dietary fibers using an in vitro continuous adult fermentation model (PolyFermS), *Sci. Rep.* 8 (2018) 4318, <https://doi.org/10.1038/s41598-018-22438-y>.
- J. Isenring, A. Geirnaert, A.R. Hall, C. Jans, C. Lacroix, M.J.A. Stevens, In vitro gut modeling as a tool for adaptive evolutionary engineering of *Lactiplantibacillus plantarum*, *MSystems* 6 (2021) e01085–20, <https://doi.org/10.1128/mSystems.01085-20>.
- G.T. Macfarlane, S. Macfarlane, G.R. Gibson, Validation of a three-stage compound continuous culture system for investigating the effect of retention time on the ecology and metabolism of bacteria in the human colon, *Microb. Ecol.* 35 (1998) 180–187, <https://doi.org/10.1007/s002489900072>.
- C. Michel, T.P. Kravtchenko, A. David, S. Gueneau, F. Kozłowski, C. Cherbut, In vitro prebiotic effects of Acacia gums onto the human intestinal microbiota depends on both botanical origin and environmental pH, *Anaerobe* 4 (1998) 257–266, <https://doi.org/10.1006/anae.1998.0178>.
- S. Van Nevel, S. Koetzsch, H.-U. Weilenmann, N. Boon, F. Hammes, Routine bacterial analysis with automated flow cytometry, *J. Microbiol. Methods* 94 (2013) 73–76, <https://doi.org/10.1016/j.mimet.2013.05.007>.
- FDA, Bioanalytical method validation guidance for industry, 2018. (<https://www.fda.gov/regulatory-information/search-fda-guidance-documents/bioanalytical-method-validation-guidance-industry>), (Accessed 9 August 2022).
- EMA, Guideline on bioanalytical method validation, 2015. (https://www.ema.europa.eu/en/documents/scientific-guideline/guideline-bioanalytical-method-validation_en.pdf), (Accessed 9 August 2022).
- C.A.S. Bergström, M. Strafford, L. Lazorova, A. Avdeef, K. Luthman, P. Artursson, Absorption classification of oral drugs based on molecular surface properties, *J. Med. Chem.* 46 (2003) 558–570, <https://doi.org/10.1021/jm020986i>.
- S. Neuhoff, A.-L. Ungell, I. Zamora, P. Artursson, pH-dependent bidirectional transport of weakly basic drugs across Caco-2 monolayers: implications for drug–drug interactions, *Pharm. Res.* 20 (2003) 1141–1148, <https://doi.org/10.1023/A:1025032511040>.
- Y. Zheng, L.Z. Benet, H. Okochi, X. Chen, pH dependent but not P-gp dependent bidirectional transport study of S-propranolol: the importance of passive diffusion, *Pharm. Res.* 32 (2015) 2516–2526, <https://doi.org/10.1007/s11095-015-1640-3>.
- P. Garberg, M. Ball, N. Borg, R. Cecchelli, L. Fenart, R.D. Hurst, T. Lindmark, A. Mabondzo, J.E. Nilsson, T.J. Raub, D. Stanimirovic, T. Terasaki, J.-O. Öberg, T. Österberg, In vitro models for the blood–brain barrier, *Toxicol. Vitro* 19 (2005) 299–334, <https://doi.org/10.1016/j.tiv.2004.06.011>.
- M. Uhr, A. Tontsch, C. Namendorf, S. Ripke, S. Lucae, M. Ising, T. Dose, M. Ebinger, M. Rosenhagen, M. Kohli, S. Kloiber, D. Salyakina, T. Bettecken, M. Specht, Polymorphisms in the drug transporter gene ABCB1 predict antidepressant treatment response in depression, *Neuron* 57 (2008) 203–209, <https://doi.org/10.1016/j.neuron.2007.11.017>.
- M. Ölander, J.R. Wisniewski, P. Matsson, P. Lundquist, P. Artursson, The proteome of filter-grown Caco-2 cells with a focus on proteins involved in drug disposition, *J. Pharm. Sci.* 105 (2016) 817–827, <https://doi.org/10.1016/j.xphs.2015.10.030>.
- L. Dalgaard, C. Larsen, Metabolism and excretion of citalopram in man: identification of O-acetyl- and N-glucuronides, *Xenobiotica* 29 (1999) 1033–1041, <https://doi.org/10.1080/004982599238092>.

- [32] C. Sampath, K. Haug, S. Thanei, M. Hamburger, H. Derendorf, R. Frye, V. Butterweck, Pharmacokinetics of valerianic acid in rats after intravenous and oral administrations, *Planta Med.* 78 (2012) 575–581, <https://doi.org/10.1055/s-0031-1298301>.
- [33] A. Maier-Salamon, G. Trauner, R. Hiltcher, G. Reznicek, B. Kopp, T. Thalhammer, W. Jäger, Hepatic metabolism and biliary excretion of valerianic acid in isolated perfused rat livers: role of Mrp2 (Abcc2), *J. Pharm. Sci.* 98 (2009) 3839–3849, <https://doi.org/10.1002/jps.21671>.
- [34] H.-U. Schulz, M. Schürer, D. Bässler, D. Weiser, Investigation of pharmacokinetic data of hypericin, pseudohypericin, hyperforin and the flavonoids quercetin and isorhamnetin revealed from single and multiple oral dose studies with a *Hypericum* extract containing tablet in healthy male volunteers, *Arzneimittelforschung* 55 (2005) 561–568, <https://doi.org/10.1055/s-0031-1296905>.
- [35] V. Senthil, J.W. Longworth, C.A. Ghiron, L.I. Grossweiner, Photosensitization of aqueous model systems by hypericin, *Biochim. Biophys. Acta Gen. Subj.* 1115 (1992) 192–200, [https://doi.org/10.1016/0304-4165\(92\)90053-W](https://doi.org/10.1016/0304-4165(92)90053-W).
- [36] L. Verotta, E. Lovaglio, O. Sterner, G. Appendino, E. Bombardelli, Modulation of chemoselectivity by protein additives. Remarkable effects in the oxidation of hyperforin, *J. Org. Chem.* 69 (2004) 7869–7874, <https://doi.org/10.1021/jo048857s>.
- [37] A. Zihler Berner, S. Fuentes, A. Dostal, A.N. Payne, P. Vazquez Gutierrez, C. Chassard, F. Grattepanche, W.M. de Vos, C. Lacroix, Novel polyfermentor intestinal model (PolyFermS) for controlled ecological studies: validation and effect of pH, *PLoS One* 8 (2013), e77772, <https://doi.org/10.1371/journal.pone.0077772>.
- [38] EMA/HMPC, Community herbal monograph on *Hypericum perforatum* L., herba, 2009. (<https://www.ema.europa.eu/en/medicines/herbal/hyperici-herba>), (Accessed 13 September 2022).
- [39] A.M. Schäfer, O. Potterat, I. Seibert, O. Fertig, H.E. Meyer zu Schwabedissen, Hyperforin-induced activation of the pregnane X receptor is influenced by the organic anion-transporting polypeptide 2B1, *Mol. Pharm.* 95 (2019) 313–323, <https://doi.org/10.1124/mol.118.114066>.
- [40] M. Winker, A. Chauveau, M. Smieško, A. Areesanan, O. Potterat, A. Zimmermann-Klemd, C. Gründemann, Immunological evaluation of herbal extracts commonly used for treatment of mental diseases during pregnancy, *Sci. Rep.* (2023) (In preparation).
- [41] S.E. Pritchard, L. Marciani, K.C. Garsed, C.L. Hoad, W. Thongborisute, E. Roberts, P.A. Gowland, R.C. Spiller, Fasting and postprandial volumes of the undisturbed colon: normal values and changes in diarrhea-predominant irritable bowel syndrome measured using serial MRI, *Neurogastroenterol. Motil.* 26 (2014) 124–130, <https://doi.org/10.1111/nmo.12243>.
- [42] E.R. Kim, P.-L. Rhee, How to interpret a functional or motility test – colon transit study, *J. Neurogastroenterol. Motil.* 18 (2012) 94–99, <https://doi.org/10.5056/jnm.2012.18.1.94>.

3.2 Alkaloids in commercial preparations of California poppy – Quantification, intestinal permeability and microbiota interactions

Antoine Chauveau, Annelies Geirnaert, Angela Babst, Andrea Treyer, Christophe Lacroix, Matthias Hamburger, Olivier Potterat

Biomedicine & Pharmacotherapy, 2023, 166, 115420

doi: 10.1016/j.biopha.2023.115420

Abstract

California poppy products are commonly used for the treatment of nervousness, anxiety and sleeping disorders. Pharmacologically relevant constituents include the main alkaloids californidine, escholtzine and protopine. However, only limited information is available about the alkaloid content in commercial preparations and their intestinal absorption. Moreover, a possible metabolization of these alkaloids by the gut microbiota, and their impact on microbial activity and viability have not been investigated. Californidine, escholtzine and protopine were quantified by UHPLC-MS/MS in eight commercial California poppy products. The intestinal permeability of alkaloids was studied in Caco-2 cell as a model for absorption in the small intestine. The gut microbial biotransformation was explored in artificial gut microbiota from the in vitro PolyFermS model. In addition, the impact of these alkaloids and a California poppy extract on the microbial production of short-chain fatty acids (SCFAs) and the viability of microbiota was investigated. Contents of californidine, escholtzine and protopine in California poppy products were in the ranges of 0.13 – 2.55, 0.05 – 0.63 and 0.008 – 0.200 mg/g, respectively. In the Caco-2 cell model, californidine was low-to-moderately permeable while escholtzine and protopine were highly permeable. An active transport process was potentially involved in the transfer of the three alkaloids. The three compounds were not metabolized by the artificial gut microbiota over 24 h. Neither the California poppy extract nor the alkaloids markedly impacted microbial SCFA production and bacterial viability.

The supporting information is available in the appendix (pages 101 – 110), or at:

<https://doi.org/10.1016/j.biopha.2023.115420>

My contribution to this publication: Caco-2 cell culture; permeability experiments; sample extraction and analysis (UHPLC/MS-MS) of Caco-2, commercial plant products and microbiota samples; UHPLC/MS-MS method development and validation for compounds californidine, escholtzine, protopine, atenolol and propranolol; writing of the manuscript draft and preparation of figures and tables.



Alkaloids in commercial preparations of California poppy – Quantification, intestinal permeability and microbiota interactions

Antoine Chauveau^a, Annelies Geirnaert^b, Angela Babst^b, Andrea Treyer^a, Christophe Lacroix^b, Matthias Hamburger^{a,*}, Olivier Potterat^{a,*}

^a Division of Pharmaceutical Biology, Department of Pharmaceutical Sciences, University of Basel, Basel, Switzerland

^b Laboratory of Food Biotechnology, Institute of Food, Nutrition and Health, Department of Health Science and Technology, ETH Zurich, Zurich, Switzerland

ARTICLE INFO

Keywords:

Californidine

Escholtzine

Protopine

Eschscholzia californica

Caco-2 cells

Gut microbiota

ABSTRACT

California poppy products are commonly used for the treatment of nervousness, anxiety and sleeping disorders. Pharmacologically relevant constituents include the main alkaloids californidine, escholtzine and protopine. However, only limited information is available about the alkaloid content in commercial preparations and their intestinal absorption. Moreover, a possible metabolization of these alkaloids by the gut microbiota, and their impact on microbial activity and viability have not been investigated. Californidine, escholtzine and protopine were quantified by UHPLC-MS/MS in eight commercial California poppy products. The intestinal permeability of alkaloids was studied in Caco-2 cell as a model for absorption in the small intestine. The gut microbial biotransformation was explored in artificial gut microbiota from the in vitro PolyFermS model. In addition, the impact of these alkaloids and a California poppy extract on the microbial production of short-chain fatty acids (SCFAs) and the viability of microbiota was investigated. Contents of californidine, escholtzine and protopine in California poppy products were in the ranges of 0.13–2.55, 0.05–0.63 and 0.008–0.200 mg/g, respectively. In the Caco-2 cell model, californidine was low-to-moderately permeable while escholtzine and protopine were highly permeable. An active transport process was potentially involved in the transfer of the three alkaloids. The three compounds were not metabolized by the artificial gut microbiota over 24 h. Neither the California poppy extract nor the alkaloids markedly impacted microbial SCFA production and bacterial viability.

1. Introduction

Phytomedicines containing California poppy (*Eschscholzia californica*, Cham., Papaveraceae) are widely used for the treatment of nervousness, anxiety and sleeping disorders [1]. Reported pharmacological activities include modulation of γ -aminobutyric acid (GABA) receptor activity [2], serotonin receptor binding [3], and modulation of catecholamine metabolism [1,4]. The sedative, anxiolytic and analgesic effects of California poppy are associated, at least in part, with the alkaloids present in the plant. These include californidine, escholtzine and protopine (Fig. 1), with californidine as the most abundant, followed by escholtzine [1]. Previous studies have shown that these compounds could be involved in herb-drug interactions. Escholtzine was reported to increase CYP3A4 and CYP1A2 expression in HepG2 cells via activation of the pregnane X receptor (PXR), while californidine, escholtzine and protopine were found to inhibit the activity of certain cytochrome P450

enzymes (CYPs) using human liver microsomes and P-glycoprotein (P-gp) in MDCK-II cells [5].

The gut microbiota is highly diverse and ensures key functions in human health by regulating host immunity, modulating the intestinal barrier, protecting against pathogenic microbials, or providing energy to the host by metabolizing undigested food such as dietary fibers [6]. Dietary fibers and plant-based polysaccharides are precursors of short-chain fatty acids (SCFAs) [7], which serve as an energy source for intestinal cells, as signaling molecules, modulators of lipid metabolism, and as regulators of the intestinal immunity [8]. Besides these essential functions for human health, the gut microbiota has significant metabolic activity [9]. There is a growing number of studies identifying microbial biotransformation of ingested compounds (xenobiotics) by human fecal microbiota, or by single bacteria and synthetic bacterial consortia [10–13]. As a relevant in vitro system to study the metabolic activity and viability of gut microbiota, the artificial gut fermentation model

* Correspondence to: Division of Pharmaceutical Biology, Department of Pharmaceutical Sciences, University of Basel, Klingelbergstrasse 50, 4056 Basel, Switzerland.

E-mail addresses: matthias.hamburger@unibas.ch (M. Hamburger), olivier.potterat@unibas.ch (O. Potterat).

<https://doi.org/10.1016/j.bioph.2023.115420>

Received 28 June 2023; Received in revised form 25 August 2023; Accepted 30 August 2023

Available online 8 September 2023

0753-3322/© 2023 The Authors.

Published by Elsevier Masson SAS. This is an open access article under the CC BY license

(<http://creativecommons.org/licenses/by/4.0/>).

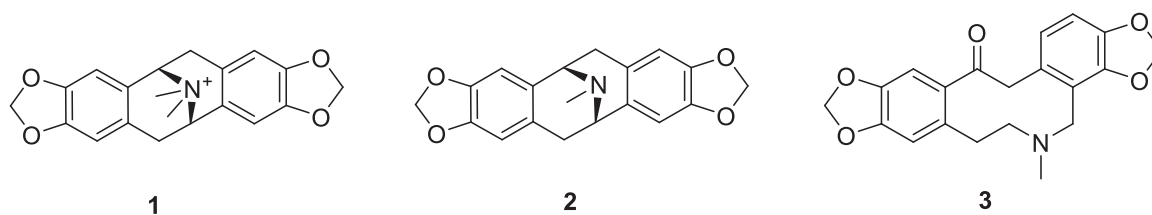


Fig. 1. Chemical structures of californidine (1), escholtzine (2) and protopine (3).

Polyfermentor Intestinal Model (PolyFermS) enables reproducible and stable cultivation of colon bacterial communities derived from a single human fecal donor [14]. The model has been previously used to study the gut microbiota interactions with constituents from St. John's wort and valerian [15].

Information on the alkaloidal content in commercial products of California poppy remains limited. Furthermore, the intestinal absorption and a possible metabolization by the gut microbiota of these alkaloids have not been investigated up to now. The impact of these alkaloids and of a California poppy extract on the viability and metabolic activity of gut microbiota has also not been explored. In this study, californidine, escholtzine and protopine were quantified in eight California poppy products sold as phytomedicines or food supplements. The bidirectional transport of californidine, escholtzine and protopine in the Caco-2 cell model, and their stability in artificial gut microbiota from the in vitro PolyFermS model were investigated. In addition, the impact of these alkaloids and of a California poppy extract on bacterial viability and microbial SCFAs production was studied.

2. Materials and methods

2.1. Cell lines, chemicals and biochemicals

The Caco-2 cell line was kindly provided by Prof. Per Artursson, Uppsala University, Sweden. Dulbecco's Modified Eagle's Medium (DMEM, with high glucose, L-glutamine, phenol red, without sodium pyruvate), Dulbecco's phosphate-buffered saline (DPBS, without calcium/magnesium, without phenol red), fetal bovine serum (FBS), MEM non-essential amino acids solution (NEAA, without L-glutamine), penicillin-streptomycin (PEST, 10,000 U/mL), and trypsin (2.5%, without phenol red) were purchased from Gibco (Paisley, UK). Hank's balanced salt solution (HBSS, without phenol red), 4-(2-hydroxyethyl) piperazine-1-ethanesulfonic acid (HEPES), 4-morpholineethanesulfonic acid monohydrate (MES), sodium bicarbonate (NaHCO₃), bovine serum albumin (BSA), dimethyl sulfoxide (DMSO), cellobiose, soluble potato starch, amylase, meat extract, mucin from porcine stomach type II, arabinogalactan from larch wood, Tween 80, hemin, NaHCO₃, KCl, MgSO₄, CaCl₂·2H₂O, MnCl₂, FeSO₄·7H₂O, ZnSO₄·7H₂O, 4-aminobenzoic acid (PABA), nicotinic acid, biotin, folic acid, cyanocobalamin, thiamine, riboflavin, phyloquinone, menadione, and pantothenate were purchased from Sigma-Aldrich (Saint-Louis, MO, USA). Xylan from oat spelts, and bacto tryptone were from Chemie Brunschwig (Basel, Switzerland). Inulin was provided by Cosucra (Warcoir, Belgium), and yeast extract by Lesaffre (Marcq-en-Barœul, France). Bile salts were purchased from Thermo Fischer Diagnostics (Pratteln, Switzerland). KH₂PO₄, NaCl, pyridoxine-HCl (Vit. B6), folic acid and menadione were obtained from VWR International (Dietikon, Switzerland). Ethylenediaminetetraacetic acid (EDTA, 0.2% in PBS, without calcium/magnesium) was purchased from MP biomedical (Santa Ana, CA, USA). Culture flasks (75 cm²), bottle top filters (pore size 0.22 μm), and 12-well Costar® plates, 12-well Transwell® plates (with 0.4 μm pore polycarbonate membrane inserts) were purchased from Corning Inc. (Corning, NY, USA). Sodium fluorescein salt, atenolol, propranolol HCl, verapamil HCl were purchased from Sigma-Aldrich (Saint-Louis, MO, USA). Californidine perchlorate (CAS n° 17939-31-0) was obtained

from Phytolab (Vestenbergsgreuth, Germany), and protopine (CAS n° 130-86-9) from Extrasynthese (Genay, France). Escholtzine (CAS n° 4040-75-9) was isolated from *E. californica* aerial parts (See [Supplementary Material](#)).

Acetonitrile (MeCN) and acetone were from Supelco (Bellefonte, PA, USA). Methanol (MeOH), isopropanol (i-PrOH) and ethanol (EtOH) were obtained from Macron Fine Chemicals (Radnor, PA, USA). *n*-Butanol (BuOH) and ethyl acetate (EtOAc) were purchased from Scharlau (Sentmenat, Spain). All solvents were of UHPLC grade. HPLC grade water was obtained from a Milli-Q integral water purification system (Millipore Merck, Darmstadt, Germany). Materials for flow cytometry were purchased from Beckman Coulter International (Nyon, Switzerland), except for stains SYBR Green I and propidium iodide which were from Life Technologies Europe (Zug, Switzerland).

2.2. Plant material and extraction

California poppy commercial preparations included different galenic forms. Three preparations were capsules or tablets containing dry flowering parts of the plant: Arkogélules® Escholtzia (Arkopharma, Carros, France), Herbes & Plantes Escholtzia Bio (Herbes et Plantes, Magescq, France), and Nature & Plantes Escholtzia (Planète au naturel, Magescq, France). Three preparations were fluid extracts of flowering aerial parts: Sommeil Pavot jaune de Californie Bio (Weleda, Arlesheim, Switzerland), Sommeil Pavot jaune de Californie (Boiron, Messimy, France), and Escholtzia (Naturalma, Bologna, Italy). Phytostandard Escholtzia Valériane consisted of tablets containing extracts of valerian roots and California poppy flowering aerial parts (PiLeJe laboratoire, Paris, France). Elusanes Eschscholtzia were capsules containing an extract of flowering aerial parts (Pierre Fabre, Castres, France). Manufacturer's information on the composition of all preparations is provided in [Table S1](#). Capsules or tablets of flowering parts were extracted with 100% MeOH utilizing pressurized liquid extraction (PLE) with a Dionex ASE 200 instrument (Sunnyvale, CA, USA). Three cycles of extraction of 5 min each at a temperature of 70 °C and a pressure of 120 bar were applied. The extracts were evaporated under reduced pressure and lyophilized.

The plant material used for the batch fermentation experiments and for the isolation of escholtzine was of Ph. Eur. grade and was purchased from Galke (Bad Grund, Germany). A voucher specimen (No 1234) has been deposited at the Division of Pharmaceutical Biology, University of Basel. The material was extracted by PLE with 70% EtOH. Three extraction cycles of 5 min were performed at a temperature of 70 °C and a pressure of 120 bar. The herbal extract has been previously characterized [16].

2.3. Caco-2 cell model and permeability experiments

2.3.1. Cell culture and permeability experiments

Cell culture and assay conditions were as previously published [15]. Briefly, cells were grown in 75 cm² culture flasks using DMEM (supplemented with 10% FBS, 1% NEAA, 1% PEST) in a humidified atmosphere (95%) with 10% CO₂, at a temperature of 37 °C. When confluence of 90–95% was reached, cells were subcultured by dissociation with trypsin solution (0.25% trypsin, 0.2% EDTA). To

prepare monolayers for permeability experiments, cells were seeded at a density of 4.5×10^5 cells/cm² and cultivated on Transwell® inserts for 22–28 days. The medium was changed three times a week. The seeding on inserts was performed with cells corresponding to passage number 94–108.

Permeability across Caco-2 monolayers was studied in both directions, from apical to basolateral (AB), and from basolateral to apical (BA) at a final concentration of 10 μ M of test compounds in the donor chamber and with 1% DMSO as co-solvent, over 60 min with 15 min sampling time intervals. Sampling volume was 0.6 mL or 0.2 mL from the basolateral chamber or apical chamber, respectively, and the sampling volume was replaced by fresh transport buffer. To simulate physiological conditions found in the human small intestine, transport buffers were adjusted to pH 6.5 in the apical chamber (10 mM MES, 4.2 mM NaHCO₃ in HBSS), and to pH 7.4 in the basolateral chamber (25 mM HEPES, 4.2 mM NaHCO₃ in HBSS). Permeability experiments were performed in triplicate. Collected samples were precipitated with MeCN and stored at -80°C until UHPLC-MS/MS analysis. Cumulative fraction curves for each experiment of all compounds are shown in Figs. S1–S5.

2.3.2. Cell lysis

Following permeability experiments, cell monolayers were washed quickly with HBSS/HEPES buffer at pH 7.4 and lysed with MeCN for 30 min. Cell lysis experiments were performed in duplicate. Samples were stored at -80°C until UHPLC-MS/MS analysis.

2.3.3. Control of Caco-2 cell monolayer integrity

Monolayer integrity was controlled using transepithelial electrical resistance (TEER) and the paracellular leakage marker fluorescein as described before [15]. Only monolayers with TEER values above 200 Ω cm² were used (Table S2) and a passage below 1% of fluorescein per hour was used as an indicator of monolayer integrity (Table S2) [17]. As an additional control, atenolol and propranolol were included as references for low-to-moderately and highly permeable drugs, respectively.

2.3.4. Experiments on cell-free inserts

Control experiments with cell-free inserts were performed to assess the passage of the compounds in absence of cells. As for the permeability experiments, study compounds were added to the donor chamber and incubated for 1 h at 37°C under shaking (450 rpm). At the end of the experiment, aliquots were taken from donor and receiver chambers, and stored at -80°C until analysis by UHPLC-MS/MS.

2.3.5. Determination of apparent permeability coefficients, efflux ratio and recoveries

Apparent permeability coefficients (P_{app}), efflux ratio and recovery values (recovery considering A and B chambers (Re_{AB}), and recovery considering A, B and the cell fraction (Re_{ABC})) were calculated as previously reported [15]. Equations are given in the supplementary material.

2.4. In vitro gut microbiota experiments

2.4.1. Anaerobic batch fermentation experiments with artificial gut microbiota and California poppy extracts or compounds

To assess the gut microbial biotransformation capacity, anaerobic batch fermentations with artificial gut microbiota and California poppy extract and compounds were performed using the same setup as previously reported for valerian and St. John's wort compounds [15].

The two artificial human gut microbiota used in this study were derived from independent stable PolyFermS bioreactors that were both inoculated with immobilized fecal microbiota from two healthy female individuals (age 25–35) and operated as previously described [15]. The PolyFermS system is designed and operated to mimic the proximal colon

conditions and allows to continuously cultivate the proximal colon microbiota akin to donor profile [18,19]. For each anaerobic batch experiment the artificial human colon microbiota from a single stabilized PolyFermS bioreactor were completely harvested under anaerobic conditions (10% CO₂, 5% H₂ and 85% N₂) in an anaerobic tent (Coy Laboratories, MA, USA).

PolyFermS microbiota were incubated with herbal compounds to monitor the colon microbial biotransformation potential and impact on fermentation metabolites and bacterial viability as described before [15]. In short, fresh and metabolically highly active PolyFermS colon microbiota effluent was supplemented with nutritive medium (MacFarlane medium) at a ratio of 7:3, and adjusted to pH 6.5. The high microbiota to medium ratio was chosen to enable the evaluation of the microbial biotransformation of the compounds and impact of the compounds on microbial viability under limited growth conditions. California poppy extract and compounds (californidine, escholtzine, protopine) were dissolved in DMSO and added to 10 mL microbiota mixture, at a final concentration of 500 μ g/mL or 30 μ g/mL, respectively. The final DMSO content was set to 0.2% (v/v) for single compounds and to 0.5% (v/v) for the plant extract, based on previous experiments showing low impact on SCFA production at these concentrations [15]. Microbiota-nutrient-compound mixtures were prepared under anaerobic conditions and filled into sterile serum flasks that were closed with sterile butyl rubber septa. Incubations were performed in the dark, at 37°C , and shaking (100 rpm) for 24 h, and under strict anaerobic conditions. 1 mL sample was withdrawn before (T0h) and after 24 h (T24h) of incubation and stored at -80°C until extraction and UHPLC-MS/MS analysis. For each experiment, DMSO controls with 0%, 0.2% and 0.5% DMSO (v/v) and 0.001% sodium perchlorate (w/v) were included. A 1 mL sample of microbial content was collected at the end of the experiment for SCFAs and bacterial cell quantification. All incubation experiments were performed in triplicate with the two artificial microbiota. Additionally, study compounds were incubated under same conditions with microbial-free (sterilization through 0.20 μ m filter) incubation mixture to assess degradation in abiotic conditions.

2.4.2. Fermentation metabolite quantification

To evaluate the impact of California poppy compounds or extract exposure on microbial metabolism, the fermentation metabolites acetate, propionate, butyrate, succinate, valerate, isovalerate and isobutyrate were quantified in collected fermentation samples as described before [15]. In short, supernatant of 1 mL fermentation samples (13'000 cfm for 10 min at 4°C) was filtered (0.2 μ m nylon filter) and analyzed by HPLC (LaChrom, Merck-Hitachi, Germany, or Accela, Thermo Fisher Scientific, Reinach, Switzerland) equipped with a Security Guard Cartridge Carbo-H (4×3.0 mm) and a Rezex ROA-Organic Acid H+ (300×7.8 mm) column (Phenomenex, Basel, Switzerland) and a refractive index detector (Thermo Fisher Scientific). The injection volume was 20 μ L (Accela HPLC) or 40 μ L (LaChrom HPLC). The mobile phase used was 10 mM H₂SO₄ at a flow rate of 0.4 mL/min at 40°C for 60 min per sample under isocratic conditions. The metabolites were quantified by external standard calibration.

2.4.3. Bacterial cell quantification

Bacterial flow cytometry was used to determine the total viable and dead bacterial cell counts of microbiota incubated with or without California poppy compounds or extract. The assay is based on a bacterial cell staining with a live/dead staining that consists of two DNA-binding fluorescent stains: SYBR® Green I and propidium iodide (PI). The former penetrates all cells and results in a green fluorescence, the latter penetrates only cells with a damaged cell membrane resulting in red fluorescence. After staining, the amount of cells with intact (viable) and permeable (dead) membrane were determined in each sample with a flow cytometer (Cytomics FC 500, Beckman Coulter) following the same protocol as described before [15]. The collected cell concentrations were exported to Microsoft Excel and converted to cell count/mL, taking into

account the sample dilution factor.

2.4.4. Microbiota sample extractions

Microbiota samples were thawed and directly processed by sequential liquid-liquid extractions with EtOAc and *n*-BuOH. Aliquots of 1 mL were extracted with 1 mL EtOAc and centrifuged for 10 min at 20 °C and 3000 rpm (Centrifuge 5810 R, Eppendorf, Hamburg, Germany). Then, the supernatant was collected and further extracted with 1 mL EtOAc, followed by 1 mL *n*-BuOH. The extracts were combined, evaporated to dryness using a rotary evaporator (Buchi, Flawil, Switzerland) and stored at -80 °C until analysis by UHPLC-MS/MS.

2.5. UHPLC-MS/MS analysis

2.5.1. Instrumentation and chromatographic conditions

California poppy, Caco-2 and microbiota samples were analyzed by ultrahigh performance liquid chromatography (UHPLC) coupled to electrospray ionization (ESI) tandem mass spectrometry (MS/MS) in multiple reaction monitoring (MRM) mode and with verapamil as internal standard (IS).

Californidine, escholtzine, protopine, atenolol and propranolol were analyzed on a 1290 Infinity UHPLC system consisting of a binary pump, an autosampler and a thermostatted column compartment coupled to a 6460 triple quadrupole mass spectrometer (all Agilent, Waldbronn, Germany). MS parameters (MRM transitions, cone voltage and collision energy) for MRM were optimized using the Agilent MassHunter program Optimizer and are presented in Table S3. UHPLC parameters of all study compounds such as gradient, flow rate, run time, eluents, column, injection volume, column temperature and autosampler temperature are listed in Table S4.

2.5.2. Sample preparation prior to UHPLC-MS/MS of California poppy samples

Dry extracts were reconstituted in appropriate volume of DMSO to reach a final concentration of 10 mg/mL, sonicated for 15 min, and centrifuged for 20 min (3500 rpm, 25 °C). 20 µL of supernatant were collected and further diluted with DMSO. The liquid preparations of California poppy were diluted with DMSO.

50 µL of analyte (californidine, escholtzine or protopine) diluted in DMSO were precipitated with 200 µL MeOH containing the IS at a concentration of 800 ng/mL, and then centrifuged for 20 min (12,700 rpm, 10 °C). 100 µL supernatant was collected and analysed by UHPLC/MS-MS.

2.5.3. Sample preparation prior to UHPLC-MS/MS analysis of Caco-2 samples

2.5.3.1. Californidine. To 50 µL of analyte in a mixture of HBSS and MeCN (1:1) were added 150 µL of ice-cold MeOH (containing the IS at a concentration of 1000 ng/mL). The samples were mixed for 10 min at room temperature on an Eppendorf MixMate (Hamburg, Germany), and centrifuged for 20 min (12,700 rpm, 10 °C). 100 µL supernatant were collected in 96-deepwell plate (96-DPW, Biotage, Uppsala, Sweden) and analysed by UHPLC/MS-MS.

2.5.3.2. Escholtzine. To 200 µL of analyte in a mixture of HBSS and MeCN (1:1) were added 900 µL of ice-cold MeCN (containing the IS at a concentration of 100 ng/mL). The samples were mixed for 10 min at room temperature, and centrifuged for 20 min (12,700 rpm, 10 °C). 750 µL supernatant were collected and transferred into a 96-deepwell plate (96-DPW, Biotage) and dried under nitrogen gas flow (Evaporex EVX-96, Apricot Designs, Covina, CA, USA). Samples were redissolved with 200 µL of a mixture of water and MeCN (65:35), both containing 0.1% of formic acid, followed by 30 min of shaking on an Eppendorf MixMate.

2.5.3.3. Protopine. The UHPLC-MS/MS method used for protopine quantification in Caco-2 samples has been previously reported [20].

To 200 µL of analyte in a mixture of HBSS and MeCN (1:1) were added 200 µL of 6% BSA in water, 100 µL of MeOH (containing the IS at a concentration of 1000 ng/mL) and 800 µL of ice-cold MeCN. The samples were mixed for 10 min at room temperature on an Eppendorf MixMate, and centrifuged at 10 °C for 20 min at 12,700 rpm. An aliquot of 750 µL supernatant was collected and transferred into a 96-deepwell plate (96-DPW, Biotage) and dried under nitrogen gas flow (Evaporex EVX-96). Samples were redissolved with 200 µL of a mixture of water and MeCN (65:35), both containing 0.1% of formic acid, followed by 30 min of shaking on an Eppendorf MixMate.

2.5.3.4. Atenolol and propranolol. To 200 µL of analyte in a mixture of HBSS and MeCN (1:1) were added 100 µL of 6% BSA in water and 900 µL of ice-cold MeCN (containing the IS at a concentration of 100 ng/mL). The samples were mixed for 10 min at room temperature on an Eppendorf MixMate, and centrifuged at 10 °C for 30 min at 3500 rpm. An aliquot of supernatant was collected (800 µL for atenolol, 300 µL for propranolol) and transferred into a 96-deepwell plate (96-DPW, Biotage) and dried under nitrogen gas flow (Evaporex EVX-96). Samples were redissolved with 100 µL (atenolol) or 200 µL (propranolol) of a mixture of water and MeCN (65:35), both containing 0.1% of formic acid, followed by 30 min of shaking on an Eppendorf MixMate [15].

2.5.4. Sample preparation prior to UHPLC-MS/MS of microbiota samples

Microbiota samples were extracted as mentioned above (Section 2.4.4). Microbiota dry samples T0h and T24h were reconstituted with DMSO (containing the corresponding internal standard at a concentration of 500 ng/mL) and analysed by UHPLC-MS/MS. Chromatographic and MS/MS conditions were as for California poppy and Caco-2 sample analysis.

2.5.5. UHPLC-MS/MS quantification methods and acceptance criteria

UHPLC-MS/MS methods for absolute quantification of study compounds in analytical samples from California poppy products and Caco-2 experiments consisted in the injection of 2 sets of 7 calibrator samples validated with 2 sets of 3 quality control (QC) samples from the low, middle and high level of the calibration curve. Calibrators, QC and analytical samples were processed with the same sample preparation protocol, and prepared fresh prior to UHPLC-MS/MS analysis. To be accepted, a bioanalytical run was required to have a coefficient of determination (R^2) higher than 0.96 with at least 75% of all calibrators valid. Additionally, for the lower limit of quantification (LLOQ) and upper limit of quantification (ULOQ), at most one value could be excluded. Furthermore, between bioanalytical runs, the imprecision (CV %) had to be lower than 15% (20% at the LLOQ), and the inaccuracy (RE %) had to be within $\pm 15\%$ ($\pm 20\%$ at the LLOQ). The above mentioned criteria were in accordance with requirements of the US Food and Drug Administration (FDA) and the European Medicines Agency (EMA) for bioanalytical methods [21,22]. For California poppy extract samples analysis, calibration range was from 2.5 to 1000 ng/mL for californidine, from 2.5 to 250 ng/mL for escholtzine, and from 2.5 to 500 ng/mL for protopine. For analysis of Caco-2 samples, the calibration range was from 0.1 to 125 ng/mL for californidine, from 10 to 1000 ng/mL for escholtzine, and from 2.5 to 500 ng/mL for protopine. For the control compounds propranolol and atenolol, the range was from 10 to 2000 ng/mL. For very low concentrated samples of atenolol, an additional UHPLC-MS/MS method was developed in a lower range of 0.05–10 ng/mL [15]. Calibration curves are provided in Figs. S6–S14, and curve parameters, calibrator and QC samples are in Tables S5–S22. Additionally, carry-over values were determined to not exceed 20% for the analyte, and 5% for the internal standard (Tables S23–S24).

Table 1

Content of californidine, escholtzine and protopine in commercial products of flowering aerial parts of California poppy. Data are reported as mg/g (for solid preparations), or mg/mL (for liquid preparations) \pm SD.

Product n°	Galenic form	Californidine	Escholtzine	Protopine
1	Dry powder	2.00 \pm 0.08	0.39 \pm 0.01	0.17 \pm 0.01
2	Dry powder	1.78 \pm 0.05	0.63 \pm 0.02	0.145 \pm 0.004
3	Dry powder	1.57 \pm 0.04	0.42 \pm 0.01	0.104 \pm 0.004
4	Dry extract	2.55 \pm 0.02	0.38 \pm 0.01	0.20 \pm 0.01
5	Dry extract	0.76 \pm 0.12	0.39 \pm 0.02	0.11 \pm 0.01
6	Fluid extract	0.153 \pm 0.005	0.085 \pm 0.001	0.058 \pm 0.002
7	Fluid extract	0.152 \pm 0.004	0.054 \pm 0.001	0.0081 \pm 0.0003
8	Fluid extract	0.131 \pm 0.004	0.084 \pm 0.002	0.015 \pm 0.001

2.6. Data acquisition and statistical analysis

UHPLC-MS/MS data were acquired and processed using Agilent MassHunter version 10.0, or Waters MassLynx V4.1 software. Statistical analysis was performed and graphs drawn with GraphPad Prism 9.3.1.

3. Results and discussion

3.1. Quantification of californidine, escholtzine and protopine in commercial preparations

Highly sensitive and selective UHPLC-MS/MS methods in the MRM detection mode were developed for the quantification of californidine, escholtzine and protopine in commercial preparations (Section 2.5.5). For each method, the imprecision (expressed as CV%) and inaccuracy (expressed as CV%) of calibration levels and QC levels were both below 15% (20% at the LLOQ) (Tables S5–S10), showing that the methods were precise and accurate [21,22]. Also, carry-over values were below 20% for the analyte and below 5% for the IS, showing that carry-over had no impact on quantification (Table S23). Therefore, the methods were reliable for the quantification of the alkaloids in commercial formulations of California poppy.

The methods were applied for the determination of californidine, escholtzine and protopine in eight commercial preparations of flowering aerial parts of California poppy containing dry herbal powder (preparations 1–3), dry extract (preparations 4 and 5), or fluid extract (preparations 6–8) as the active ingredient (Tables 1, S1). All preparations

showed a similar alkaloid pattern, but with variations in absolute amounts of compounds. Californidine was the most abundant, followed by escholtzine and protopine. The contents in dry powders (preparations 1–3) were comparable, with contents in californidine, escholtzine and protopine of 1.57–2.00, 0.39–0.63, and 0.10–0.17 mg/g, respectively. In contrast, important differences were noticed between dry extracts, with respective amounts of californidine, escholtzine and protopine of 2.55, 0.38 and 0.20 mg/g in preparation 4, and of 0.76, 0.39 and 0.11 mg/g in preparation 5. In fluid extracts (preparations 6–8), contents of californidine, escholtzine and protopine were in the ranges of 0.131–0.153, 0.054–0.085, and 0.008–0.058 mg/g, respectively. The concentration of protopine, in particular, differed strongly between the products (Table 1). The differences observed in the extract-containing products are likely due, at least in part, to differing extraction procedures.

There have been a few studies on the contents of these three alkaloids in commercially available preparations of California poppy. The contents determined by HPLC-UV in two herbal powders and one solid extract were in a similar range for californidine and protopine, while the contents of escholtzine were up to ten times higher compared to the values found in preparations 1–5 [23]. The contents of californidine and escholtzine determined by capillary electrophoresis in a commercial tincture of California poppy were comparable to those in preparations 6–8, whereas the content of the major alkaloid protopine was comparable to that of preparation 7 [24].

Based on our data and the dosage recommendations of the manufacturers, the maximum amounts of californidine, escholtzine and protopine ingested per day were calculated to range between 0.16 and 2.97 mg/day (californidine), 0.10–1.11 mg/day (escholtzine), and 0.02–0.31 mg/day (protopine) (Fig. 2). Thus, considerable differences in the daily intake of californidine, escholtzine and protopine are expected for patients using different California poppy products.

3.2. Permeability across Caco-2 monolayers

The intestinal absorption of californidine, escholtzine and protopine was assessed by means of permeability across Caco-2 cell monolayers. The apparent permeability coefficients (P_{app}) from apical to basolateral (AB), and from basolateral to apical (BA) for each of the compounds were determined. Atenolol and propranolol were used as controls as previously described [15] and results were within the reference range (Table 2).

Californidine showed a mean P_{appAB} of 0.58×10^{-6} cm/s, a mean P_{appBA} of 4.93×10^{-6} cm/s, and a calculated ER of 8.6. Re_{AB} values in AB direction and BA direction were 90.3% and 114%, respectively.

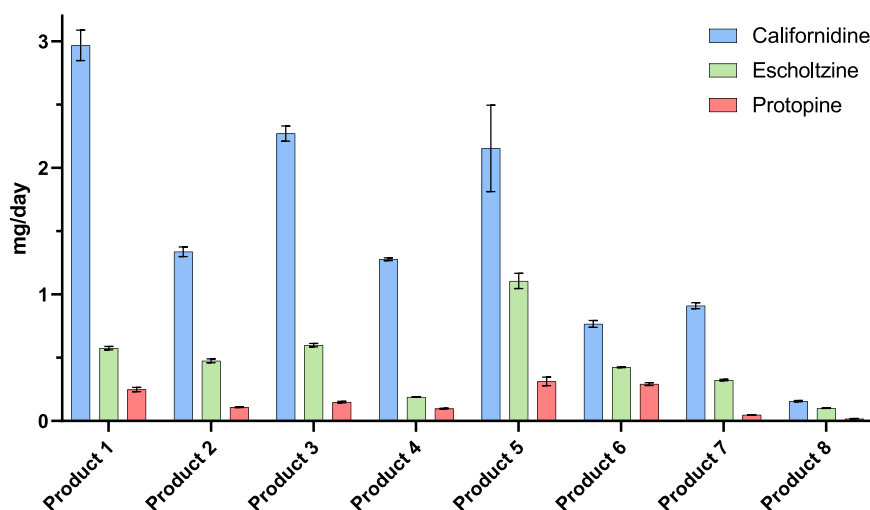


Fig. 2. Maximum daily intake of californidine, escholtzine and protopine for commercial products 1–8. Calculations are based on contents (Table 1) and dosage recommendations provided by the manufacturer (Table S1). Data are reported in mg / day \pm SD.

Table 2

Permeability data of californidine, escholtzine, protopine, atenolol, and propranolol across Caco-2 monolayers. Data are presented as mean \pm SD. (n = 3). Cumulative fraction curves for each individual monolayer are shown in Figs. S1–S5.

Compounds	AB direction			BA direction			
	P_{appAB} ($\times 10^{-6}$ cm/s)	Re_{AB}^a (%)	Re_{ABC}^b (%)	P_{appBA} ($\times 10^{-6}$ cm/s)	Re_{AB} (%)	Re_{ABC} (%)	ER ^c
Californidine	0.58 \pm 0.13	90.3 \pm 2.7	98.2	4.93 \pm 0.89	114 \pm 60	115	8.6
Escholtzine	82.5 \pm 4.1	17.7 \pm 4.4	37.6	175 \pm 5	42.8 \pm 11.1	53.6	2.1
Protopine	39.2 \pm 2.4	36.7 \pm 1.5	38.8	144 \pm 4	11.9 \pm 5.0	13.0	3.7
Atenolol ^d	0.11 \pm 0.03	88.7 \pm 6.3	92.8	0.14 \pm 0.02	118 \pm 22	118	1.3
Propranolol ^d	53.4 \pm 5.3	39.5 \pm 1.1	58.1	121 \pm 4	61.8 \pm 5.2	69.8	2.3

^a Recovery considering apical and basolateral compartments

^b Recovery considering apical and basolateral compartments, and cell fraction

^c Efflux ratio

^d Values from our previous study [15].

Re_{ABC} values in AB direction and BA direction were 98.2% and 115%, respectively (Table 2). Permeability experiments across empty inserts revealed that the passage of californidine was not restricted (Fig. S15). The P_{appAB} classified californidine as a low-to-moderately permeable compound. Californidine is a quaternary ammonium compound carrying a permanent charge, which is expected to restrain its permeability across epithelial barriers [25]. The calculated ER of 8.6 suggests that an active efflux process could be involved in the transport of californidine [26].

For escholtzine, the mean P_{appAB} was 82.5×10^{-6} cm/s, the mean P_{appBA} 175×10^{-6} cm/s, and the ER 2.1. In AB direction, the Re_{AB} was 17.7%, and Re_{ABC} was 37.6%. In BA direction, the Re_{AB} was 42.8%, and Re_{ABC} was 53.6% (Table 2). Protopine showed a mean P_{appAB} of 39.2×10^{-6} cm/s and a mean P_{appBA} of 144×10^{-6} cm/s, with a calculated ER of 3.7. Re_{AB} values in AB direction and BA direction were of 36.7% and of 11.9%, respectively. Re_{ABC} values in AB direction and BA direction were of 38.8% and of 13.0%, respectively (Table 2). Both alkaloids were classified as highly permeable compounds [26]. Data for protopine were consistent with previously reported pharmacokinetic data in various animal models [27]. The obtained ER values suggest that an active efflux transport could be involved in the transfer of both compounds. Further experiments at lower compound concentration to reduce possible transport saturation and/or with specific carrier-protein inhibitors would be needed to confirm the involvement of active efflux processes. The low recovery values (Table 2) suggest that escholtzine and protopine may be metabolized given that solubility issues could be ruled out (Fig. S15). In Caco-2 cells, levels of phase I metabolizing enzymes are known to be low, while phase II enzymes such as UDP-glucuronosyltransferases (UGTs), sulfotransferases (SULTs) and glutathione S-transferases (GSTs) are highly expressed [28] which could possibly have contributed to the low recovery. In agreement with this, protopine glucuronide conjugates have been detected in rat urine samples [27].

As a limitation inherent to the Caco-2 cell model the P_{app} values are considered to be slightly underestimated for values of recovery below 80%, and should, therefore, be seen as a qualitative readout [26]. This was the case for escholtzine and protopine, as well as for the control propranolol.

3.3. Stability of compounds during *in vitro* gut microbiota fermentation

Incubation experiments in artificial microbiota were performed to assess a possible biotransformation of californidine, escholtzine and protopine by human gut microbiota. Two microbiota derived from two different healthy adult female fecal donors were used for the experiments. The metabolic activity of both microbiota over the incubation time was confirmed by the determination of SCFA levels in control incubations with and without DMSO (Fig. S16). All the alkaloids were stable over 24 h in abiotic incubations with microbe-free PolyFermS effluent with 30% nutritive medium buffered at pH 6.5. No major

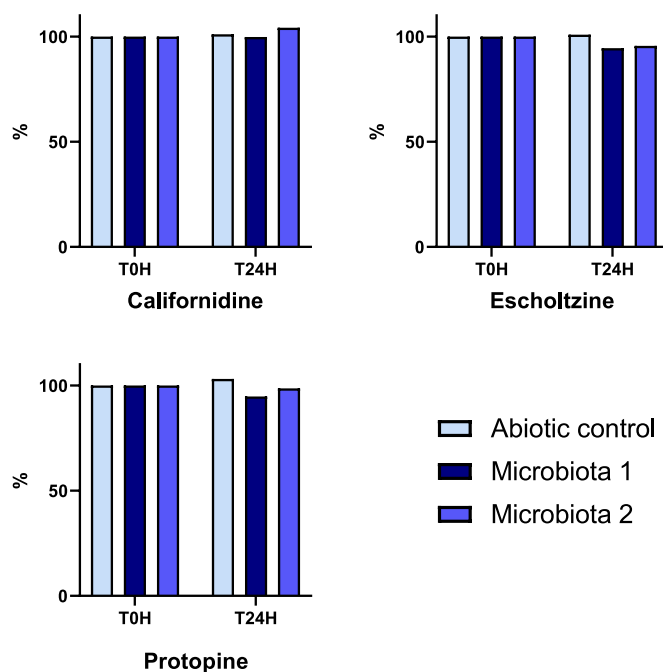


Fig. 3. Stability of compounds after 24 h incubation in PolyFermS effluent without active microbiota (abiotic), and in viable PolyFermS microbiota of donors 1 and 2 supplemented with 30% nutritive medium. All incubations contained 20 μ L DMSO. Mean concentration values (n = 2) are normalized to 100%. The individual values of the two replicates are given in Table S25.

differences were observed between abiotic and microbiota incubations, suggesting that no microbiota-mediated metabolism of studied alkaloids occurred (Fig. 3).

Upon ingestion of herbal medicines, phytochemicals are transported through the gastrointestinal tract and can be absorbed in the small intestine. The permeability experiments with the Caco-2 cell model indicated that californidine is low-to-moderately permeable (Table 2). Thus, relevant concentrations could possibly be reached in the colon. Moreover, our results with two different gut microbiota suggest that biotransformation of californidine in the colon is not to be expected. In contrast, escholtzine and protopine were found to be highly permeable in the Caco-2 cell model, which in turn would imply only low concentrations in the colon (Table 2). However, if a small fraction of these two alkaloids would not be absorbed in the small intestine, the results from microbiota incubation experiments suggest that they also would not be metabolized by the gut microbiota. While the disposition of escholtzine has not been investigated, protopine was found to have an absolute bioavailability of 25.8% in rats [29] and to undergo phase I/II metabolism [27]. In addition, excretion studies in rats have shown that

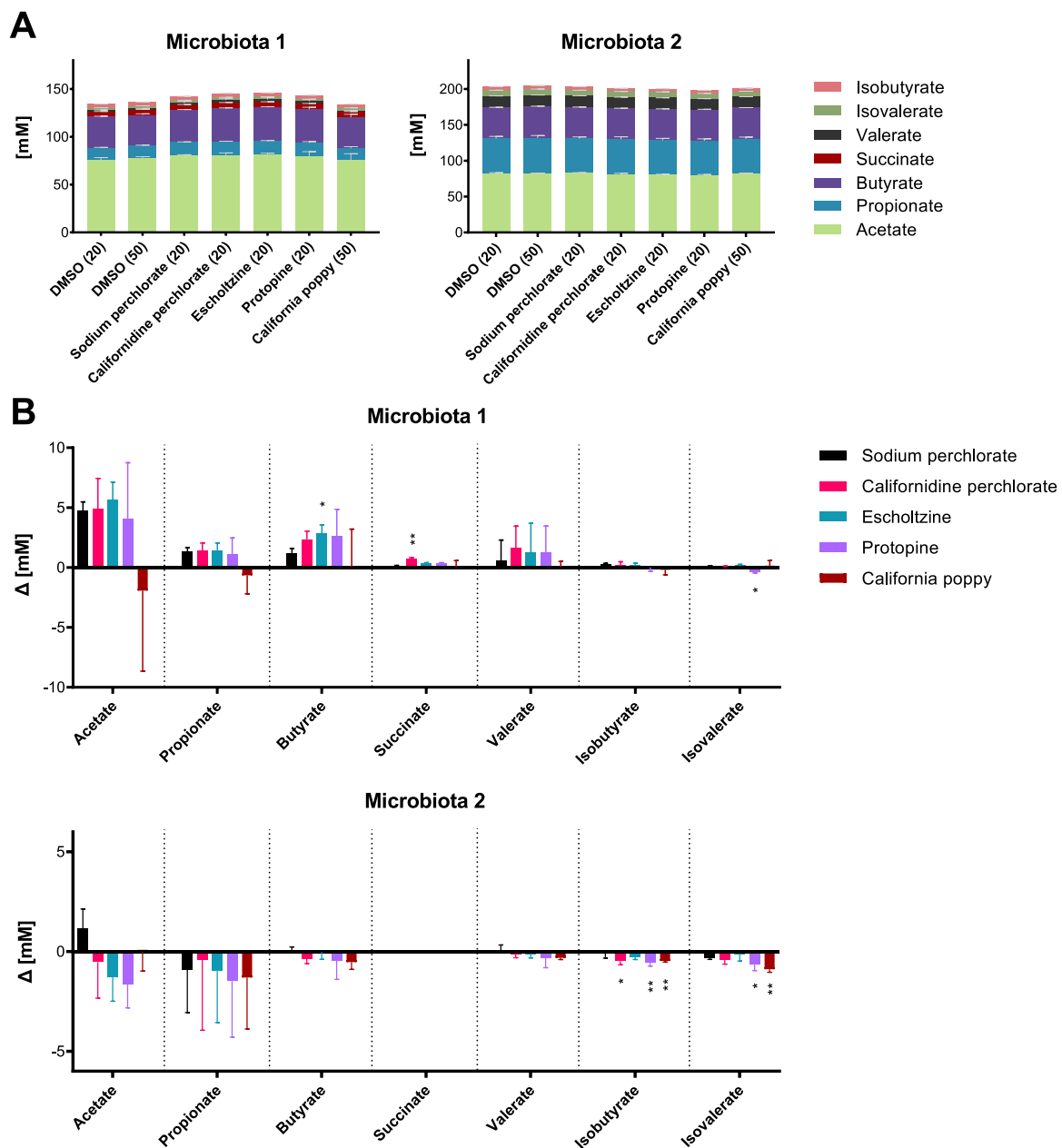


Fig. 4. (A) Fermentation metabolite concentrations after 24 h incubation of PolyFermS microbiota of donors 1 and 2, respectively. Incubations were supplemented with 30% nutritive medium and DMSO, with or without herbal compounds or extracts. Averages \pm SD. ($n = 3$). (B) Difference (Δ) after 24 h of short-chain fatty acid concentrations in compound vs DMSO control fermentation. Averages \pm SD. ($n = 3$). Asterisks indicate significant differences in average metabolite concentration between compound fermentation and respective DMSO control, analyzed by one-way ANOVA.

protopine was mainly excreted in metabolized form (>99%) [29]. Therefore, metabolites of protopine excreted via the hepatobiliary system could possibly transit over the gastrointestinal tract and interact with the gut microbiota. In the absence of data, this can also not be excluded for escholtzine.

3.4. Impact of compounds and plant extracts on microbiota activity and viability

Next, the impact of the California poppy extract and its compounds on the SCFA production by the two artificial gut microbiota was assessed. The main SCFAs (acetate, propionate, butyrate) and other minor organic acids (succinate, valerate, isovalerate, isobutyrate) were quantified and used as readout for the carbohydrate fermentation

activity, which is a key metabolic function of the human gut microbiome [7]. The artificial microbiota derived from the two female fecal donors were of two distinct but prevalent microbiota types. Microbiota 1 was producing more butyrate (butyrogenic), while microbiota 2 was producing more propionate (propionogenic) (Fig. 4A). Californidine, escholtzine, protopine and the California poppy extract did not markedly impact the total SCFA levels (Fig. 4A). In microbiota 1, butyrate production increased by 9% in the presence of escholtzine, succinate production by 13% in presence of californidine, and isovalerate production decreased by 14% in the presence of protopine, while the effect of California poppy extract on individual SFCAs was negligible (Fig. 4B). In microbiota 2, isobutyrate levels decreased in the presence of californidine (−10%), protopine (−11%), and California poppy extract (−9%), while levels of isovalerate decreased in the presence of protopine

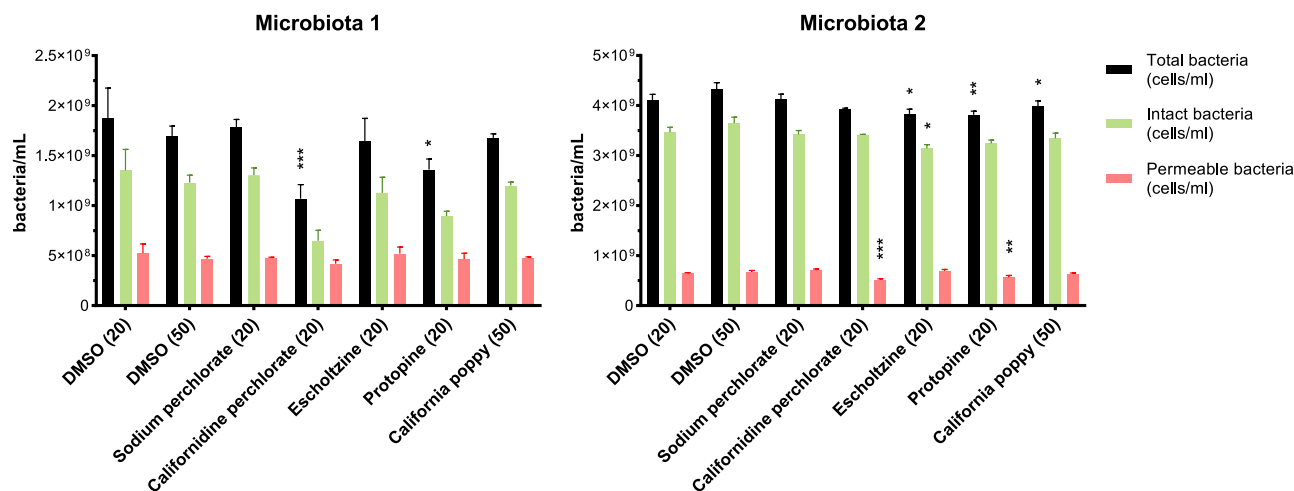


Fig. 5. Concentration of total (black), viable (intact, green) and dead (permeable, red) bacteria after 24 h incubation in PolyFermS microbiota of donor microbiota 1 and 2. Microbiota were supplemented with 30% nutritive medium and DMSO, with or without single compounds or herbal extract. Averages on bacteria/mL \pm SD ($n = 3$). Asterisks indicate significant differences in average bacterial concentration between compound fermentation and respective DMSO control fermentation analyzed by one-way ANOVA.

(−8%) and California poppy extract (−10%) (Fig. 4B).

Additionally, the impact of californidine, escholtzine, protopine and California poppy extract on bacterial concentration and viability was assessed by flow cytometry, whereby the total concentration of viable and dead bacteria in the microbiota after 24 h of incubation was determined. In microbiota 1, the alkaloids californidine and protopine resulted in significantly lower total bacteria concentrations (43% and 28% lower, respectively) compared to the control, which may be explained by a lower fraction of viable cells (trend, not significant) (Fig. 5). In microbiota 2, a small antimicrobial effect was noticed for californidine (with a decrease of 21% in permeable cells), escholtzine (with a decrease of 7% total bacteria and 9% in intact cells), protopine (with a decrease of 7% total bacteria and 13% in permeable cells) and the California poppy extract (with a decrease of 8% total bacteria) (Fig. 5).

Our data suggest that exposure to californidine, escholtzine, protopine and California poppy extract does not markedly affect the microbial fermentation activity and bacterial viability at the tested concentrations (30 μ g/mL for compounds, and 500 μ g/mL for the extract). However, it cannot be excluded that with higher test concentrations in the batch fermentation assays and with a long-term exposure in continuous fermentation experiments the SCFA metabolism and bacterial viability could be affected.

The quantitative analysis of the major alkaloids in commercial preparations of California poppy, together with manufacturer's dosage recommendations, showed that the maximum ingested amounts of californidine, escholtzine and protopine are in the range of 0.16–2.97, 0.10–1.11, and 0.02–0.31 mg/day, respectively (Fig. 2). Considering these amounts, an average volume of 200 mL of the proximal colon [30], and a colonic retention time of 8 h resulting in 600 mL proximal colon suspension per day [18,31], and assuming stability and no absorption of compounds in the upper parts of the gastrointestinal tract, the calculated concentrations of californidine, escholtzine and protopine in the colon would be in the range of 0.3–4.9, 0.2–1.8, and 0.03–0.52 μ g/mL, respectively. Assuming a homogenous dispersion of compounds in the proximal colon, the concentrations used in our experiments were above the expected maximum theoretical colonic concentrations (about 6-fold for californidine, 17-fold for escholtzine, and 58-fold for protopine). Thus, one can reasonably assume that upon oral intake of California poppy herbal products the alkaloids would not substantially impair the fermentation capacities and the bacterial viability of microbiota. As to the California poppy extract, concentrations used in our experiments were up to 4-fold lower than those theoretically expected with a

maximum recommended daily intake, where intestinal concentrations of 0.7–2.1 mg/mL could be reached. For the herbal products themselves an impact on microbiota balance cannot be excluded at this point. However, experiments with a higher number of individual PolyFermS microbiota would be needed to further substantiate the findings. Further, our experiments with high inoculation ratio were designed to assess the effect of the compounds on the microbial metabolite production and overall viability under limited growth [32]. Therefore, future in vitro continuous gut fermentations may allow to monitor long-term impact of alkaloids on microbial community structure and diversity.

4. Conclusions

The contents in californidine, escholtzine and protopine in eight commercial California poppy products were determined by UHPLC-MS/MS. In all products californidine was the major alkaloid, followed by escholtzine. The alkaloid content in the analyzed products varied significantly, ranging from 0.13 to 2.55 mg/g for californidine, 0.05–0.63 for escholtzine, and 0.008–0.200 mg/g for protopine. Based on the dosage recommended by manufacturers, maximal daily doses for the three alkaloids were calculated to be between 0.16 and 2.97, 0.10 and 1.11, and 0.02 and 0.31 mg/day, respectively.

Californidine was found to be low-to-moderately permeable, whereas escholtzine and protopine were highly permeable in the Caco-2 cell assay. The transport of each compound was possibly involving an active process. Escholtzine and protopine were also likely metabolized in Caco-2 cells.

The three alkaloids were not metabolized in the two PolyFermS artificial gut microbiota obtained from two different healthy female fecal donors. This suggests a negligible role of the gut microbiota in the disposition of the three alkaloids. The alkaloids and the extract did not markedly impact the SCFA production or the bacterial viability of microbiota. Thus, use of California poppy does not seem to affect gut microbiota metabolism, at least in short-term exposure. However, given the high interindividual variability of gut microbiota, studies with a larger number of microbiota and with continuous fermentations models are warranted to assess a possible effect on microbiota composition produced by a prolonged exposure.

With the calculated maximal daily intake in alkaloids, and assuming a 100% bioavailability, a rough estimation of the alkaloid concentrations in body fluids [33,34] for an average adult (40 years-old, 170 cm, and 70 kg) would theoretically result in maximal plasma concentrations

of 0.22, 0.08 and 0.02 μM for californidine, escholtzine and protopine, respectively. However, lower concentrations can be assumed for californidine due to its limited intestinal permeability. As for protopine, lower concentrations are also likely, given that intensive phase I and phase II metabolism has been shown in pharmacokinetic studies in rats [35]. Given the lowest IC_{50} values reported for these alkaloids in the study of Manda et al. (2016) [5] (IC_{50} of 100 μM for inhibition of any CYPs by californidine, IC_{50} of 0.3 μM for inhibition of CYP2C19 by escholtzine, and IC_{50} of 0.03 μM for inhibition of CYP2D6 by protopine), it seems unlikely that they could be responsible for herb-drug interactions.

Ethics approval and consent to participate

The Ethics Committee of ETH Zürich exempted this study from review because the sample collection procedure has not been performed under conditions of intervention. Informed written consent was obtained from fecal donors.

CRedit authorship contribution statement

Antoine Chauveau: Conceptualization, Methodology, Validation, Investigation, Writing – original draft. **Annélies Geirnaert:** Conceptualization, Methodology, Validation, Investigation, Writing – review & editing, Supervision. **Angela Babst:** Investigation. **Andrea Treyer:** Conceptualization, Methodology, Validation, Investigation, Writing – review & editing, Supervision. **Christophe Lacroix:** Conceptualization, Methodology, Validation, Supervision, Project administration, Funding acquisition. **Matthias Hamburger:** Conceptualization, Methodology, Validation, Formal analysis, Resources, Writing – review & editing, Supervision, Project administration, Funding acquisition. **Olivier Potterat:** Conceptualization, Methodology, Validation, Formal analysis, Resources, Writing – review & editing, Supervision, Project administration, Funding acquisition.

Declaration of Competing Interest

The authors declare no competing interests.

Acknowledgments

This work was supported by the Swiss National Science Foundation [CRSII5_177260; Herbal Safety in Pregnancy]. We thank Morris Keller, Dr. Jakob Reinhardt and Orlando Fertig (Division of Pharmaceutical Biology, University of Basel) for the isolation and characterization of escholtzine, and Alfonso Die (Laboratory of Food Biotechnology, ETH Zurich) for HPLC-RI analysis.

Appendix A. Supporting information

Supplementary data associated with this article can be found in the online version at [doi:10.1016/j.biopha.2023.115420](https://doi.org/10.1016/j.biopha.2023.115420).

References

- [1] EMA/HMPC, Assessment Report on *Eschscholzia californica* Cham., herba, 2015. (https://www.ema.europa.eu/en/documents/herbal-report/final-assessment-report-eschscholzia-californica-cham-herba_en.pdf) (Accessed March 20, 2023).
- [2] A. Rolland, J. Fleurentin, M.C. Lanhers, R. Misslin, F. Mortier, Neurophysiological effects of an extract of *Eschscholzia californica* Cham. (Papaveraceae), *Phytother. Res.* 15 (2001) 377–381, <https://doi.org/10.1002/ptr.884>.
- [3] S. Gafner, B.M. Dietz, K.L. McPhail, I.M. Scott, J.A. Glinski, F.E. Russell, M. McCollom, J.W. Budzinski, B.C. Foster, C. Bergeron, M.-R. Rhyu, J.L. Bolton, Alkaloids from *Eschscholzia californica* and their capacity to inhibit binding of [3H] 8-Hydroxy-2-(di-N-propylamino)tetralin to 5-HT_{1A} receptors in vitro, *J. Nat. Prod.* 69 (2006) 432–435, <https://doi.org/10.1021/np058114h>.
- [4] E. Kleber, W. Schneider, H.L. Schäfer, E.F. Elstner, Modulation of key reactions of the catecholamine metabolism by extracts from *Eschscholzia californica* and *Corydalis cava*, *Arzneimittelforschung* 45 (1995) 127–131.
- [5] V.K. Manda, M.A. Ibrahim, O.R. Dale, M. Kumarihamy, S.J. Cutler, I.A. Khan, L. A. Walker, I. Muhammad, S.I. Khan, Modulation of CYPs, P-gp, and PXR by *Eschscholzia californica* (California poppy) and its alkaloids, *Planta Med.* 82 (2016) 551–558, <https://doi.org/10.1055/s-0042-103689>.
- [6] E. Thursby, N. Juge, Introduction to the human gut microbiota, *Biochem. J.* 474 (2017) 1823–1836, <https://doi.org/10.1042/BCJ20160510>.
- [7] A. Koh, F. De Vadder, P. Kovatcheva-Datchary, F. Bäckhed, From dietary fiber to host physiology: short-chain fatty acids as key bacterial metabolites, *Cell* 165 (2016) 1332–1345, <https://doi.org/10.1016/j.cell.2016.05.041>.
- [8] E.M. Bik, J.A. Ugalde, J. Cousins, A.D. Goddard, J. Richman, Z.S. Apte, Microbial biotransformations in the human distal gut, *Br. J. Pharmacol.* 175 (2018) 4404–4414, <https://doi.org/10.1111/bph.14085>.
- [9] J. Qin, R. Li, J. Raes, M. Arumugam, K.S. Burgdorf, C. Manichanh, T. Nielsen, N. Pons, F. Levenez, T. Yamada, D.R. Mende, J. Li, J. Xu, S. Li, D. Li, J. Cao, B. Wang, H. Liang, H. Zheng, Y. Xie, J. Tap, P. Lepage, M. Bertalan, J.-M. Batto, T. Hansen, D. Le Paslier, A. Linneberg, H.B. Nielsen, E. Pelletier, P. Renault, T. Sicheritz-Ponten, K. Turner, H. Zhu, C. Yu, S. Li, M. Jian, Y. Zhou, Y. Li, X. Zhang, S. Li, N. Qin, H. Yang, J. Wang, S. Brunak, J. Doré, F. Guarner, K. Kristiansen, O. Pedersen, J. Parkhill, J. Weissenbach, P. Bork, S.D. Ehrlich, J. Wang, A human gut microbial gene catalogue established by metagenomic sequencing, *Nature* 464 (2010) 59–65, <https://doi.org/10.1038/nature08821>.
- [10] R.N. Carmody, P.J. Turnbaugh, Host-microbial interactions in the metabolism of therapeutic and diet-derived xenobiotics, *J. Clin. Investig.* 124 (2014) 4173–4181, <https://doi.org/10.1172/JCI72335>.
- [11] N. Koppel, V. Maini Rekdal, E.P. Balskus, Chemical transformation of xenobiotics by the human gut microbiota, *eaag2770*, *Science* 356 (2017), <https://doi.org/10.1126/science.aag2770>.
- [12] L. Maier, M. Pruteanu, M. Kuhn, G. Zeller, A. Telzerow, E.E. Anderson, A. R. Brochado, K.C. Fernandez, H. Dose, H. Mori, K.R. Patil, P. Bork, A. Typas, Extensive impact of non-antibiotic drugs on human gut bacteria, *Nature* 555 (2018) 623–628, <https://doi.org/10.1038/nature25979>.
- [13] M. Zimmermann, M. Zimmermann-Kogadeeva, R. Wegmann, A.L. Goodman, Mapping human microbiome drug metabolism by gut bacteria and their genes, *Nature* 570 (2019) 462–467, <https://doi.org/10.1038/s41586-019-1291-3>.
- [14] A. Zihler Berner, S. Fuentes, A. Dostal, A.N. Payne, P. Vazquez Gutierrez, C. Chassard, F. Grattepanche, W.M. de Vos, C. Lacroix, Novel polyfermentor intestinal model (PolyFermS) for controlled ecological studies: validation and effect of pH, *PLoS ONE* 8 (2013), e77772, <https://doi.org/10.1371/journal.pone.0077772>.
- [15] A. Chauveau, A. Treyer, A. Geirnaert, L. Bircher, A. Babst, V.F. Abegg, A.P. Simões-Wüst, C. Lacroix, O. Potterat, M. Hamburger, Intestinal permeability and gut microbiota interactions of pharmacologically active compounds in valerian and St. John's wort, *Biomol. Pharmacother.* 162 (2023), 114652, <https://doi.org/10.1016/j.biopha.2023.114652>.
- [16] D. Spiess, M. Winker, A. Chauveau, V.F. Abegg, O. Potterat, M. Hamburger, C. Gründemann, A.P. Simões-Wüst, Medicinal plants for the treatment of mental diseases in pregnancy: an in vitro safety assessment, *Planta Med.* 88 (2021) 1036–1046, <https://doi.org/10.1055/a-1628-8132>.
- [17] K. Cattoor, M. Bracke, D. Deforce, D. De Keukeleire, A. Heyerick, Transport of hop bitter acids across intestinal Caco-2 cell monolayers, *J. Agric. Food Chem.* 58 (2010) 4132–4140, <https://doi.org/10.1021/jf904079h>.
- [18] S.A. Poeker, A. Geirnaert, L. Berchtold, A. Greppi, L. Krych, R.E. Steinert, T. de Wouters, C. Lacroix, Understanding the prebiotic potential of different dietary fibers using an in vitro continuous adult fermentation model (PolyFermS), *Sci. Rep.* 8 (2018) 4318, <https://doi.org/10.1038/s41598-018-22438-y>.
- [19] J. Isenring, A. Geirnaert, A.R. Hall, C. Jans, C. Lacroix, M.J.A. Stevens, In vitro gut modeling as a tool for adaptive evolutionary engineering of *Lactiplantibacillus plantarum*, *mSystems* 6 (2021) e01085–20, <https://doi.org/10.1128/mSystems.01085-20>.
- [20] D. Spiess, V.F. Abegg, A. Chauveau, A. Treyer, M. Reinehr, M. Oufir, E. Duong, O. Potterat, M. Hamburger, A.P. Simões-Wüst, Placental passage of protopine in an ex vivo human perfusion system, *Planta Med.* 89 (2022) 194–207, <https://doi.org/10.1055/a-1829-9546>.
- [21] EMA, Guideline on Bioanalytical Method Validation, 2015. (https://www.ema.europa.eu/en/documents/scientific-guideline/guideline-bioanalytical-method-validation_en.pdf) (Accessed August 9, 2022).
- [22] F.D.A., Bioanalytical Method Validation Guidance for industry, 2018. (<https://www.fda.gov/regulatory-information/search-fda-guidance-documents/bioanalytical-method-validation-guidance-industry>) (Accessed August 9, 2022).
- [23] F. Tomè, M.L. Colombo, L. Caldiroli, A comparative investigation on alkaloid composition in different populations of *Eschscholzia californica* Cham, *Phytochem. Anal.* 10 (1999) 264–267, [https://doi.org/10.1002/\(SICI\)1099-1565\(199909/10\)10:5<264::AID-PCA469>3.0.CO;2-4](https://doi.org/10.1002/(SICI)1099-1565(199909/10)10:5<264::AID-PCA469>3.0.CO;2-4).
- [24] H. Stuppner, S. Sturm, N. Mulinacci, F. Vincieri, Capillary zone electrophoretic analysis of the main alkaloids from *Eschscholzia californica*, *Chromatographia* 37 (1993) 579–583, <https://doi.org/10.1007/BF02274105>.
- [25] D. Dahlgren, H. Lennernäs, Intestinal permeability and drug absorption: predictive experimental, computational and in vivo approaches, *Pharmaceutics* 11 (2019) 411, <https://doi.org/10.3390/pharmaceutics11080411>.
- [26] I. Hubatsch, E.G.E. Ragnarsson, P. Artursson, Determination of drug permeability and prediction of drug absorption in Caco-2 monolayers, *Nat. Protoc.* 2 (2007) 2111–2119, <https://doi.org/10.1038/nprot.2007.303>.
- [27] W. Huang, L. Kong, Y. Cao, L. Yan, Identification and quantification, metabolism and pharmacokinetics, pharmacological activities, and botanical preparations of protopine: a review, *Molecules* 27 (2022) 215, <https://doi.org/10.3390/molecules27010215>.

- [28] M. Ölander, J.R. Wiśniewski, P. Matsson, P. Lundquist, P. Artursson, The proteome of filter-grown Caco-2 cells with a focus on proteins involved in drug disposition, *J. Pharm. Sci.* 105 (2016) 817–827, <https://doi.org/10.1016/j.xphs.2015.10.030>.
- [29] C. Guo, Y. Jiang, L. Li, L. Hong, Y. Wang, Q. Shen, Y. Lou, H. Hu, H. Zhou, L. Yu, H. Jiang, S. Zeng, Application of a liquid chromatography–tandem mass spectrometry method to the pharmacokinetics, tissue distribution and excretion studies of *Dactylicapnos scandens* in rats, *J. Pharm. Biomed. Anal.* 74 (2013) 92–100, <https://doi.org/10.1016/j.jpba.2012.10.011>.
- [30] S.E. Pritchard, L. Marciari, K.C. Garsed, C.L. Hoad, W. Thongborisute, E. Roberts, P.A. Gowland, R.C. Spiller, Fasting and postprandial volumes of the undisturbed colon: normal values and changes in diarrhea-predominant irritable bowel syndrome measured using serial MRI, *Neurogastroenterol. Motil.* 26 (2014) 124–130, <https://doi.org/10.1111/nmo.12243>.
- [31] E.R. Kim, P.-L. Rhee, How to interpret a functional or motility test - Colon transit study, *J. Neurogastroenterol. Motil.* 18 (2012) 94–99, <https://doi.org/10.5056/jnm.2012.18.1.94>.
- [32] J. Isenring, L. Bircher, A. Geirnaert, C. Lacroix, In vitro human gut microbiota fermentation models: opportunities, challenges, and pitfalls, *Microbiome Res. Rep.* 2 (2023) 2, <https://doi.org/10.20517/mrr.2022.15>.
- [33] MSD, Calculators: Total Body Water in Men (Watson formula), 2022. (<https://www.msmanuals.com/professional/multimedia/clinical-calculator/total-body-water-in-men-watson-formula>) (Accessed April 11, 2023).
- [34] P.E. Watson, I.D. Watson, R.D. Batt, Total body water volumes for adult males and females estimated from simple anthropometric measurements, *Am. J. Clin. Nutr.* 33 (1980) 27–39, <https://doi.org/10.1093/ajcn/33.1.27>.
- [35] P. Huang, Z.-Y. Cheng, S.-J. Zhang, Z.-L. Tian, J.-G. Sun, Z.-Y. Zeng, Liu, Biotransformation and tissue distribution of protopine and allocryptopine and effects of plume poppy total alkaloid on liver drug-metabolizing enzymes, *Sci. Rep.* 8 (2018) 537, <https://doi.org/10.1038/s41598-017-18816-7>.

4 Conclusions and outlook

In this work, an assessment of intestinal absorption and gut microbiota interactions of pharmacologically relevant constituents from herbal medicines used commonly to treat depressive, anxiety and sleeping disorders, was conducted. Intestinal permeability of valerenic acid from valerian, hyperforin and hypericin from St. John's wort, as well as, californidine, escholtzine and protopine from California poppy, was studied by means of Caco-2 cell monolayers, as a model of the human small intestine. In addition, gut microbiota interactions of these herbal constituents, namely their possible microbiota-mediated biotransformation or the impact of these herbal compounds and extracts exposure on microbiota metabolic activity (production of SCFAs) and bacterial viability, were investigated with batch fermentation experiments with two *in vitro* human gut microbiota (PolyFermS) derived from a different healthy adult female fecal donor. Furthermore, the contents of alkaloids californidine, escholtzine and protopine were determined in eight commercial preparations of California poppy sold as phytomedicines or food supplements. Selective and sensitive UHPLC-MS/MS methods were developed and validated for each compound, to analyze Caco-2, microbiota and California poppy product samples.

Valerenic acid showed a P_{appAB} of 199×10^{-6} cm/s and a P_{appBA} of 60.4×10^{-6} cm/s, with an ER of 0.3. This suggests that valerenic acid is highly absorbed in the small intestine, and possibly with the involvement of a carrier-mediated uptake mechanism. Also, the low recovery values of 43 – 69 % obtained in the Caco-2 assay support that the compound is possibly metabolized in Caco-2 cells. Phase II metabolizing enzymes including UDP-glucuronosyltransferases, sulfotransferases or glutathione S-transferases are highly expressed in Caco-2 cells, in contrast to phase I enzymes [58]. Hepatic phase I and phase II metabolism of valerenic acid was shown in isolated perfused rat livers [149], and in pooled human liver microsomes (Manuscript in preparation). In addition, an absolute bioavailability of 34%, and an extensive first-pass metabolism of valerenic acid was reported in a pharmacokinetic study with rats [132]. Whether an intestinal metabolism contributes to the first pass metabolism of valerenic acid, deserves to be further investigated, using complementary *in vitro* systems such as human intestinal microsomes, that express both phase I and phase II enzymes [150]. As a highly permeable compound in the Caco-2 cell model, there is a low chance for valerenic acid to reach the colon at relevant concentrations. However, compounds absorbed in the small intestine can possibly undergo enterohepatic circulation [109,151]. While *in vitro* data in rats have shown that valerenic acid and their hepatic metabolites were excreted through the hepatobiliary pathway [149], a pharmacokinetic study in rats have suggested that valerenic acid underwent enterohepatic recycling, due to a pharmacokinetic profile in multiple peaks [132]. Valerenic acid was stable in batch fermentation experiments, ruling out microbiota-mediated metabolism. Whether valerenic acid conjugates produced in the liver and excreted via the biliary duct can be converted back into valerenic acid by the gut microbiota, remains to be further investigated.

For hyperforin, a P_{appAB} of 4.76×10^{-6} cm/s, a P_{appBA} of 6.38×10^{-6} cm/s and an ER of 1.3 were found, suggesting a high permeability in the small intestine, with a transport by transcellular passive diffusion.

For hypericin, a P_{appAB} of 0.48×10^{-6} cm/s, a P_{appBA} of 0.39×10^{-6} cm/s and an ER of 1.2, suggest a low-to-moderate absorption in the small intestine, with transcellular passive diffusion as permeation mechanism. These findings are in accordance with previous *in vitro* permeability data [139–141] and with a previous pharmacokinetic study in two volunteers that reported a low absolute bioavailability (14%) for hypericin [138]. Thus, unlike hyperforin, there is a high potential for relevant concentrations of hypericin to be found in the colon. Incubation experiments with the artificial human microbiota showed that a metabolism by gut bacteria is not to be expected, for both compounds. At the moment, it cannot be excluded that hyperforin and hypericin metabolites interact with the gut microbiota, given the absence of data regarding their excretion routes.

For californidine, P_{appAB} , P_{appBA} and ER were of 0.58×10^{-6} cm/s, 4.93×10^{-6} cm/s, and 8.6, respectively, which suggests that it is low-to-moderately absorbed in the human small intestine, and that an efflux transporter protein may be involved in its permeation. The low-to-moderate intestinal absorption and possible luminal efflux support that relevant concentrations of californidine might be found in the colon, increasing its potential for interacting with the gut microbiota. Californidine was stable in the artificial gut microbiota, excluding its microbiota-mediated biotransformation. For escholtzine and protopine, P_{appAB} , P_{appBA} and ER were of 82.5×10^{-6} cm/s, 175×10^{-6} cm/s, 2.1, and 39.2×10^{-6} cm/s, 144×10^{-6} cm/s, 3.7, respectively. These values suggest, for both compounds, a high intestinal permeability, with the involvement of an efflux carrier-mediated transporter. Also, the low recovery values for escholtzine (38 – 54%) and protopine (13 – 39%) pointed to a possible metabolization of both alkaloids in the Caco-2 cells. Phase I and phase II (glucuronide conjugates) metabolites of protopine were detected in urine, feces and cecal contents in rats following oral administration of protopine [152]. Whether a metabolism in the gut wall plays a role in the disposition of protopine, needs to be verified in further experiments. The permeability data obtained for escholtzine and protopine, which suggests a high absorption in the small intestine, primarily support that a contact between both alkaloids and the gut microbiota is unlikely. However, if a luminal efflux is confirmed for both alkaloids by means of experiments with appropriate inhibitors of efflux transporter proteins, there may be a potential for both compounds to reach higher levels in the colon. Escholtzine and protopine were found to be very stable in batch fermentation experiments suggesting that these are not metabolized by colonic bacteria. Excretion studies in rats found that protopine was mainly excreted in a metabolized form [148]. Given the absence of data regarding the excretion routes for both compounds, it cannot be ruled out that their potential metabolites interact with the gut microbiota.

One should emphasize that herbal medicines are multicomponent mixtures of active, partially active or inactive compounds that can possibly influence one another's bioavailability [153]. This synergistic effect was observed for hypericin, in which flavonoids from St. John's wort increased its intestinal permeability *in vitro* [141,154]; an effect that was confirmed in a pharmacokinetic study in rats [155]. In absence of data for valerianic acid, hyperforin, californidine, escholtzine and protopine, one cannot

exclude that other constituents of the corresponding herbal extract would influence their intestinal permeability. Further investigations on this are warranted.

Herbal compounds and extracts were not found to markedly impact the metabolism of microbial SCFAs in short-term (24 h) batch fermentation experiments. This implies that valerian, St. John's wort and California poppy, at the tested concentrations, do not have an indirect influence on the CNS via the modulation of the microbiota-gut-brain axis, at least not through modification of SCFAs metabolism. Moreover, the bacterial viability was not markedly affected by the exposure of the herbal compounds or extracts. These data support that at the tested concentrations, the metabolic activity and viability of the gut microbiome is not affected by the exposure of herbal extracts and compounds, supporting a safe use of these herbal extracts from a microbiome balance perspective. Nonetheless, in contrast to herbal compounds, the assayed concentrations of herbal extracts (0.5 mg/mL) were lower in comparison to the maximum colonic concentrations possibly reached in a day, upon ingestion of extracts of valerian (maximum 3 mg/mL), St. John's wort (maximum to 1.7 mg/mL) or California poppy (maximum 2.1 mg/mL). Thus, an impact of the herbal drugs on the microbial metabolic activity and bacterial viability cannot be excluded at this point. Moreover, given the high interindividual variabilities in gut microbiota, a higher number of experiments with several PolyFermS from different fecal donors is warranted. Lastly, the use of PolyFermS operated as a continuous fermentation model, would enable to assess if a prolonged exposure to the herbal compound and extracts, affects the gut microbiome metabolic activity and bacterial viability.

Further investigation of the impact of herbal compounds or extracts on the microbial metabolism of other important molecules (including vitamins, choline or purines), or on the taxonomic composition of the gut microbiome, would complete the assessment of gut microbiota interactions [81,107]. A recent study found that the polyphenol fraction of St John's wort (at relevant concentrations) stimulated the growth of beneficial gut microbial strains (*Lactiplantibacillus plantarum* and *Saccharomyces boulardii*), in isolated cultures [156]. St. John's wort extract did not affect the total bacterial growth in our batch fermentation experiments. While the use of isolated gut bacterial strains is suitable for identifying pathways, this approach does not offer the high bacterial diversity, high bacterial abundance and the presence of metabolic cross-feeding mechanisms provided by *in vitro* fermentation models [121].

UHPLC-MS/MS analysis of the eight commercial preparations of California poppy (consisting of dry powders, dry extracts or fluid extracts of flowering aerial parts of California poppy), revealed high variabilities of alkaloid contents, ranging from 0.13 to 2.55 mg/g for californidine, 0.05 to 0.63 mg/g for escholtzine and 0.008 to 0.200 mg/g for protopine. Different extraction techniques of the preparations might partly account for these high variations. From these data and the manufacturer directions, the possible maximum daily ingested contents were calculated to be 0.16 – 2.97 mg/day (californidine), 0.10 – 1.11 mg/day (escholtzine) and 0.02 – 0.31 mg/day (protopine). Thus, maximum intake in alkaloids can vary extensively in patients using different California poppy products.

In summary, valerenic acid, hyperforin, escholtzine and protopine were highly permeable in the Caco-2 cell model, whereas californidine and hypericin were low-to-moderately permeable, suggesting that the latter herbal compounds have a higher potential for interacting with the colonic gut microbiota. Batch fermentation experiments showed that all herbal compounds were not metabolized by the two *in vitro* gut microbiota (PolyFermS) over 24 h, suggesting that the gut microbiome does not impact their disposition. In addition, the overall impact of herbal compounds and extracts on the microbial metabolism of SCFAs or on the bacterial viability was minimal, supporting that short-term exposure of valerian, St. John's wort and California poppy do not exert an indirect effect on the CNS function via the modulation of SCFAs, which are important modulators of the microbiota-gut-brain axis. These data suggest that the use of valerian, St. John's wort and California poppy, at the tested concentrations, may not influence the metabolic activity and the bacterial viability of the gut microbiome, at least in short-term exposure. Further experiments with a larger number of *in vitro* gut microbiota and with continuous fermentation experiments, would ensure to take into account interindividual differences and an impact of a long-term exposure.

References

- [1] J. Caldwell, I. Gardner, N. Swales, An introduction to drug disposition: The basic principles of absorption, distribution, metabolism, and excretion, *Toxicol. Pathol.* 23 (1995) 102–114. <https://doi.org/10.1177/019262339502300202>.
- [2] K. Thelen, J.B. Dressman, Cytochrome P450-mediated metabolism in the human gut wall, *J. Pharm. Pharmacol.* 61 (2009) 541–558. <https://doi.org/10.1211/jpp.61.05.0002>.
- [3] E.H. Kerns, L. Di, *Drug-like properties: Concepts, structure design and methods*, 2008.
- [4] M.E. Soliman, A.T. Adewumi, O.B. Akawa, T.I. Subair, F.O. Okunlola, O.E. Akinsuku, S. Khan, Simulation models for prediction of bioavailability of medicinal drugs—the interface between experiment and computation, *AAPS PharmSciTech.* 23 (2022) 86. <https://doi.org/10.1208/s12249-022-02229-5>.
- [5] M. Azman, A.H. Sabri, Q.K. Anjani, M.F. Mustafa, K.A. Hamid, Intestinal absorption study: Challenges and absorption enhancement strategies in improving oral drug delivery, *Pharmaceuticals.* 15 (2022) 975. <https://doi.org/10.3390/ph15080975>.
- [6] J.N. Chu, G. Traverso, Foundations of gastrointestinal-based drug delivery and future developments, *Nat. Rev. Gastroenterol. Hepatol.* 19 (2022) 219–238. <https://doi.org/10.1038/s41575-021-00539-w>.
- [7] A. Dahan, I. González-Álvarez, Regional intestinal drug absorption: Biopharmaceutics and drug formulation, *Pharmaceutics.* 13 (2021) 272. <https://doi.org/10.3390/pharmaceutics13020272>.
- [8] Small intestine | Digestive function, structure & length | Encyclopaedia Britannica, (2023). <https://www.britannica.com/science/small-intestine> (accessed August 8, 2023).
- [9] S. Hua, Advances in oral drug delivery for regional targeting in the gastrointestinal tract - Influence of physiological, pathophysiological and pharmaceutical Factors, *Front. Pharmacol.* 11 (2020). <https://www.frontiersin.org/articles/10.3389/fphar.2020.00524> (accessed July 13, 2023).
- [10] M. Vertzoni, P. Augustijns, M. Grimm, M. Koziol, G. Lemmens, N. Parrott, C. Pentafragka, C. Reppas, J. Rubbens, J. Van Den Abeele, T. Vanuytsel, W. Weitschies, C.G. Wilson, Impact of regional differences along the gastrointestinal tract of healthy adults on oral drug absorption: An UNGAP review, *Eur. J. Pharm. Sci.* 134 (2019) 153–175. <https://doi.org/10.1016/j.ejps.2019.04.013>.
- [11] P.A. Blaker, P. Irving, Physiology and function of the small intestine, in: *Advanced Nutrition and Dietetics in Gastroenterology*, John Wiley & Sons, Ltd, 2014: pp. 21–27. <https://doi.org/10.1002/9781118872796.ch1.4>.
- [12] Y.N. Kallis, D. Westaby, Physiology and function of the pancreas, in: *Advanced Nutrition and Dietetics in Gastroenterology*, John Wiley & Sons, Ltd, 2014: pp. 33–35. <https://doi.org/10.1002/9781118872796.ch1.6>.
- [13] Y.N. Kallis, D. Westaby, Physiology and function of the hepatobiliary tract, in: *Advanced Nutrition and Dietetics in Gastroenterology*, John Wiley & Sons, Ltd, 2014: pp. 36–40. <https://doi.org/10.1002/9781118872796.ch1.7>.
- [14] P.R. Kiela, F.K. Ghishan, Physiology of intestinal absorption and secretion, *Best Pract. Res. Clin. Gastroenterol.* 30 (2016) 145–159. <https://doi.org/10.1016/j.bpg.2016.02.007>.
- [15] E.V. Carrington, S.M. Scott, Physiology and function of the colon, in: *Advanced Nutrition and Dietetics in Gastroenterology*, John Wiley & Sons, Ltd, 2014: pp. 28–32. <https://doi.org/10.1002/9781118872796.ch1.5>.
- [16] M. Vancamelbeke, S. Vermeire, The intestinal barrier: A fundamental role in health and disease, *Expert Rev. Gastroenterol. Hepatol.* 11 (2017) 821–834. <https://doi.org/10.1080/17474124.2017.1343143>.
- [17] M. Herath, S. Hosie, J.C. Bornstein, A.E. Franks, E.L. Hill-Yardin, The role of the gastrointestinal mucus system in intestinal homeostasis: Implications for neurological disorders, *Front. Cell.*

- Infect. Microbiol. 10 (2020). <https://www.frontiersin.org/articles/10.3389/fcimb.2020.00248> (accessed July 19, 2023).
- [18] M. Camilleri, B.J. Lyle, K.L. Madsen, J. Sonnenburg, K. Verbeke, G.D. Wu, Role for diet in normal gut barrier function: Developing guidance within the framework of food-labeling regulations, *Am. J. Physiol. - Gastrointest. Liver Physiol.* 317 (2019) G17–G39. <https://doi.org/10.1152/ajpgi.00063.2019>.
- [19] K.R. Groschwitz, S.P. Hogan, Intestinal barrier function: molecular regulation and disease pathogenesis, *J. Allergy Clin. Immunol.* 124 (2009) 3–20; quiz 21–22. <https://doi.org/10.1016/j.jaci.2009.05.038>.
- [20] L.W. Peterson, D. Artis, Intestinal epithelial cells: Regulators of barrier function and immune homeostasis, *Nat. Rev. Immunol.* 14 (2014) 141–153. <https://doi.org/10.1038/nri3608>.
- [21] T.K. Noah, B. Donahue, N.F. Shroyer, Intestinal development and differentiation, *Exp. Cell Res.* 317 (2011) 2702–2710. <https://doi.org/10.1016/j.yexcr.2011.09.006>.
- [22] W.W. Agace, K.D. McCoy, Regionalized development and maintenance of the intestinal adaptive immune landscape, *Immunity.* 46 (2017) 532–548. <https://doi.org/10.1016/j.immuni.2017.04.004>.
- [23] L. González-Mariscal, ed., *Tight junctions*, Springer International Publishing, Cham, 2022. <https://doi.org/10.1007/978-3-030-97204-2>.
- [24] P.R. Kvietyts, Transcapillary solute exchange, in: *The gastrointestinal circulation*, Morgan & Claypool Life Sciences, 2010. <https://www.ncbi.nlm.nih.gov/books/NBK53097/> (accessed July 24, 2023).
- [25] E. Cocucci, J.Y. Kim, Y. Bai, N. Pabla, Role of passive diffusion, transporters, and membrane trafficking-mediated processes in cellular drug transport, *Clin. Pharmacol. Ther.* 101 (2017) 121–129. <https://doi.org/10.1002/cpt.545>.
- [26] K. Sugano, M. Kansy, P. Artursson, A. Avdeef, S. Bendels, L. Di, G.F. Ecker, B. Faller, H. Fischer, G. Gerebtzoff, H. Lennernaes, F. Senner, Coexistence of passive and carrier-mediated processes in drug transport, *Nat. Rev. Drug Discov.* 9 (2010) 597–614. <https://doi.org/10.1038/nrd3187>.
- [27] W.S. Trimble, S. Grinstein, Barriers to the free diffusion of proteins and lipids in the plasma membrane, *J. Cell Biol.* 208 (2015) 259–271. <https://doi.org/10.1083/jcb.201410071>.
- [28] Tissue | Molecular view of the cell membrane | Encyclopædia Britannica, (2023). <https://www.britannica.com/science/tissue#/media/1/342838/45550> (accessed October 10, 2023).
- [29] A. Horowitz, S.D. Chanez-Paredes, X. Haest, J.R. Turner, Paracellular permeability and tight junction regulation in gut health and disease, *Nat. Rev. Gastroenterol. Hepatol.* 20 (2023) 417–432. <https://doi.org/10.1038/s41575-023-00766-3>.
- [30] A. Buckley, J.R. Turner, Cell biology of tight junction barrier regulation and mucosal disease, *Cold Spring Harb. Perspect. Biol.* 10 (2018) a029314. <https://doi.org/10.1101/cshperspect.a029314>.
- [31] A.G. Roberts, The structure and mechanism of drug transporters, in: S. Nagar, U.A. Argikar, D. Tweedie (Eds.), *Enzyme kinetics in drug metabolism: Fundamentals and applications*, Springer US, New York, NY, 2021: pp. 193–234. https://doi.org/10.1007/978-1-0716-1554-6_8.
- [32] M. Harwood, M. Zhang, S. Pathak, S. Neuhoff, The regional-specific relative and absolute expression of gut transporters in adult Caucasians: A meta-analysis, *Drug Metab. Dispos.* (2019). <https://doi.org/10.1124/dmd.119.086959>.
- [33] X. Liang, K.M. Staiger, E. Riddle, J. Hao, Y. Lai, Chapter 10 - Role of transporters in drug disposition and drug-drug interactions, in: S. Ma, S.K. Chowdhury (Eds.), *Identification and quantification of drugs, metabolites, drug metabolizing enzymes, and transporters* (Second Edition), Elsevier, Amsterdam, 2020: pp. 311–337. <https://doi.org/10.1016/B978-0-12-820018-6.00010-7>.
- [34] K.M. Giacomini, S.-M. Huang, D.J. Tweedie, L.Z. Benet, K.L.R. Brouwer, X. Chu, A. Dahlin, R. Evers, V. Fischer, K.M. Hillgren, K.A. Hoffmaster, T. Ishikawa, D. Keppler, R.B. Kim, C.A. Lee,

- M. Niemi, J.W. Polli, Y. Sugiyama, P.W. Swaan, J.A. Ware, S.H. Wright, S. Wah Yee, M.J. Zamek-Gliszczynski, L. Zhang, The international transporter consortium, membrane transporters in drug development, *Nat. Rev. Drug Discov.* 9 (2010) 215–236. <https://doi.org/10.1038/nrd3028>.
- [35] M.J. Zamek-Gliszczynski, M.E. Taub, P.P. Chothe, X. Chu, K.M. Giacomini, R.B. Kim, A.S. Ray, S.L. Stocker, J.D. Unadkat, M.B. Wittwer, C. Xia, S.-W. Yee, L. Zhang, Y. Zhang, I.T. Consortium, Transporters in drug development: 2018 ITC recommendations for transporters of emerging clinical importance, *Clin. Pharmacol. Ther.* 104 (2018) 890–899. <https://doi.org/10.1002/cpt.1112>.
- [36] M. Drozdziak, C. Gröer, J. Penski, J. Lapczuk, M. Ostrowski, Y. Lai, B. Prasad, J.D. Unadkat, W. Siegmund, S. Oswald, Protein abundance of clinically relevant multidrug transporters along the entire length of the human intestine, *Mol. Pharm.* 11 (2014) 3547–3555. <https://doi.org/10.1021/mp500330y>.
- [37] J. König, F. Müller, M.F. Fromm, Transporters and drug-drug interactions: Important determinants of drug disposition and effects, *Pharmacol. Rev.* 65 (2013) 944–966. <https://doi.org/10.1124/pr.113.007518>.
- [38] W. Kramer, Transporters, Trojan horses and therapeutics: suitability of bile acid and peptide transporters for drug delivery, *Biol. Chem.* 392 (2011) 77–94. <https://doi.org/10.1515/bc.2011.017>.
- [39] S.W. Yee, D.J. Brackman, E.A. Ennis, Y. Sugiyama, L.K. Kamdem, R. Blanchard, A. Galetin, L. Zhang, K.M. Giacomini, Influence of transporter polymorphisms on drug disposition and response: A perspective from the international transporter consortium, *Clin. Pharmacol. Ther.* 104 (2018) 803–817. <https://doi.org/10.1002/cpt.1098>.
- [40] C.R. Jones, O.J.D. Hatley, A.-L. Ungell, C. Hilgendorf, S.A. Peters, A. Rostami-Hodjegan, Gut wall metabolism. Application of pre-clinical models for the prediction of human drug absorption and first-pass elimination, *AAPS J.* 18 (2016) 589–604. <https://doi.org/10.1208/s12248-016-9889-y>.
- [41] R. Iswandana, M.I. Irianti, D. Oosterhuis, H.S. Hofker, M.T. Merema, M.H. de Jager, H.A.M. Mutsaers, P. Olinga, Regional differences in human intestinal drug metabolism, *Drug Metab. Dispos.* 46 (2018) 1879–1885. <https://doi.org/10.1124/dmd.118.083428>.
- [42] S.A. Peters, C.R. Jones, A.-L. Ungell, O.J.D. Hatley, Predicting drug extraction in the human gut wall: Assessing contributions from drug metabolizing enzymes and transporter proteins using preclinical models, *Clin. Pharmacokinet.* 55 (2016) 673–696. <https://doi.org/10.1007/s40262-015-0351-6>.
- [43] G. Clarke, K.V. Sandhu, B.T. Griffin, T.G. Dinan, J.F. Cryan, N.P. Hyland, Gut reactions: Breaking down xenobiotic-microbiome interactions, *Pharmacol. Rev.* 71 (2019) 198–224. <https://doi.org/10.1124/pr.118.015768>.
- [44] V.J. Wacher, L. Salphati, L.Z. Benet, Active secretion and enterocytic drug metabolism barriers to drug absorption, *Adv. Drug Deliv. Rev.* 46 (2001) 89–102. [https://doi.org/10.1016/s0169-409x\(00\)00126-5](https://doi.org/10.1016/s0169-409x(00)00126-5).
- [45] F. Xie, X. Ding, Q.-Y. Zhang, An update on the role of intestinal cytochrome P450 enzymes in drug disposition, *Acta Pharm. Sin. B.* 6 (2016) 374–383. <https://doi.org/10.1016/j.apsb.2016.07.012>.
- [46] K. Yoshida, P. Zhao, L. Zhang, D.R. Abernethy, D. Rekić, K.S. Reynolds, A. Galetin, S.-M. Huang, *In vitro–in vivo* extrapolation of metabolism- and transporter-mediated drug–drug interactions—Overview of basic prediction methods, *J. Pharm. Sci.* 106 (2017) 2209–2213. <https://doi.org/10.1016/j.xphs.2017.04.045>.
- [47] P. Stenberg, U. Norinder, K. Luthman, P. Artursson, Experimental and computational screening models for the prediction of intestinal drug absorption, *J. Med. Chem.* 44 (2001) 1927–1937. <https://doi.org/10.1021/jm001101a>.

- [48] I. Hubatsch, E.G.E. Ragnarsson, P. Artursson, Determination of drug permeability and prediction of drug absorption in Caco-2 monolayers, *Nat. Protoc.* 2 (2007) 2111–2119. <https://doi.org/10.1038/nprot.2007.303>.
- [49] T. Lea, Caco-2 cell line, in: K. Verhoeckx, P. Cotter, I. López-Expósito, C. Kleiveland, T. Lea, A. Mackie, T. Requena, D. Swiatecka, H. Wichers (Eds.), *The impact of food bioactives on health: In vitro and ex vivo models*, Springer International Publishing, Cham, 2015: pp. 103–111. https://doi.org/10.1007/978-3-319-16104-4_10.
- [50] J. Fogh, J. Fogh, T. Orfeo, One hundred and twenty-seven cultured human tumor cell lines producing tumors in nude mice, *J. Natl. Cancer Inst.* 59 (1977). <https://doi.org/10.1093/jnci/59.1.221>.
- [51] J. Fogh, W.C. Wright, J.D. Loveless, Absence of HeLa cell contamination in 169 cell lines derived from human tumors, *J. Natl. Cancer Inst.* 58 (1977) 209–214. <https://doi.org/10.1093/jnci/58.2.209>.
- [52] M. Pinto, Enterocyte-like differentiation and polarization of the human colon carcinoma cell line Caco-2 cell culture, *Biol. Cell.* 47 (1983) 323–330.
- [53] R.T. Borchardt, Hidalgo, I. J., Raub, T. J., and Borchardt, R. T.: Characterization of the human colon carcinoma cell line (Caco-2) as a model system for intestinal epithelial permeability, *Gastroenterology*, 96, 736–749, 1989—The backstory, *AAPS J.* 13 (2011) 323–327. <https://doi.org/10.1208/s12248-011-9283-8>.
- [54] I.J. Hidalgo, T.J. Raub, R.T. Borchardt, Characterization of the human colon carcinoma cell line (Caco-2) as a model system for intestinal epithelial permeability, *Gastroenterology*. 96 (1989) 736–749.
- [55] D.J. Brayden, Per Artursson’s major contributions to the Caco-2 Cell literature in pharmaceutical sciences, *J. Pharm. Sci.* 110 (2021) 12–16. <https://doi.org/10.1016/j.xphs.2020.08.016>.
- [56] P. Artursson, Epithelial transport of drugs in cell culture. I: A model for studying the passive diffusion of drugs over intestinal absorptive (Caco-2) cells, *J. Pharm. Sci.* 79 (1990) 476–482. <https://doi.org/10.1002/jps.2600790604>.
- [57] P. Artursson, J. Karlsson, Correlation between oral drug absorption in humans and apparent drug permeability coefficients in human intestinal epithelial (Caco-2) cells, *Biochem. Biophys. Res. Commun.* 175 (1991) 880–885. [https://doi.org/10.1016/0006-291X\(91\)91647-U](https://doi.org/10.1016/0006-291X(91)91647-U).
- [58] M. Ölander, J.R. Wiśniewski, P. Matsson, P. Lundquist, P. Artursson, The proteome of filter-grown Caco-2 cells with a focus on proteins involved in drug disposition, *J. Pharm. Sci.* 105 (2016) 817–827. <https://doi.org/10.1016/j.xphs.2015.10.030>.
- [59] T. Takenaka, N. Harada, J. Kuze, M. Chiba, T. Iwao, T. Matsunaga, Human small intestinal epithelial cells differentiated from adult intestinal stem cells as a novel system for predicting oral drug absorption in humans, *Drug Metab. Dispos.* 42 (2014) 1947–1954. <https://doi.org/10.1124/dmd.114.059493>.
- [60] B. Srinivasan, A.R. Kolli, M.B. Esch, H.E. Abaci, M.L. Shuler, J.J. Hickman, TEER measurement techniques for *in vitro* barrier model systems, *J. Lab. Autom.* 20 (2015) 107–126. <https://doi.org/10.1177/2211068214561025>.
- [61] Y. Uchida, S. Ohtsuki, J. Kamiie, K. Ohmine, R. Iwase, T. Terasaki, Quantitative targeted absolute proteomics for 28 human transporters in plasma membrane of Caco-2 cell monolayer cultured for 2, 3, and 4 weeks, *Drug Metab. Pharmacokinet.* 30 (2015) 205–208. <https://doi.org/10.1016/j.dmpk.2014.11.002>.
- [62] G. Englund, F. Rorsman, A. Rönnblom, U. Karlbom, L. Lazorova, J. Gråsjö, A. Kindmark, P. Artursson, Regional levels of drug transporters along the human intestinal tract: Co-expression of ABC and SLC transporters and comparison with Caco-2 cells, *Eur. J. Pharm. Sci.* 29 (2006) 269–277. <https://doi.org/10.1016/j.ejps.2006.04.010>.
- [63] S. Tavelin, J. Gråsjö, J. Taipalensuu, G. Ocklind, P. Artursson, Applications of epithelial cell culture in studies of drug transport, in: *Epithelial cell culture protocols*, Humana Press, New Jersey, 2002: pp. 233–272. <https://doi.org/10.1385/1-59259-185-X:233>.

- [64] C.A.S. Bergström, M. Strafford, L. Lazorova, A. Avdeef, K. Luthman, P. Artursson, Absorption classification of oral drugs based on molecular surface properties, *J. Med. Chem.* 46 (2003) 558–570. <https://doi.org/10.1021/jm020986i>.
- [65] S. Neuhoff, P. Artursson, A.-L. Ungell, Advantages and disadvantages of using bovine serum albumin and/or Cremophor EL as extracellular additives during transport studies of lipophilic compounds across Caco-2 monolayers, *J. Drug Deliv. Sci. Technol.* 17 (2007) 259–266. [https://doi.org/10.1016/S1773-2247\(07\)50093-6](https://doi.org/10.1016/S1773-2247(07)50093-6).
- [66] P. Artursson, K. Palm, K. Luthman, Caco-2 monolayers in experimental and theoretical predictions of drug transport, *Adv. Drug Deliv. Rev.* 64 (2012) 280–289. <https://doi.org/10.1016/j.addr.2012.09.005>.
- [67] C.A. Lipinski, F. Lombardo, B.W. Dominy, P.J. Feeney, Experimental and computational approaches to estimate solubility and permeability in drug discovery and development settings, *Adv. Drug Deliv. Rev.* 23 (1997) 3–25. [https://doi.org/10.1016/S0169-409X\(96\)00423-1](https://doi.org/10.1016/S0169-409X(96)00423-1).
- [68] M.D. Shultz, Two decades under the Influence of the rule of five and the changing properties of approved oral drugs, *J. Med. Chem.* 62 (2019) 1701–1714. <https://doi.org/10.1021/acs.jmedchem.8b00686>.
- [69] R.J. Young, P.D. Leeson, Mapping the efficiency and physicochemical trajectories of successful optimizations, *J. Med. Chem.* 61 (2018) 6421–6467. <https://doi.org/10.1021/acs.jmedchem.8b00180>.
- [70] Y. Xu, N. Shrestha, V. Pr at, A. Beloqui, An overview of *in vitro*, *ex vivo* and *in vivo* models for studying the transport of drugs across intestinal barriers, *Adv. Drug Deliv. Rev.* 175 (2021) 113795. <https://doi.org/10.1016/j.addr.2021.05.005>.
- [71] H. Almeida, A.C.F. Vieira, J. Teixeira, M.J. Gomes, P. Barrocas, T. Vasconcelos, B. Sarmento, Cell-based intestinal *in vitro* models for drug absorption screening, in: F.J. Hock, M.R. Gralinski, M.K. Pugsley (Eds.), *Drug discovery and evaluation: Safety and pharmacokinetic assays*, Springer International Publishing, Cham, 2022: pp. 1–22. https://doi.org/10.1007/978-3-030-73317-9_94-1.
- [72] I.V. Hartung, B.R. Huck, A. Crespo, Rules were made to be broken, *Nat. Rev. Chem.* 7 (2023) 3–4. <https://doi.org/10.1038/s41570-022-00451-0>.
- [73] C.A.S. Bergstr m, *In silico* predictions of drug solubility and permeability: two rate-limiting barriers to oral drug absorption, *Basic Clin. Pharmacol. Toxicol.* 96 (2005) 156–161. <https://doi.org/10.1111/j.1742-7843.2005.pto960303.x>.
- [74] P. Matsson, C.A.S. Bergstr m, N. Nagahara, S. Tavelin, U. Norinder, P. Artursson, Exploring the role of different drug transport routes in permeability screening, *J. Med. Chem.* 48 (2005) 604–613. <https://doi.org/10.1021/jm049711o>.
- [75] P.V. Balimane, S. Chong, R.A. Morrison, Current methodologies used for evaluation of intestinal permeability and absorption, *J. Pharmacol. Toxicol. Methods.* 44 (2000) 301–312. [https://doi.org/10.1016/S1056-8719\(00\)00113-1](https://doi.org/10.1016/S1056-8719(00)00113-1).
- [76] J.D. Irvine, L. Takahashi, K. Lockhart, J. Cheong, J.W. Tolan, H.E. Selick, J.R. Grove, MDCK (Madin–Darby canine kidney) cells: A tool for membrane permeability screening, *J. Pharm. Sci.* 88 (1999) 28–33. <https://doi.org/10.1021/js9803205>.
- [77] S. Tavelin, J. Taipalensuu, F. Hallb ock, K.-S. Vellonen, V. Moore, P. Artursson, An improved cell culture model based on 2/4/A1 cell monolayers for studies of intestinal drug transport: characterization of transport routes, *Pharm. Res.* 20 (2003) 373–381. <https://doi.org/10.1023/a:1022643802296>.
- [78] S. Youhanna, V.M. Lauschke, The past, present and future of intestinal *in vitro* cell systems for drug absorption studies, *J. Pharm. Sci.* 110 (2021) 50–65. <https://doi.org/10.1016/j.xphs.2020.07.001>.
- [79] Y.L. Franco, L. Da Silva, R. Cristofolletti, Navigating through cell-based *in vitro* models available for prediction of intestinal permeability and metabolism: Are we ready for 3D?, *AAPS J.* 24 (2021) 2. <https://doi.org/10.1208/s12248-021-00665-y>.

- [80] E. Thursby, N. Juge, Introduction to the human gut microbiota, *Biochem. J.* 474 (2017) 1823–1836. <https://doi.org/10.1042/BCJ20160510>.
- [81] A.E. Lindell, M. Zimmermann-Kogadeeva, K.R. Patil, Multimodal interactions of drugs, natural compounds and pollutants with the gut microbiota, *Nat. Rev. Microbiol.* 20 (2022) 431–443. <https://doi.org/10.1038/s41579-022-00681-5>.
- [82] S.M. Tsunoda, C. Gonzales, A.K. Jarmusch, J.D. Momper, J.D. Ma, Contribution of the gut microbiome to drug disposition, pharmacokinetic and pharmacodynamic variability, *Clin. Pharmacokinet.* 60 (2021) 971–984. <https://doi.org/10.1007/s40262-021-01032-y>.
- [83] R. Sender, S. Fuchs, R. Milo, Revised estimates for the number of human and bacteria cells in the body, *PLoS Biol.* 14 (2016) e1002533. <https://doi.org/10.1371/journal.pbio.1002533>.
- [84] J. Qin, R. Li, J. Raes, M. Arumugam, K.S. Burgdorf, C. Manichanh, T. Nielsen, N. Pons, F. Levenez, T. Yamada, D.R. Mende, J. Li, J. Xu, S. Li, D. Li, J. Cao, B. Wang, H. Liang, H. Zheng, Y. Xie, J. Tap, P. Lepage, M. Bertalan, J.-M. Batto, T. Hansen, D. Le Paslier, A. Linneberg, H.B. Nielsen, E. Pelletier, P. Renault, T. Sicheritz-Ponten, K. Turner, H. Zhu, C. Yu, S. Li, M. Jian, Y. Zhou, Y. Li, X. Zhang, S. Li, N. Qin, H. Yang, J. Wang, S. Brunak, J. Doré, F. Guarner, K. Kristiansen, O. Pedersen, J. Parkhill, J. Weissenbach, P. Bork, S.D. Ehrlich, J. Wang, A human gut microbial gene catalogue established by metagenomic sequencing, *Nature.* 464 (2010) 59–65. <https://doi.org/10.1038/nature08821>.
- [85] S. Leviatan, S. Shoer, D. Rothschild, M. Gorodetski, E. Segal, An expanded reference map of the human gut microbiome reveals hundreds of previously unknown species, *Nat. Commun.* 13 (2022) 3863. <https://doi.org/10.1038/s41467-022-31502-1>.
- [86] A.M. Mowat, W.W. Agace, Regional specialization within the intestinal immune system, *Nat. Rev. Immunol.* 14 (2014) 667–685. <https://doi.org/10.1038/nri3738>.
- [87] W. Ruan, M.A. Engevik, J.K. Spinler, J. Versalovic, Healthy human gastrointestinal microbiome: Composition and function after a decade of exploration, *Dig. Dis. Sci.* 65 (2020) 695–705. <https://doi.org/10.1007/s10620-020-06118-4>.
- [88] G. Falony, M. Joossens, S. Vieira-Silva, J. Wang, Y. Darzi, K. Faust, A. Kurilshikov, M.J. Bonder, M. Valles-Colomer, D. Vandeputte, R.Y. Tito, S. Chaffron, L. Rymenans, C. Verspecht, L. De Sutter, G. Lima-Mendez, K. D’hoë, K. Jonckheere, D. Homola, R. Garcia, E.F. Tigchelaar, L. Eeckhaut, J. Fu, L. Henckaerts, A. Zhernakova, C. Wijmenga, J. Raes, Population-level analysis of gut microbiome variation, *Science.* 352 (2016) 560–564. <https://doi.org/10.1126/science.aad3503>.
- [89] C. Huttenhower, D. Gevers, R. Knight, S. Abubucker, J.H. Badger, A.T. Chinwalla, H.H. Creasy, A.M. Earl, M.G. FitzGerald, R.S. Fulton, M.G. Giglio, K. Hallsworth-Pepin, E.A. Lobos, R. Madupu, V. Magrini, J.C. Martin, M. Mitreva, D.M. Muzny, E.J. Sodergren, J. Versalovic, A.M. Wollam, K.C. Worley, J.R. Wortman, S.K. Young, Q. Zeng, K.M. Aagaard, O.O. Abolude, E. Allen-Vercoe, E.J. Alm, L. Alvarado, G.L. Andersen, S. Anderson, E. Appelbaum, H.M. Arachchi, G. Armitage, C.A. Arze, T. Ayvaz, C.C. Baker, L. Begg, T. Belachew, V. Bhonagiri, M. Bihan, M.J. Blaser, T. Bloom, V. Bonazzi, J. Paul Brooks, G.A. Buck, C.J. Buhay, D.A. Busam, J.L. Campbell, S.R. Canon, B.L. Cantarel, P.S.G. Chain, I.-M.A. Chen, L. Chen, S. Chhibba, K. Chu, D.M. Ciulla, J.C. Clemente, S.W. Clifton, S. Conlan, J. Crabtree, M.A. Cutting, N.J. Davidovics, C.C. Davis, T.Z. DeSantis, C. Deal, K.D. Delehaunty, F.E. Dewhirst, E. Deych, Y. Ding, D.J. Dooling, S.P. Dugan, W. Michael Dunne, A. Scott Durkin, R.C. Edgar, R.L. Erlich, C.N. Farmer, R.M. Farrell, K. Faust, M. Feldgarden, V.M. Felix, S. Fisher, A.A. Fodor, L.J. Forney, L. Foster, V. Di Francesco, J. Friedrich, D.C. Friedrich, C.C. Fronick, L.L. Fulton, H. Gao, N. Garcia, G. Giannoukos, C. Giblin, M.Y. Giovanni, J.M. Goldberg, J. Goll, A. Gonzalez, A. Griggs, S. Gujja, S. Kinder Haake, B.J. Haas, H.A. Hamilton, E.L. Harris, T.A. Hepburn, B. Herter, D.E. Hoffmann, M.E. Holder, C. Howarth, K.H. Huang, S.M. Huse, J. Izard, J.K. Jansson, H. Jiang, C. Jordan, V. Joshi, J.A. Katancik, W.A. Keitel, S.T. Kelley, C. Kells, N.B. King, D. Knights, H.H. Kong, O. Koren, S. Koren, K.C. Kota, C.L. Kovar, N.C. Kyrpides, P.S. La Rosa, S.L. Lee, K.P. Lemon, N. Lennon, C.M. Lewis, L. Lewis, R.E. Ley, K. Li, K. Liolios, B. Liu, Y. Liu, C.-C. Lo, C.A. Lozupone, R. Dwayne Lunsford, T. Madden, A.A. Mahurkar, P.J. Mannon, E.R. Mardis, V.M. Markowitz, K. Mavromatis, J.M. McCarrison, D. McDonald, J. McEwen, A.L.

- McGuire, P. McInnes, T. Mehta, K.A. Mihindukulasuriya, J.R. Miller, P.J. Minx, I. Newsham, C. Nusbaum, M. O’Laughlin, J. Orvis, I. Pagani, K. Palaniappan, S.M. Patel, M. Pearson, J. Peterson, M. Podar, C. Pohl, K.S. Pollard, M. Pop, M.E. Priest, L.M. Proctor, X. Qin, J. Raes, J. Ravel, J.G. Reid, M. Rho, R. Rhodes, K.P. Riehle, M.C. Rivera, B. Rodriguez-Mueller, Y.-H. Rogers, M.C. Ross, C. Russ, R.K. Sanka, P. Sankar, J. Fah Sathirapongsasuti, J.A. Schloss, P.D. Schloss, T.M. Schmidt, M. Scholz, L. Schriml, A.M. Schubert, N. Segata, J.A. Segre, W.D. Shannon, R.R. Sharp, T.J. Sharpton, N. Shenoy, N.U. Sheth, G.A. Simone, I. Singh, C.S. Smillie, J.D. Sobel, D.D. Sommer, P. Spicer, G.G. Sutton, S.M. Sykes, D.G. Tabbaa, M. Thiagarajan, C.M. Tomlinson, M. Torralba, T.J. Treangen, R.M. Truty, T.A. Vishnivetskaya, J. Walker, L. Wang, Z. Wang, D.V. Ward, W. Warren, M.A. Watson, C. Wellington, K.A. Wetterstrand, J.R. White, K. Wilczek-Boney, Y. Wu, K.M. Wylie, T. Wylie, C. Yandava, L. Ye, Y. Ye, S. Yooseph, B.P. Youmans, L. Zhang, Y. Zhou, Y. Zhu, L. Zoloth, J.D. Zucker, B.W. Birren, R.A. Gibbs, S.K. Highlander, B.A. Methé, K.E. Nelson, J.F. Petrosino, G.M. Weinstock, R.K. Wilson, O. White, The Human Microbiome Project Consortium, Structure, function and diversity of the healthy human microbiome, *Nature*. 486 (2012) 207–214. <https://doi.org/10.1038/nature11234>.
- [90] K.S. Betts, A study in balance: How microbiomes are changing the shape of environmental health, *Environ. Health Perspect.* 119 (2011) a340–a346. <https://doi.org/10.1289/ehp.119-a340>.
- [91] S.R. Gill, M. Pop, R.T. DeBoy, P.B. Eckburg, P.J. Turnbaugh, B.S. Samuel, J.I. Gordon, D.A. Relman, C.M. Fraser-Liggett, K.E. Nelson, Metagenomic analysis of the human distal gut microbiome, *Science*. 312 (2006) 1355–1359. <https://doi.org/10.1126/science.1124234>.
- [92] B. van der Hee, J.M. Wells, Microbial regulation of host physiology by short-chain fatty acids, *Trends Microbiol.* 29 (2021) 700–712. <https://doi.org/10.1016/j.tim.2021.02.001>.
- [93] E. Capuano, The behavior of dietary fiber in the gastrointestinal tract determines its physiological effect, *Crit. Rev. Food Sci. Nutr.* 57 (2017) 3543–3564. <https://doi.org/10.1080/10408398.2016.1180501>.
- [94] A. Koh, F. De Vadder, P. Kovatcheva-Datchary, F. Bäckhed, From dietary fiber to host physiology: Short-chain fatty acids as key bacterial metabolites, *Cell*. 165 (2016) 1332–1345. <https://doi.org/10.1016/j.cell.2016.05.041>.
- [95] E.M. Bik, J.A. Ugalde, J. Cousins, A.D. Goddard, J. Richman, Z.S. Apte, Microbial biotransformations in the human distal gut, *Br. J. Pharmacol.* 175 (2018) 4404–4414. <https://doi.org/10.1111/bph.14085>.
- [96] K.J. Portune, M. Beaumont, A.-M. Davila, D. Tomé, F. Blachier, Y. Sanz, Gut microbiota role in dietary protein metabolism and health-related outcomes: The two sides of the coin, *Trends Food Sci. Technol.* 57 (2016) 213–232. <https://doi.org/10.1016/j.tifs.2016.08.011>.
- [97] P. Louis, G.L. Hold, H.J. Flint, The gut microbiota, bacterial metabolites and colorectal cancer, *Nat. Rev. Microbiol.* 12 (2014) 661–672. <https://doi.org/10.1038/nrmicro3344>.
- [98] G. den Besten, K. van Eunen, A.K. Groen, K. Venema, D.-J. Reijngoud, B.M. Bakker, The role of short-chain fatty acids in the interplay between diet, gut microbiota, and host energy metabolism, *J. Lipid Res.* 54 (2013) 2325–2340. <https://doi.org/10.1194/jlr.R036012>.
- [99] I. Rowland, G. Gibson, A. Heinken, K. Scott, J. Swann, I. Thiele, K. Tuohy, Gut microbiota functions: Metabolism of nutrients and other food components, *Eur. J. Nutr.* 57 (2018) 1–24. <https://doi.org/10.1007/s00394-017-1445-8>.
- [100] D.J. Morrison, T. Preston, Formation of short chain fatty acids by the gut microbiota and their impact on human metabolism, *Gut Microbes.* 7 (2016) 189–200. <https://doi.org/10.1080/19490976.2015.1134082>.
- [101] B. Dalile, L. Van Oudenhove, B. Vervliet, K. Verbeke, The role of short-chain fatty acids in microbiota–gut–brain communication, *Nat. Rev. Gastroenterol. Hepatol.* 16 (2019) 461–478. <https://doi.org/10.1038/s41575-019-0157-3>.
- [102] K.J. O’Riordan, M.K. Collins, G.M. Moloney, E.G. Knox, M.R. Aburto, C. Fülling, S.J. Morley, G. Clarke, H. Schellekens, J.F. Cryan, Short chain fatty acids: Microbial metabolites for

- gut-brain axis signalling, *Mol. Cell. Endocrinol.* 546 (2022) 111572. <https://doi.org/10.1016/j.mce.2022.111572>.
- [103] L. Liu, J.R. Huh, K. Shah, Microbiota and the gut-brain-axis: Implications for new therapeutic design in the CNS, *eBioMedicine.* 77 (2022) 103908. <https://doi.org/10.1016/j.ebiom.2022.103908>.
- [104] M. van de Wouw, M. Boehme, J.M. Lyte, N. Wiley, C. Strain, O. O’Sullivan, G. Clarke, C. Stanton, T.G. Dinan, J.F. Cryan, Short-chain fatty acids: Microbial metabolites that alleviate stress-induced brain-gut axis alterations, *J. Physiol.* 596 (2018) 4923–4944. <https://doi.org/10.1113/JP276431>.
- [105] P.A. Gill, M.C. van Zelm, J.G. Muir, P.R. Gibson, Review article: Short chain fatty acids as potential therapeutic agents in human gastrointestinal and inflammatory disorders, *Aliment. Pharmacol. Ther.* 48 (2018) 15–34. <https://doi.org/10.1111/apt.14689>.
- [106] R.N. Carmody, P.J. Turnbaugh, Host-microbial interactions in the metabolism of therapeutic and diet-derived xenobiotics, *J. Clin. Invest.* 124 (2014) 4173–4181. <https://doi.org/10.1172/JCI72335>.
- [107] N. Koppel, V. Maini Rekdal, E.P. Balskus, Chemical transformation of xenobiotics by the human gut microbiota, *Science.* 356 (2017) eaag2770. <https://doi.org/10.1126/science.aag2770>.
- [108] M.A. Beliaeva, M. Wilmanns, M. Zimmermann, Decipher enzymes from human microbiota for drug discovery and development, *Curr. Opin. Struct. Biol.* 80 (2023) 102567. <https://doi.org/10.1016/j.sbi.2023.102567>.
- [109] P. Spanogiannopoulos, E.N. Bess, R.N. Carmody, P.J. Turnbaugh, The microbial pharmacists within us: A metagenomic view of xenobiotic metabolism, *Nat. Rev. Microbiol.* 14 (2016) 273–287. <https://doi.org/10.1038/nrmicro.2016.17>.
- [110] H.J. Haiser, P.J. Turnbaugh, Developing a metagenomic view of xenobiotic metabolism, *Pharmacol. Res.* 69 (2013) 21–31. <https://doi.org/10.1016/j.phrs.2012.07.009>.
- [111] M. Zimmermann, M. Zimmermann-Kogadeeva, R. Wegmann, A.L. Goodman, Mapping human microbiome drug metabolism by gut bacteria and their genes, *Nature.* 570 (2019) 462–467. <https://doi.org/10.1038/s41586-019-1291-3>.
- [112] B. Javdan, J.G. Lopez, P. Chankhamjon, Y.-C.J. Lee, R. Hull, Q. Wu, X. Wang, S. Chatterjee, M.S. Donia, Personalized mapping of drug metabolism by the human gut microbiome, *Cell.* 181 (2020) 1661-1679.e22. <https://doi.org/10.1016/j.cell.2020.05.001>.
- [113] R. Feng, J.-W. Shou, Z.-X. Zhao, C.-Y. He, C. Ma, M. Huang, J. Fu, X.-S. Tan, X.-Y. Li, B.-Y. Wen, X. Chen, X.-Y. Yang, G. Ren, Y. Lin, Y. Chen, X.-F. You, Y. Wang, J.-D. Jiang, Transforming berberine into its intestine-absorbable form by the gut microbiota, *Sci. Rep.* 5 (2015) 12155. <https://doi.org/10.1038/srep12155>.
- [114] H. Hasegawa, Proof of the mysterious efficacy of ginseng: Basic and clinical trials: Metabolic activation of ginsenoside: Deglycosylation by intestinal bacteria and esterification with fatty acid, *J. Pharmacol. Sci.* 95 (2004) 153–157. <https://doi.org/10.1254/jphs.fmj04001x4>.
- [115] R. García-Villalba, J.A. Giménez-Bastida, A. Cortés-Martín, M.Á. Ávila-Gálvez, F.A. Tomás-Barberán, M.V. Selma, J.C. Espín, A. González-Sarrías, Urolithins: a comprehensive update on their metabolism, bioactivity, and associated gut microbiota, *Mol. Nutr. Food Res.* 66 (2022) 2101019. <https://doi.org/10.1002/mnfr.202101019>.
- [116] J.G. LeBlanc, C. Milani, G.S. de Giori, F. Sesma, D. van Sinderen, M. Ventura, Bacteria as vitamin suppliers to their host: a gut microbiota perspective, *Curr. Opin. Biotechnol.* 24 (2013) 160–168. <https://doi.org/10.1016/j.copbio.2012.08.005>.
- [117] F. Cabreiro, C. Au, K.-Y. Leung, N. Vergara-Irigaray, H.M. Cochemé, T. Noori, D. Weinkove, E. Schuster, N.D.E. Greene, D. Gems, Metformin retards aging in *C. elegans* by altering microbial folate and methionine metabolism, *Cell.* 153 (2013) 228–239. <https://doi.org/10.1016/j.cell.2013.02.035>.

- [118] R. Pryor, D. Martinez-Martinez, L. Quintaneiro, F. Cabreiro, The role of the microbiome in drug response, *Annu. Rev. Pharmacol. Toxicol.* 60 (2020) 417–435. <https://doi.org/10.1146/annurev-pharmtox-010919-023612>.
- [119] M. Klünemann, S. Andrejev, S. Blasche, A. Mateus, P. Phapale, S. Devendran, J. Vappiani, B. Simon, T.A. Scott, E. Kafkia, D. Konstantinidis, K. Zimngibl, E. Mastrorilli, M. Banzhaf, M.-T. Mackmull, F. Hövelmann, L. Nesme, A.R. Brochado, L. Maier, T. Bock, V. Periwal, M. Kumar, Y. Kim, M. Tramontano, C. Schultz, M. Beck, J. Hennig, M. Zimmermann, D.C. Sévin, F. Cabreiro, M.M. Savitski, P. Bork, A. Typas, K.R. Patil, Bioaccumulation of therapeutic drugs by human gut bacteria, *Nature*. 597 (2021) 533–538. <https://doi.org/10.1038/s41586-021-03891-8>.
- [120] A. Zihler Berner, S. Fuentes, A. Dostal, A.N. Payne, P. Vazquez Gutierrez, C. Chassard, F. Grattepanche, W.M. de Vos, C. Lacroix, Novel polyfermentor intestinal model (PolyFermS) for controlled ecological studies: Validation and effect of pH, *PLoS ONE*. 8 (2013) e77772. <https://doi.org/10.1371/journal.pone.0077772>.
- [121] J. Isenring, L. Bircher, A. Geirnaert, C. Lacroix, *In vitro* human gut microbiota fermentation models: opportunities, challenges, and pitfalls, *Microbiome Res. Rep.* 2 (2023) 2. <https://doi.org/10.20517/mrr.2022.15>.
- [122] C. Cinquin, G. Le Blay, I. Fliss, C. Lacroix, New three-stage *in vitro* model for infant colonic fermentation with immobilized fecal microbiota, *FEMS Microbiol. Ecol.* 57 (2006) 324–336. <https://doi.org/10.1111/j.1574-6941.2006.00117.x>.
- [123] G.T. Macfarlane, S. Macfarlane, G.R. Gibson, Validation of a three-stage compound continuous culture system for investigating the effect of retention time on the ecology and metabolism of bacteria in the human colon, *Microb. Ecol.* 35 (1998) 180–187. <https://doi.org/10.1007/s002489900072>.
- [124] L. Nissen, F. Casciano, A. Gianotti, Intestinal fermentation *in vitro* models to study food-induced gut microbiota shift: An updated review, *FEMS Microbiol. Lett.* 367 (2020) fnaa097. <https://doi.org/10.1093/femsle/fnaa097>.
- [125] M.M. O'Donnell, M.C. Rea, F. Shanahan, R.P. Ross, The use of a mini-bioreactor fermentation system as a reproducible, high-throughput *ex vivo* batch model of the distal colon, *Front. Microbiol.* 9 (2018). <https://www.frontiersin.org/articles/10.3389/fmicb.2018.01844> (accessed October 2, 2023).
- [126] F.-S. Li, J.-K. Weng, Demystifying traditional herbal medicine with modern approach, *Nat. Plants*. 3 (2017) 1–7. <https://doi.org/10.1038/nplants.2017.109>.
- [127] A.N. Welz, A. Emberger-Klein, K. Menrad, Why people use herbal medicine: insights from a focus-group study in Germany, *BMC Complement. Altern. Med.* 18 (2018) 92. <https://doi.org/10.1186/s12906-018-2160-6>.
- [128] WHO, Mental disorders, (2022). <https://www.who.int/news-room/fact-sheets/detail/mental-disorders> (accessed September 5, 2023).
- [129] EMA/HMPC, Final european union herbal monograph on *Valeriana officinalis* L., radix, (2016). <https://www.ema.europa.eu/en/medicines/herbal/valerianae-radix> (accessed September 12, 2022).
- [130] T. Smith, K. Kawa, V. Eckl, C. Morton, R. Stredney, Herbal supplements sales in US increased 8.5% in 2017, topping \$8 billion, *HerbalGram*. (2018). <http://herbalgram.org/resources/herbalgram/issues/119/table-of-contents/hg119-herbmktrpt/> (accessed September 12, 2022).
- [131] A. Becker, F. Felgentreff, H. Schröder, B. Meier, A. Brattström, The anxiolytic effects of a valerian extract is based on valerenic acid, *BMC Complement. Altern. Med.* 14 (2014) 267. <https://doi.org/10.1186/1472-6882-14-267>.
- [132] C. Sampath, K. Haug, S. Thanei, M. Hamburger, H. Derendorf, R. Frye, V. Butterweck, Pharmacokinetics of valerenic acid in rats after intravenous and oral administrations, *Planta Med.* 78 (2012) 575–581. <https://doi.org/10.1055/s-0031-1298301>.

- [133] G.D. Anderson, G.W. Elmer, D.M. Taibi, M.V. Vitiello, E. Kantor, T.F. Kalhorn, W.N. Howald, S. Barsness, C.A. Landis, Pharmacokinetics of valerianic acid after single and multiple doses of valerian in older women, *Phytother. Res.* 24 (2010) 1442–1446. <https://doi.org/10.1002/ptr.3151>.
- [134] EMA/HMPC, Assessment report on *Hypericum perforatum* L., herba, European Medicines Agency. (2021). <https://www.ema.europa.eu/en/medicines/herbal/hyperici-herba> (accessed October 4, 2023).
- [135] V. Butterweck, Mechanism of action of St. John's wort in depression, *CNS Drugs.* 17 (2003) 539–562. <https://doi.org/10.2165/00023210-200317080-00001>.
- [136] M. Schmidt, V. Butterweck, The mechanisms of action of St. John's wort: an update, *Wien. Med. Wochenschr.* 165 (2015) 229–235. <https://doi.org/10.1007/s10354-015-0372-7>.
- [137] H.-U. Schulz, M. Schürer, D. Bässler, D. Weiser, Investigation of the bioavailability of hypericin, pseudohypericin, hyperforin and the flavonoids quercetin and isorhamnetin following single and multiple oral dosing of a *Hypericum* extract containing tablet, *Arzneimittelforschung.* (2005) 8.
- [138] R. Kerb, J. Brockmöller, B. Staffeldt, M. Ploch, I. Roots, Single-dose and steady-state pharmacokinetics of hypericin and pseudohypericin, *Antimicrob. Agents Chemother.* 40 (1996) 2087–2093. <https://doi.org/10.1128/AAC.40.9.2087>.
- [139] A.R. Kamuhabwa, P. Augustijns, P.A. de Witte, *In vitro* transport and uptake of protohypericin and hypericin in the Caco-2 model, *Int. J. Pharm.* 188 (1999) 81–86. [https://doi.org/10.1016/S0378-5173\(99\)00203-3](https://doi.org/10.1016/S0378-5173(99)00203-3).
- [140] S. Verjee, D. Brügger, H. Abdel-Aziz, V. Butterweck, Permeation characteristics of hypericin across Caco-2 monolayers in the absence or presence of quercitrin – A mass balance study, *Planta Med.* 81 (2015) 1111–1120. <https://doi.org/10.1055/s-0035-1546034>.
- [141] K. Forsch, B. Siewert, J. Drewe, G. Fricker, L. Disch, Sustained release for St. John's wort: A rational idea?, *J. Bioequiv. Availab.* 09 (2017) 565–576. <https://doi.org/10.4172/jbb.1000363>.
- [142] EMA/HMPC, Assessment report on *Eschscholzia californica* Cham., herba, (2015). https://www.ema.europa.eu/en/documents/herbal-report/final-assessment-report-eschscholzia-californica-cham-herba_en.pdf (accessed March 20, 2023).
- [143] A. Rolland, J. Fleurentin, M.C. Lanhers, R. Misslin, F. Mortier, Neurophysiological effects of an extract of *Eschscholzia californica* Cham. (Papaveraceae), *Phytother. Res.* 15 (2001) 377–381. <https://doi.org/10.1002/ptr.884>.
- [144] S. Gafner, B.M. Dietz, K.L. McPhail, I.M. Scott, J.A. Glinski, F.E. Russell, M.M. McCollom, J.W. Budzinski, B.C. Foster, C. Bergeron, M.-R. Rhyu, J.L. Bolton, Alkaloids from *Eschscholzia californica* and their capacity to inhibit binding of [³H]8-Hydroxy-2-(di-N-propylamino)tetralin to 5-HT_{1A} receptors *in vitro*, *J. Nat. Prod.* 69 (2006) 432–435. <https://doi.org/10.1021/np058114h>.
- [145] E. Kleber, W. Schneider, H.L. Schäfer, E.F. Elstner, Modulation of key reactions of the catecholamine metabolism by extracts from *Eschscholtzia californica* and *Corydalis cava*, *Arzneimittelforschung.* 45 (1995) 127–131.
- [146] H. Stuppner, S. Sturm, N. Mulinacci, F. Vincieri, Capillary zone electrophoretic analysis of the main alkaloids from *Eschscholtzia californica*, *Chromatographia.* 37 (1993) 579–583. <https://doi.org/10.1007/BF02274105>.
- [147] F. Tomè, M.L. Colombo, L. Caldiroli, A comparative investigation on alkaloid composition in different populations of *Eschscholtzia californica* Cham., *Phytochem. Anal.* 10 (1999) 264–267. [https://doi.org/10.1002/\(SICI\)1099-1565\(199909/10\)10:5<264::AID-PCA469>3.0.CO;2-4](https://doi.org/10.1002/(SICI)1099-1565(199909/10)10:5<264::AID-PCA469>3.0.CO;2-4).
- [148] C. Guo, Y. Jiang, L. Li, L. Hong, Y. Wang, Q. Shen, Y. Lou, H. Hu, H. Zhou, L. Yu, H. Jiang, S. Zeng, Application of a liquid chromatography–tandem mass spectrometry method to the pharmacokinetics, tissue distribution and excretion studies of *Dactylicapnos scandens* in rats, *J. Pharm. Biomed. Anal.* 74 (2013) 92–100. <https://doi.org/10.1016/j.jpba.2012.10.011>.

- [149] A. Maier-Salamon, G. Trauner, R. Hiltcher, G. Reznicek, B. Kopp, T. Thalhammer, W. Jäger, Hepatic metabolism and biliary excretion of valerianic acid in isolated perfused rat livers: Role of Mrp2 (Abcc2), *J. Pharm. Sci.* 98 (2009) 3839–3849. <https://doi.org/10.1002/jps.21671>.
- [150] M. Davies, P. Peramuhendige, L. King, M. Golding, A. Kotian, M. Penney, S. Shah, N. Manevski, Evaluation of *in vitro* models for assessment of human intestinal metabolism in drug discovery, *Drug Metab. Dispos.* (2020). <https://doi.org/10.1124/dmd.120.000111>.
- [151] M.S. Roberts, B.M. Magnusson, F.J. Burczynski, M. Weiss, Enterohepatic circulation, *Clin. Pharmacokinet.* 41 (2002) 751–790. <https://doi.org/10.2165/00003088-200241100-00005>.
- [152] Huang, P. Cheng, Z.-Y. Zhang, S.-J. Tian, Z.-L. Sun, J.-G. Zeng, Z.-Y. Liu, Biotransformation and tissue distribution of protopine and allocryptopine and effects of *Plume poppy* total alkaloid on liver drug-metabolizing enzymes, *Sci. Rep.* 8 (2018) 537. <https://doi.org/10.1038/s41598-017-18816-7>.
- [153] J. Gertsch, Botanical drugs, synergy, and network pharmacology: Forth and back to intelligent mixtures, *Planta Med.* 77 (2011) 1086–1098. <https://doi.org/10.1055/s-0030-1270904>.
- [154] S. Verjee, O. Kelber, C. Kolb, H. Abdel-Aziz, V. Butterweck, Permeation characteristics of hypericin across Caco-2 monolayers in the presence of single flavonoids, defined flavonoid mixtures or *Hypericum* extract matrix, *J. Pharm. Pharmacol.* 71 (2018) 58–69. <https://doi.org/10.1111/jphp.12717>.
- [155] V. Butterweck, U. Liefländer-Wulf, H. Winterhoff, A. Nahrstedt, Plasma levels of hypericin in presence of procyanidin B2 and hyperoside: A pharmacokinetic study in rats, *Planta Med.* 69 (2003) 189–192. <https://doi.org/10.1055/s-2003-38495>.
- [156] M. Milutinović, S. Dimitrijević-Branković, M. Rajilić-Stojanović, Plant extracts rich in polyphenols as potent modulators in the growth of probiotic and pathogenic intestinal microorganisms, *Front. Nutr.* 8 (2021) 1–11. <https://doi.org/10.3389/fnut.2021.688843>.

Appendix

Supporting information

Intestinal permeability and gut microbiota interactions of pharmacologically active compounds in valerian and St. John's wort

Antoine Chauveau^a, Andrea Treyer^a, Annelies Geirnaert^b, Lea Bircher^b, Angela Babst^b, Vanessa Fabienne Abegg^a, Ana Paula Simões-Wüst^c, Christophe Lacroix^b, Olivier Potterat^{a*}, Matthias Hamburger^{a,d*}

Affiliations

^aDivision of Pharmaceutical Biology, Department of Pharmaceutical Sciences, University of Basel, Basel, Switzerland

^bLaboratory of Food Biotechnology, Institute of Food, Nutrition and Health, Department of Health Science and Technology, ETH Zurich, Zurich, Switzerland

^cDepartment of Obstetrics, University Hospital Zurich, University of Zurich, Zurich, Switzerland

* Corresponding authors

Prof. Dr. Matthias Hamburger
Division of Pharmaceutical Biology, Department of Pharmaceutical Sciences, University of Basel,
Klingelbergstrasse 50, 4056 Basel, Switzerland
matthias.hamburger@unibas.ch
Tel. +41 61 207 14 25

Prof. Dr. Olivier Potterat
Division of Pharmaceutical Biology, Department of Pharmaceutical Sciences, University of Basel,
Klingelbergstrasse 50, 4056 Basel, Switzerland
olivier.potterat@unibas.ch
Tel. +41 61 207 14 25

Determination of the cumulative fraction transported (FA_{cum})

FA_{cum} was calculated according to the following equation:

$$FA_{cum} = \frac{1}{A} \sum_{k=1}^i \frac{[C_R(t_k) - f C_D(t_{k-1})] V_R}{[C_D(t_{k-1}) + C_D(t_k)] V_D} \quad (A.1)$$

V_R is the receiver chamber volume, t_k is the time point for the sampling occasion k , $C_D(t_k)$ is the measured concentration in the donor chamber at sample occasion k , $C_R(t_k)$ is the measured concentration in the receiver chamber at sample occasion k . The sample replacement factor f is defined as $f = (1 - V_S/V_R)$, where V_S is the sample volume and V_R is the receiver chamber volume.

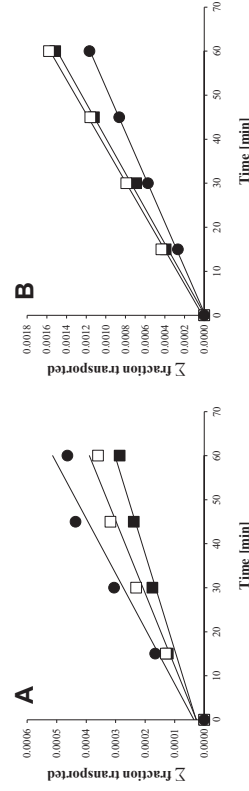


Fig. S1. Atenolol transport across Caco-2 monolayers in AB direction (A) and in BA direction (B) over 60 min. The cumulative fraction for three individual monolayers is shown; (■) monolayer 1, (□) monolayer 2, and (●) monolayer 3.

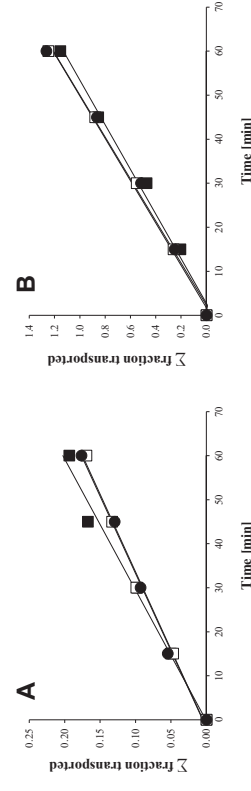


Fig. S2. Propranolol transport across Caco-2 monolayers in AB direction (A) and in BA direction (B) over 60 min. The cumulative fraction for three individual monolayers is shown; (■) monolayer 1, (□) monolayer 2, and (●) monolayer 3.

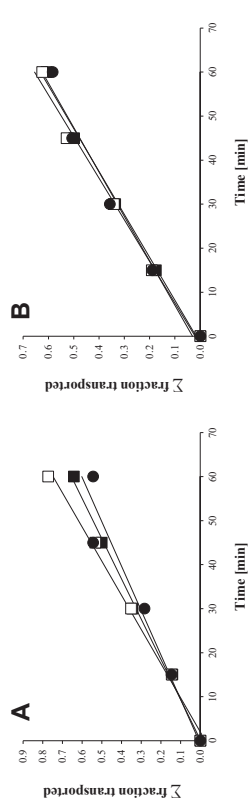


Fig. S3. Valerianic acid transport across Caco-2 monolayers in AB direction (A) and in BA direction (B) over 60 min. The cumulative fraction for three individual monolayers is shown; (■) monolayer 1, (□) monolayer 2, and (●) monolayer 3.

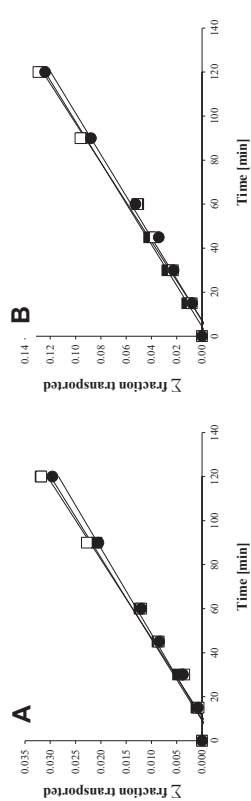


Fig. S4. Hyperforin transport across Caco-2 monolayers in AB direction (A) and in BA direction (B) over 60 min. The cumulative fraction for three individual monolayers is shown; (■) monolayer 1, (□) monolayer 2, and (●) monolayer 3.

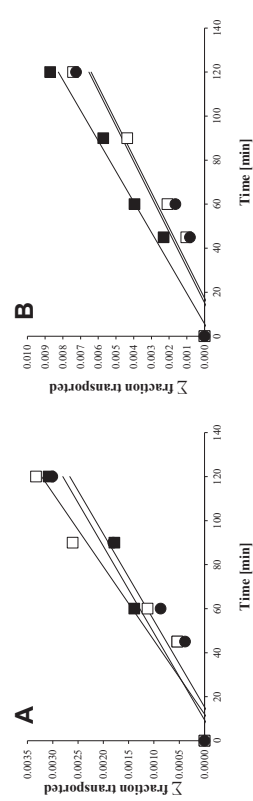


Fig. S5. Hypericin transport across Caco-2 monolayers in AB direction (A) and in BA direction (B) over 120 min. The cumulative fraction for three individual monolayers is shown; (■) monolayer 1, (□) monolayer 2 and (●) monolayer 3. For all monolayers, the hypericin concentrations were below the lower limit of quantification at timepoints < 45 min.

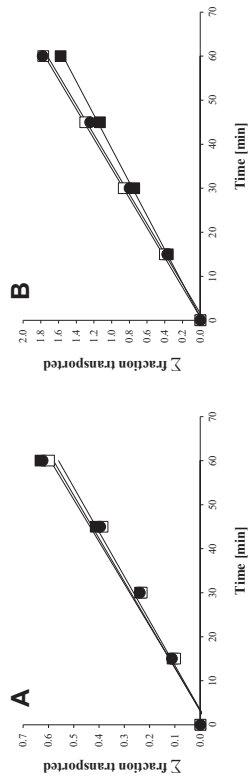


Fig. S6. Diazepam transport across Caco-2 monolayers in AB direction (A) and in BA direction (B) over 60 min. The cumulative fraction for three individual monolayers is shown; (■) monolayer 1, (□) monolayer 2 and (●) monolayer 3.

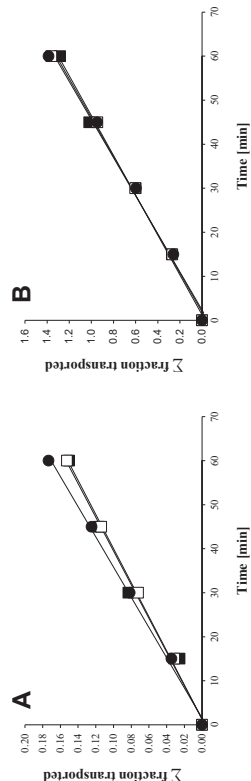


Fig. S7. Citalopram transport across Caco-2 monolayers in AB direction (A) and in BA direction (B) over 60 min. The cumulative fraction for three individual monolayers is shown; (■) monolayer 1, (□) monolayer 2 and (●) monolayer 3.

Table S1. Trans epithelial electrical resistance (TEER) values of Caco-2 cell monolayers before (n=6) and after (n=2) experiments, and fluorescein fluxes across Caco-2 cell monolayers, performed after transport experiments (n=2).

Compounds	Pre-experiment TEER (Ω ·cm ²) (Mean \pm SD)	Post-experiment TEER (Ω ·cm ²) (values of 2 replicates)	Fluorescein flux (%) (values of 2 replicates)
Valerianic acid	260 \pm 12.7	250 240	0.68 0.48
Hyperforin	331 \pm 8.45	286 235	0.33 0.72
Hypericin	321 \pm 12.8	282 288	0.94 0.57
Diazepam	267 \pm 6.65	255 236	0.16 0.20
Citalopram	314 \pm 7.28	291 295	0.21 0.86
Atenolol	279 \pm 8.09	235 236	0.51 0.28
Propamamol	255 \pm 5.56	247	0.79

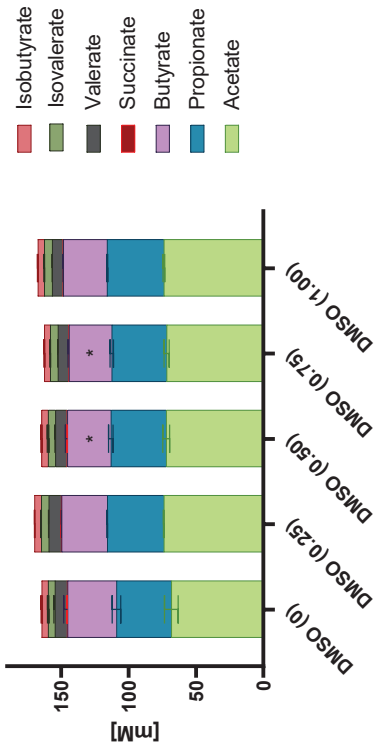


Fig. S8. Fermentation metabolite concentration after 24 h incubation of PolyfermS microbiota supplemented with 30% nutritive medium and different DMSO concentrations (0, 0.25, 0.50, 0.75 or 1.00 % (v/v)). Averages \pm s.d. (n=3). Asterisks indicate significant difference in average metabolite concentration compared to DMSO (0) control ($p < 0.05$).

Table S2. Optimized MS/MS parameters for valeric acid, hypericin, citalopram, citalopram-D₄, digoxin, on the Waters UHPLC-MS/MS system.

Compounds	Optimized MS/MS parameters		
	ESI mode	MRM transitions	Collision energy (V)
Valeric acid	Negative	232.8 → 84 (Q)	20
	Negative	232.8 → 41 (q)	20
Hypericin	Negative	503.2 → 433.1 (Q)	52
	Negative	503.2 → 405 (q)	64
Citalopram	Positive	324.9 → 109.1 (Q)	30
Citalopram-D ₄ (IS)	Positive	324.9 → 262.1 (q)	20
Digoxin (IS)	Negative	329.3 → 113	27
Digoxin (Q)	Negative	779.5 → 85.1	78

Table S3. Optimized MS/MS parameters for atenolol, propranolol HCl, verapamil HCl, diazepam, diazepam-D₅, hyperforin DCHA, warfarin, on the Agilent UHPLC-MS/MS system

Compounds	Optimized MS/MS parameters		
	ESI mode	MRM transitions	Collision energy (eV)
Hyperforin DCHA	Negative	535.38 → 383.2 (Q)	30
	Negative	535.38 → 313.2 (q)	34
Diazepam	Positive	285.08 → 154 (Q)	26
	Positive	285.08 → 193.1 (q)	34
Atenolol	Positive	267.17 → 56.1 (Q)	30
	Positive	267.17 → 91.1 (q)	54
Propranolol HCl	Positive	260.17 → 56.1 (Q)	26
	Positive	260.17 → 72.1 (q)	18
Verapamil HCl (IS)	Positive	455.29 → 77.1	125
Diazepam-D ₅ (IS)	Positive	290.11 → 198.1	34
Warfarin (IS)	Negative	307.09 → 161.1	18

Q: Quantifier; q: Qualifier

Table S4. Optimized UHPLC parameters of all studied compounds

Compounds	Gradient	Flow rate (ml/min)	Total run time (min)	Eluent	Column	Injection vol. (μl)	Column temp. (°C)	Autosampler temp. (°C)
Valeric acid	5% to 70% in 6 mins, 100% for 1 min	0.4	8	A: Water + 0.1% NH ₄ OH, pH 10.7 B: Acetonitrile mixed with A at a ratio 9:1	Waters Acuity UPLC® BEH C18, 1.7 μm, 2.1 × 50 mm	2	55	4
Hypericin	5% to 70% in 6 mins, 100% for 1 min	0.4	8	A: Water + 0.1% NH ₄ OH, pH 10.7 B: Acetonitrile mixed with A at a ratio 9:1	Waters Acuity UPLC® BEH C18, 1.7 μm, 2.1 × 50 mm	2	55	4
Hyperforin	5% to 100% in 1 mins, 100% for 2 mins	0.4	5	A: Water + 0.1% Formic acid (FA) B: Acetonitrile + 0.1% FA	Waters Acuity UPLC® CSH19 Phenyl-Hexyl, 1.7 μm, 2.1 × 50 mm	2	45	18
Diazepam	5% to 90% in 3.5 mins, 100% for 0.5 mins	0.4	6	A: Water + 0.1% FA B: Acetonitrile + 0.1% FA	Phenomenex Kinetex® XB-C18, 1.7 μm, 2.1 × 100 mm	5	45	4
Citalopram	5% to 100% in 2 mins, 100% for 1 min	0.4	5	A: Water + 0.1% FA B: Acetonitrile + 0.1% FA	Waters Acuity UPLC® HSS T3, 1.8 μm, 2.1 × 100 mm	2	55	10
Atenolol	5% to 100% in 2 mins, 100% for 1 min	0.5	5	A: Water + 0.1% FA B: Acetonitrile + 0.1% FA	Waters Acuity UPLC® HSS T3, 1.8 μm, 2.1 × 100 mm	2	45	4
Propranolol	5% to 100% in 2 mins, 100% for 1 min	0.5	5	A: Water + 0.1% FA B: Acetonitrile + 0.1% FA	Waters Acuity UPLC® HSS T3, 1.8 μm, 2.1 × 100 mm	2	45	4

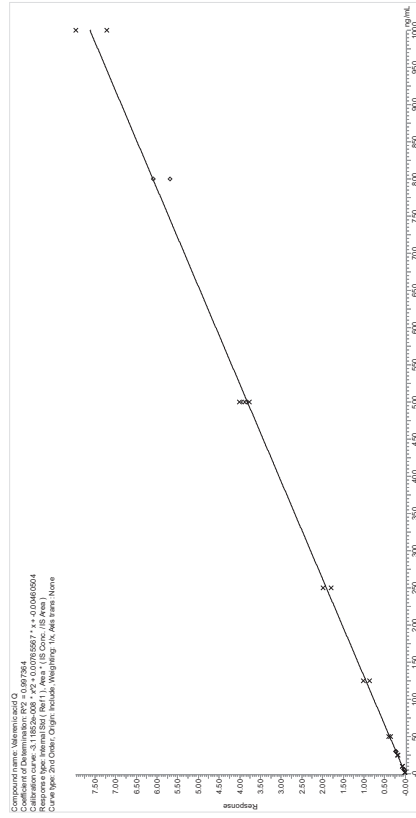


Fig. S9. Calibration curve of valeric acid (calibrators are shown as crosses, and quality controls as squares).

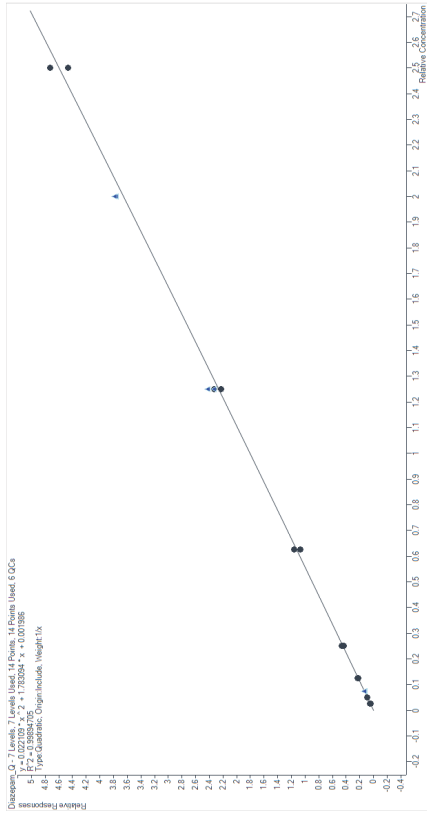


Fig. S12. Calibration curve of diazepam (calibrators are shown as black dots, and quality controls as blue triangles).

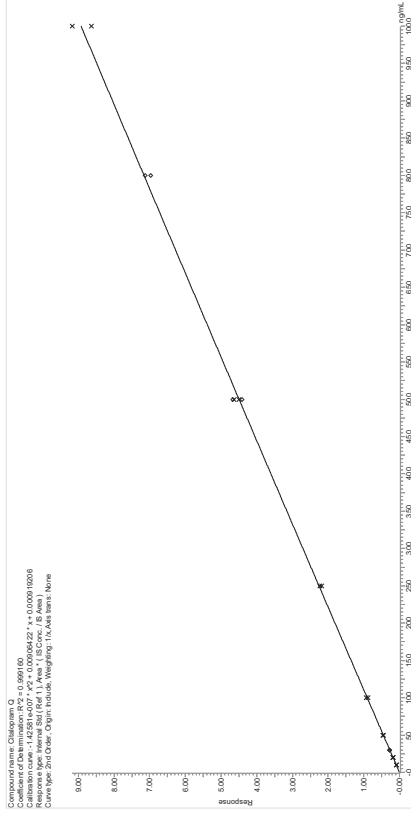


Fig. S13. Calibration curve of citalopram (calibrators are shown as crosses, and quality controls as squares).

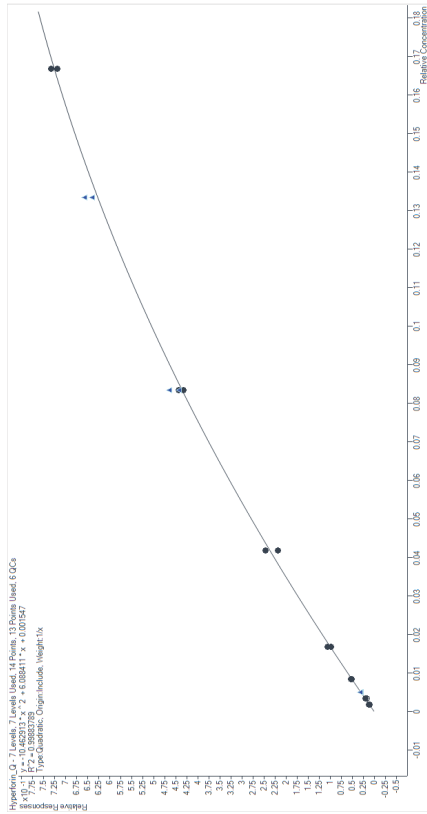


Fig. S10. Calibration curve of hypericin (calibrators are shown as black dots, and quality controls as blue triangles).

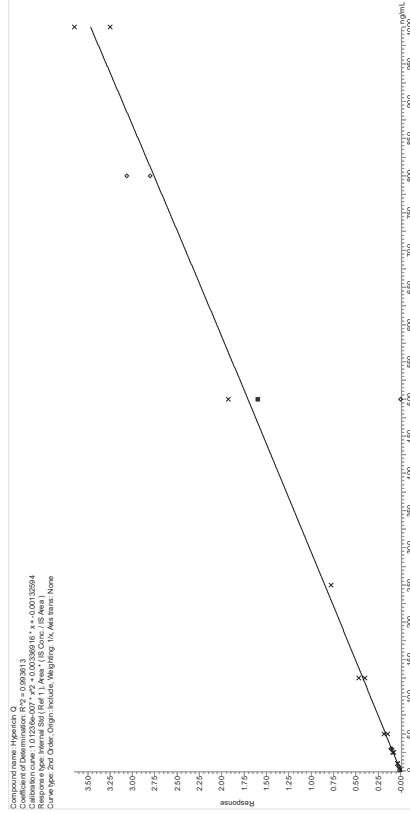


Fig. S11. Calibration curve of hypericin (calibrators are shown as crosses, and quality controls as squares).

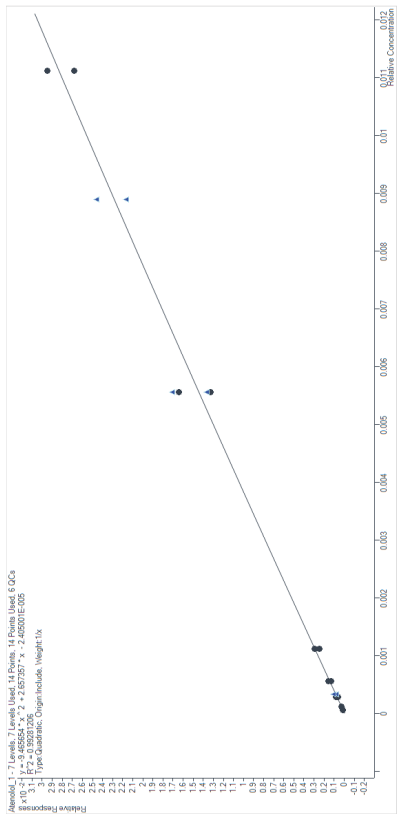


Fig. S14. Calibration curve of atenolol, low range (calibrators are shown as black dots, and quality controls as blue triangles).

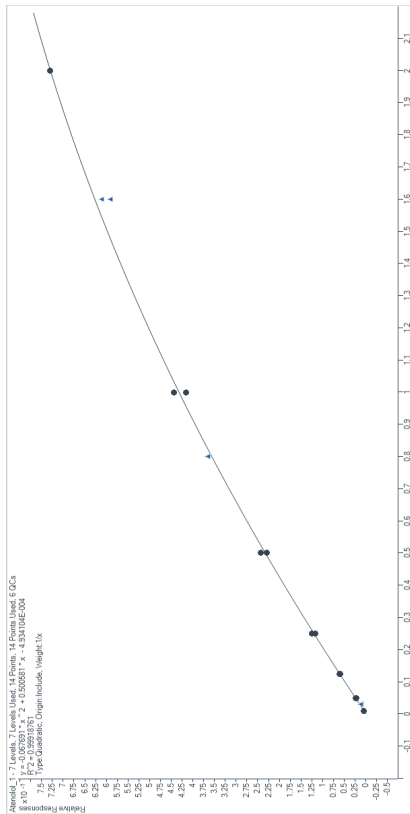


Fig. S15. Calibration curve of atenolol, high range (calibrators are shown as black dots, and quality controls as blue triangles).

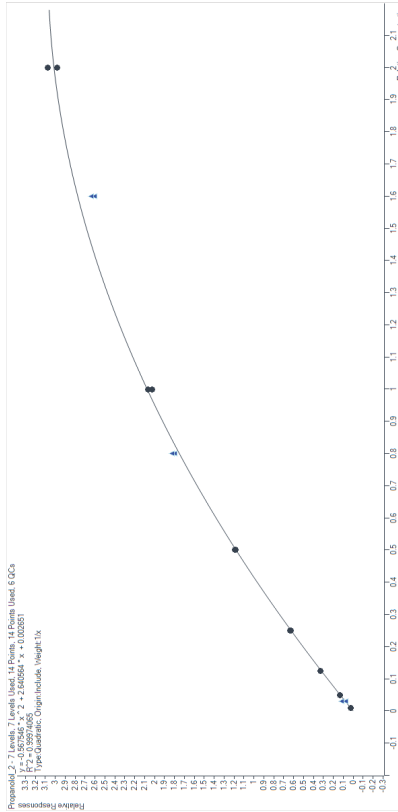


Fig. S16. Calibration curve of propranolol (calibrators are shown as black dots, and quality controls as blue triangles).

Table S5. Calibrators and calibration curve parameters for valerenic acid.

Response: $A \times Conc^2 + B \times Conc + C$, 1/X weighing, Quadratic regression, included origin (n=4)

	Concentration (ng/mL)				Regression parameters							
	2.00	10.00	25.00	50.00	A	B	C	R ²				
Mean	1.95	9.73	23.20	49.95	120.95	250.40	510.55	995.23	3.61E-08	0.0057	-0.0033	0.9982
SD	0.17	0.80	1.16	2.62	8.15	11.14	14.60	43.83	9.52E-08	-	-	-
CV%	8.88	8.24	5.01	5.24	6.74	4.45	2.86	4.40	-	-	-	-
RE%	-2.50	-2.75	-7.20	-0.10	-3.24	0.16	2.11	-0.48	-	-	-	-

Table S6. Calibrators and calibration curve parameters for hyperforin.

Response: $A \times Conc^2 + B \times Conc + C$, 1/X weighing, Quadratic regression, included origin (n=4)

	Concentration (ng/mL)				Regression parameters						
	2.50	5.00	12.50	25.00	62.50	125.00	250.00	A	B	C	R ²
Mean	2.47	4.90	12.66	25.81	61.29	125.23	250.22	-8.12468	5.61870	0.00186	0.99775
SD	0.06	0.16	0.27	1.98	5.65	5.08	3.88	2.02855	-	-	-
CV%	2.53	3.22	2.16	7.67	9.22	4.06	1.55	-	-	-	-
RE%	-1.31	-1.99	1.30	3.25	-1.93	0.19	0.09	-	-	-	-

Table S7. Calibrators and calibration curve parameters for hypericin.

Response: $A \times Conc^2 + B \times Conc + C$, 1/X weighing, Quadratic regression, included origin (n=4)

	Concentration (ng/mL)						Regression parameters			R ²	
	10.00	20.00	50.00	100.00	250.00	500.00	1000.00	A	B		C
Mean	9.55	24.83	50.93	132.73	248.30	512.25	994.35	1.07E-07	0.00240	-0.00121	0.98973
SD	0.13	2.06	7.05	13.42	21.16	56.08	97.41	8.43E-09	-	-	-
CV%	1.35	8.30	13.84	10.11	8.52	10.95	9.80	-	-	-	-
RE%	-4.50	-0.67	1.87	6.19	-0.68	2.45	-0.56	-	-	-	-

Table S8. Calibrators and calibration curve parameters for diazepam.

Response: $A \times Conc^2 + B \times Conc + C$, 1/X weighing, Quadratic regression, included origin (n=4)

	Concentration (ng/mL)						Regression parameters			R ²	
	10.00	20.00	50.00	100.00	250.00	500.00	1000.00	A	B		C
Mean	9.97	20.13	50.02	99.65	249.93	500.47	999.79	0.02870	1.86999	0.00095	0.99862
SD	0.72	1.35	2.35	6.01	11.26	22.88	30.68	0.00933	-	-	-
CV%	7.25	6.72	4.69	6.03	4.51	4.57	3.07	-	-	-	-
RE%	-0.31	0.67	0.04	-0.35	-0.03	0.09	-0.02	-	-	-	-

Table S9. Calibrators and calibration curve parameters for citalopram.

Response: $A \times Conc^2 + B \times Conc + C$, 1/X weighing, Quadratic regression, included origin (n=6)

	Concentration (ng/mL)						Regression parameters			R ²	
	10.00	20.00	50.00	100.00	250.00	500.00	1000.00	A	B		C
Mean	10.03	20.42	47.93	102.25	248.22	497.56	996.10	-3.39E-07	0.00942	-0.00190	0.99689
SD	0.10	1.05	3.76	5.17	6.06	13.14	36.06	3.18E-07	-	-	-
CV%	1.03	5.12	7.85	5.05	2.44	2.64	3.62	-	-	-	-
RE%	0.33	2.08	-4.13	2.25	-0.71	-0.49	-0.39	-	-	-	-

Table S10. Calibrators and calibration curve parameters for atenolol (high range).

Response: $A \times Conc^2 + B \times Conc + C$, 1/X weighing, Quadratic regression, included origin (n=4)

	Concentration (ng/mL)						Regression parameters			R ²	
	10.00	50.00	125.00	250.00	500.00	1000.00	2000.00	A	B		C
Mean	10.22	46.80	123.14	251.51	509.03	988.65	2005.13	-0.07347	0.51651	-0.00021	0.99918
SD	0.60	1.85	3.58	6.20	14.06	34.59	13.85	0.00848	-	-	-
CV%	5.90	3.95	2.91	2.47	2.76	3.50	0.69	-	-	-	-
RE%	2.16	-6.40	-1.49	0.60	1.81	-1.13	0.26	-	-	-	-

Table S11. Calibrators and calibration curve parameters for atenolol (low range).

Response: $A \times Conc^2 + B \times Conc + C$, 1/X weighing, Quadratic regression, included origin (n=4)

	Concentration (ng/mL)						Regression parameters			R ²	
	0.050	0.100	0.250	0.500	1.000	5.000	10.000	A	B		C
Mean	0.047	0.103	0.258	0.493	1.024	5.177	10.028	-9.49216	2.66480	-0.00002	0.99256
SD	0.002	0.009	0.036	0.059	0.014	0.646	0.580	0.03748	-	-	-
CV%	3.808	8.738	13.955	11.949	1.331	12.486	5.783	-	-	-	-
RE%	-5.154	2.565	3.270	-1.406	2.430	3.549	0.280	-	-	-	-

Table S12. Calibrators and calibration curve parameters for propranolol.

Response: $A \times Conc^2 + B \times Conc + C$, 1/X weighing, Quadratic regression, included origin (n=4)

	Concentration (ng/mL)						Regression parameters			R ²	
	10.00	50.00	125.00	250.00	500.00	1000.00	2000.00	A	B		C
Mean	9.65	50.77	127.73	250.86	503.12	981.20	2053.78	-0.60147	2.69910	0.00234	0.99977
SD	0.12	0.33	0.94	1.54	6.29	14.41	195.62	0.04797	-	-	-
CV%	1.24	0.64	0.74	0.61	1.25	1.47	9.52	-	-	-	-
RE%	-3.54	1.55	2.18	0.34	0.62	-1.88	2.69	-	-	-	-

Table S13. Quality control samples of valeric acid (n=4).

	QCL			QCM			QCH		
	6.00	500.00	800.00	125.00	500.00	800.00	125.00	500.00	800.00
Mean	5.63	520.78	787.13	5.63	520.78	787.13	5.63	520.78	787.13
SD	0.51	15.24	37.87	0.51	15.24	37.87	0.51	15.24	37.87
CV%	9.11	2.93	4.81	9.11	2.93	4.81	9.11	2.93	4.81
RE%	-6.11	4.16	-1.61	-6.11	4.16	-1.61	-6.11	4.16	-1.61

Table S14. Quality control samples of hyperforin (n=4).

	QCL			QCM			QCH		
	7.50 <th>125.00</th> <th>200.00</th> <th>125.00</th> <th>500.00</th> <th>800.00</th> <th>125.00</th> <th>500.00</th> <th>800.00</th>	125.00	200.00	125.00	500.00	800.00	125.00	500.00	800.00
Mean	7.95	130.78	205.29	7.95	130.78	205.29	7.95	130.78	205.29
SD	0.36	5.09	8.44	0.36	5.09	8.44	0.36	5.09	8.44
CV%	4.56	3.89	4.11	4.56	3.89	4.11	4.56	3.89	4.11
RE%	5.97	4.62	2.64	5.97	4.62	2.64	5.97	4.62	2.64

Table S15. Quality control samples of hypericin (n=4).

	QCL			QCM			QCH		
	30.00	500.00	800.00	30.00	500.00	800.00	30.00	500.00	800.00
Mean	30.08	501.97	847.48	30.08	501.97	847.48	30.08	501.97	847.48
SD	2.60	57.97	45.27	2.60	57.97	45.27	2.60	57.97	45.27
CV%	8.66	11.55	5.34	8.66	11.55	5.34	8.66	11.55	5.34
RE%	0.25	0.39	5.93	0.25	0.39	5.93	0.25	0.39	5.93

Table S16. Quality control samples of diazepam (n=4).

	QCL	OCM	QCH
	30.00	500.00	800.00
Mean	30.53	511.82	816.42
SD	1.29	21.85	16.23
CV%	4.21	4.27	1.99
RE%	1.78	2.36	2.05

Table S17. Quality control samples of citalopram (n=6).

	QCL	OCM	QCH
	30.00	500.00	800.00
Mean	30.65	501.40	812.90
SD	0.88	11.00	30.83
CV%	2.88	2.19	3.79
RE%	2.17	0.28	1.61

Table S18. Quality control samples of atenolol, high range (n=4).

	QCL	OCM	QCH
	30.00	800.00	1600.00
Mean	25.76	827.17	1505.27
SD	0.87	3.74	29.58
CV%	3.39	0.45	1.97
RE%	-14.14	3.40	-5.92

Table S19. Quality control samples of atenolol, low range (n=4).

	QCL	OCM	QCH
	0.300	5.000	8.000
Mean	0.297	4.783	8.169
SD	0.003	0.064	0.618
CV%	0.843	1.331	7.564
RE%	-0.969	-4.346	2.116

Table S20. Quality control samples of propranolol (n=4).

	QCL	OCM	QCH
	30.00	800.00	1600.00
Mean	34.00	830.23	1417.46
SD	4.89	11.77	35.11
CV%	14.38	1.42	2.48
RE%	13.33	3.78	-11.41

Table S21. Carry-over assessment for all analytes and corresponding internal standards (I.S.) (n= 4)

Compound	Mean carry-over (%)
Valeric acid	6.652
I.S.	0.059
Hyperforin	9.242
I.S.	0.018
Hypericin	12.347
I.S.	0.068
Diazepam	2.693
I.S.	0.055
Citalopram	3.041
I.S.	0.052
Atenolol – high range	0.702
I.S.	0.047
Atenolol – low range	5.592
I.S.	0.102
Propranolol	4.890
I.S.	0.036

Table S22. Physicochemical properties of study compounds. Parameters were predicted with software ACD/Percepta (ACD/Labs release 2020.1.1).

Compounds	Molecular weight (g/mol)	pKa	clogP	clogP_{at 6.5}	clogP_{at 7.4}
Valeric acid	234.334	4,9	4.63	3.0	2.1
Hyperforin	536.785	4,5	10.23	8.2	7.4
Hypericin	504.443	6,9	7.89	7.7	7.1
Diazepam	284.740	2,5	2.73	2.7	2.7
Citalopram	324.392	9,6	3.39	0.6	1.3
Atenolol	266.336	9,4	0.24	-2.5	-1.9
Propranolol	259.343	9,5	3.26	0.5	1.1

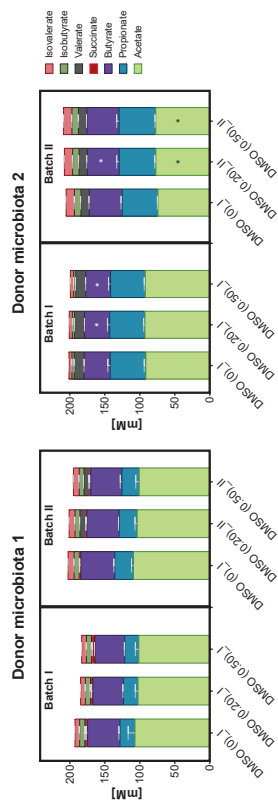


Fig. S18. Short chain fatty acid concentration after 24 h incubation of PolyfermS microbiota 1 and 2 supplemented with 30% nutritive medium and different DMSO concentrations (0, 20 or 50 μ L) that served as controls for compounds dissolved in DMSO. Two independent experiments (batch I and batch II) were performed for each microbiota. Averages \pm stdevy (n=3). Asterisks indicate significant differences in average metabolite concentration compared to DMSO (0) control ($p < 0.05$).

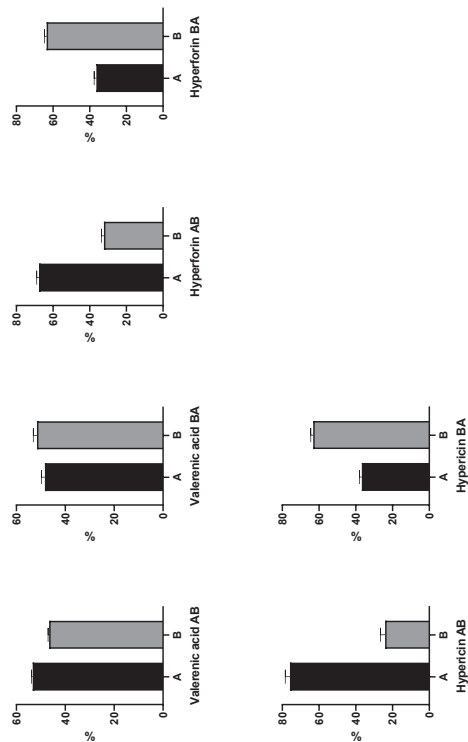


Fig. S17. Distribution of compounds on apical (A) and basolateral (B) sides in transport experiments on cell-free inserts after 1 hour (2 h for hyperforin and hypericin), with transport buffer adjusted to pH 6.5 (10 mM MES, 4.2 mM NaHCO_3 in HBSS) in the apical chamber, and at pH 7.4 in the basolateral chamber (25 mM HEPES, 4.2 mM NaHCO_3 in HBSS), both supplemented with 1% DMSO (and with 10% BSA for hyperforin and hypericin). Experiments were performed in apical to basolateral (AB) and basolateral to apical directions (BA). Data are expressed as percentage and mean \pm S.D. from three independent experiments.

Table S23. Stability of study compounds after 24h incubation with PolyfermS microbiota of donors 1 and 2, supplemented with 30% nutritive medium and 20 μ L DMSO. Values are normalized to 100%.

Compounds	Replicates	Abiotic		Female donor 1		Female donor 2	
		T 0h	T 24h	T 0h	T 24h	T 0h	T 24h
Valeric acid	Replicate 1	100.0%	109%	100.0%	92.0%	100.0%	92.2%
	Replicate 2	100.0%	97.4%	100.0%	99.9%	100.0%	93.5%
Hyperforin	Replicate 1	100.0%	99.9%	100.0%	99.7%	100.0%	97.8%
	Replicate 2	100.0%	106%	100.0%	92.3%	100.0%	96.8%
Hypericin	Replicate 1	100.0%	99.1%	100.0%	94.9%	100.0%	98.7%
	Replicate 2	100.0%	108%	100.0%	103%	100.0%	98.7%
Diazepam	Replicate 1	100.0%	93.0%	100.0%	92.9%	100.0%	88.8%
	Replicate 2	100.0%	95.5%	100.0%	91.8%	100.0%	91.1%
Citalopram	Replicate 1	100.0%	93.7%	100.0%	91.2%	100.0%	94.5%
	Replicate 2	100.0%	101%	100.0%	100%	100.0%	100%

Supplementary material

Alkaloids in commercial preparations of California poppy – quantification, intestinal permeability and microbiota interactions

Antoine Chauveaur^a, Annelies Geirnaert^b, Angela Babst^b, Andrea Treyer^a, Christophe Lacroix^b, Matthias Hamburger^{a,*}, Olivier Potterat^{a,b}

Affiliations

^aDivision of Pharmaceutical Biology, Department of Pharmaceutical Sciences, University of Basel, Basel, Switzerland

^bLaboratory of Food Biotechnology, Institute of Food, Nutrition and Health, Department of Health Science and Technology, ETH Zurich, Zurich, Switzerland

* Corresponding authors

Prof. Dr. Olivier Potterat
Division of Pharmaceutical Biology, Department of Pharmaceutical Sciences, University of Basel, Klingelbergstrasse 50, 4056 Basel, Switzerland
olivier.potterat@unibas.ch
Tel. +41 61 207 14 25

Prof. Dr. Matthias Hamburger
Division of Pharmaceutical Biology, Department of Pharmaceutical Sciences, University of Basel, Klingelbergstrasse 50, 4056 Basel, Switzerland
matthias.hamburger@unibas.ch
Tel. +41 61 207 14 25

Supplementary material table of contents

Isolation of escholtzine	2 – 4
General procedure	2 – 3
Plant material	3
Extraction and isolation	3
Analytical data of escholtzine	4
Equations	5 – 6
Determination of apparent permeability coefficients	5
Determination of efflux ratio	5
Determination of recoveries	5
Supplementary tables and figures	6 – 20

Isolation of escholtzine

General procedures

Preparative HPLC was carried out on a Preparative LC/MSD System (Agilent Technologies, Santa Clara, CA, USA) consisting of a binary pump (1260 Prep Bin Pump), a quaternary pump (Infinity II 1290), a PDA detector (1100 Series), and a 6120 single quadrupole MS detector. A SunFire Prep C18 OBD column (5 μ m, 150 \times 30 mm i.d., Waters, Milford, MA, USA), equipped with a C18 Prep Guard Cartridge (10 \times 30 mm i.d.) was used. The mobile phase consisted of water (A) and acetonitrile (B), both containing 0.1% formic acid. A flow rate of 20 mL/min was applied. A 1290 Infinity II Valve Drive manual injection system (Agilent Technologies) was used for injection. Data acquisition and processing was done by ChemStation software (Agilent Technologies).

HPLC-PDA-ELSD-ESIMS analysis were conducted on a LC-MS 8030 chromatographic system (Shimadzu, Kyoto, Japan) consisting of a degasser, auto-sampler, quaternary pump (LC-20 CE), a column oven (CTO-20AC), a photo diode array detector (SPD-M20A), connected via a T-split to a triple quadrupole MS, and an ELSD 3300 detector (Alltech, Deerfield, IL, USA). Analysis of escholtzine was carried out on a SunFire C18 column (3.5 μ m, 150 \times 3 mm i.d., Waters) equipped with a guard column (10 \times 3 mm i.d.). Solvents A and B (see above) were used as mobile phase. A gradient of 5-100% B in 30 min was applied at a flow rate of 0.4 mL/min. The LabSolutions software (Shimadzu) was used for data acquisition and processing.

Optical rotation was measured at 25 °C on a JASCO P-2000 polarimeter (Brechtöhler, Schlieren, Switzerland) equipped with a 10 cm temperature-controlled microcell.

NMR spectra were recorded on a Bruker Avance III spectrometer (Bruker BioSpin, Rheinstetten, Germany) operating at 500.13 MHz for ¹H and 125.77 MHz for ¹³C nuclei. ¹H-NMR, ¹H-COSY,

HSQC, HMBC, and NOESY spectra were recorded in CDCl₃ (ARMAR Chemicals, Dörtingen, Switzerland) in a 5 mm BBO probe at 23°C. Data were analyzed using Bruker Topspin 3.5 and ACD/Labs NMR Workbook suites (Advanced Chemistry Development, Toronto, Canada) software. Chemical shifts are reported as δ values (ppm) using the solvent signal (δ_H 7.27; δ_C 77.00, CDCl₃) as internal reference; coupling constants (*J*) are given in Hz.

Ethanol (96%) for extraction was from Brenntag Schweizerhalle AG (Switzerland). Technical grade petroleum ether (Rheuss Chemie, Tägerig, Switzerland), hydrochloric acid (37%, Merck KGaA, Darmstadt, Germany), and ammonia (ammonium hydroxide sol 25%, Hänsseler AG, Herisau, Switzerland) were used for obtaining the alkaloid enriched fraction. Before use, technical grade petroleum ether was redistilled. HPLC-grade acetonitrile (Avantor, Radnor, PA, USA) and water from a Milli-Q water purification system (Merck Millipore, Billerica, USA) were used for HPLC separations. HPLC-grade formic acid and DMSO were obtained from Scharlau (Scharlab S.L., Barcelona, Spain).

Plant material

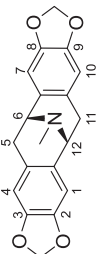
Eschscholzia californica Cham. herb was purchased from Galke (lot number 811502). A voucher specimen (no. 1234) has been deposited at the Division of Pharmaceutical Biology, University of Basel, Switzerland.

Extraction and isolation

The powdered plant material (50 g) was macerated overnight with 70% aqueous EtOH (300 mL). After filtration and drying, the oily residue was re-suspended in 2 M hydrochloric acid (500 mL, pH \approx 1–2) and partitioned with petroleum ether (3 x 300 mL). The remaining aqueous phase was basified with 25% ammonia in water (pH > 8) and partitioned 3 times with 300 mL petroleum ether. The combined organic phases were dried with sodium sulfate, filtered, and evaporated to dryness under reduced pressure to afford a crude alkaloid fraction (135 mg). Preparative HPLC of the crude alkaloid fraction applying a gradient of 10–60% B in 30 min (UV detection at 254 nm) yielded pure escholtzine (15 mg, *t_R* 10.8 min).

Analytical data of escholtzine (*synonym crychine*)

C₁₉H₁₇NO₄, M = 323.3 g/mol, white amorphous powder



ESIMS (positive ion mode) : *m/z* 323.7 [M+H]⁺

[α]_D²⁵ -79.4 (c 0.06, MeOH)

¹H and ¹³C NMR Spectroscopic Data (CDCl₃; 500 MHz for ¹H and 126 MHz for ¹³C NMR; δ in ppm)

position	δ_C , type	δ_H (<i>J</i> in Hz)
1	106.8, CH ^a	6.59, s ^a
2	146.6, C ^a	-
3	147.2, C ^a	-
2,3-OCH ₂ O-	100.9, CH ₂ ^a	5.88, dd (18.2, 1.4) ^a
4	108.6, CH ^a	6.46, s ^a
4a	123.5, C ^a	-
5	33.9, CH ₂ ^a	2.69, d (16.1) ^a , (H _a) 3.55, dd (16.7, 5.6) ^a , (H _b) 4.22, br d (5.7) ^a
6	56.7, CH ^a	-
6a	128.0, C ^a	-
7	106.8, CH ^a	6.59, s ^a
8	146.6, C ^a	-
9	147.2, C ^a	-
8,9-OCH ₂ O-	100.9, CH ₂ ^a	5.88, dd (18.2, 1.4) ^a 6.46, s ^a
10	108.6, CH ^a	-
10a	123.5, C ^a	-
11	33.9, CH ₂ ^a	2.69, d (16.1) ^a , (H _a) 3.55, dd (16.7, 5.6) ^a , (H _b) 4.22, br d (5.7) ^a
12	56.7, CH ^a	-
12a	128.0, C ^a	-
N-CH ₃	40.1, CH ₃	2.70, s ^a

^aOverlapping signals.

Chemical shifts were in agreement with previously reported data [1].

- [1] Y. Suzuki, Y. Saito, M. Goto, D.J. Newman, B.R. O'Keefe, K.H. Lee, K. Nakagawa-Goto, (-)-Neocaryachine, an antiproliferative pavine alkaloid from *Cryptocarya laevigata*, induces DNA double-strand breaks, *Journal of Natural Products*. 80 (2017) 220–224. <https://doi.org/10.1021/acs.jnatprod.6b01153>.

Equations

Determination of apparent permeability coefficients

Apparent permeability coefficients (P_{app}) were calculated according to equations described by Hubatsch et al. [1]. The apparent permeability coefficients (P_{app}), expressed in $\text{cm}^2 \cdot \text{s}^{-1}$, were calculated according to the following equation:

$$P_{app} = \left(\frac{dQ}{dt} \right) \left(\frac{1}{AC_0} \right) \quad (1)$$

Where dQ/dt is the steady-state flux ($\mu\text{M} \cdot \text{s}^{-1}$), A the surface area of the filter (cm^2), and C_0 the initial concentration in the donor chamber (μM).

The lowered donor concentration after each sampling was taken into account, and recalculated by subtracting the cumulative fraction transported (FA_{cum}) to the receiver chamber, at each time interval.

FA_{cum} was calculated according to the following equation:

$$FA_{cum} = \frac{1}{A} \sum_{k=1}^i \frac{[C_R(t_k) - C_R(t_{k-1})] V_R}{[C_D(t_{k-1}) + C_D(t_k)] V_D} \quad (2)$$

where V_R is the receiver chamber volume, t_k is the time point for the sampling occasion k , $C_D(t_k)$ is the measured concentration in the donor chamber at sampling occasion k , $C_R(t_k)$ is the measured concentration in the receiver chamber at sampling occasion k . The sample replacement factor f is defined as $f = (1 - V_S/V_R)$, where V_S is the sample volume and V_R is the receiver chamber volume.

Determination of efflux ratio

P_{app} values in apical to basolateral ($P_{app,AB}$) and P_{app} values in basolateral to apical direction ($P_{app,BA}$) were calculated to determine the efflux ratio (ER) as follows:

$$ER = \frac{P_{app,BA}}{P_{app,AB}} \quad (3)$$

Determination of recoveries

Recovery considering A and B chambers (Re_{AB}) was calculated according to the following equation [1] as:

$$Re_{AB} (\%) = (C_{D(fin)} V_D + C_{R(fin)} V_{R(fin)} + \sum (C_{S(t)} V_{S(t)})) 100 / (C_{D(0)} V_{D(0)}) \quad (4)$$

whereby $C_{D(0)}$ and $C_{D(fin)}$ are the initial or final concentration in the donor chamber, and $C_{R(0)}$ and $C_{R(fin)}$ the respective concentration on the receiver side. $C_{S(t)}$ represents the respective concentrations of samples withdrawn at different time points t , and V_D , V_R and V_S are the respective volumes.

Recovery considering A, B and cell fraction (Re_{ABC}) was calculated to evaluate the accumulation or binding of study compounds to the cells. Re_{ABC} was calculated according to the following equation:

$$Re_{ABC} (\%) = Re_{AB} + A_{cells} 100 / A_{D(0)} \quad (5)$$

whereby A_{cells} represents the amount in the cell fraction, and $A_{D(0)}$ the initial amount in the donor chamber.

[1] I. Hubatsch, E.G.E. Ragnarsson, P. Artursson, Determination of drug permeability and prediction of drug absorption in Caco-2 monolayers, *Nat. Protoc.* 2 (2007) 2111–2119. <https://doi.org/10.1038/nprot.2007.303>.

Table S1. California poppy commercial preparations specifications

Product n°	Manufacturer	Product name	Galenic formulation	Composition	Posology
1	Akepharma	Akegétules® Escholzia	Dry powder of flowering aerial parts	300 mg of powdered aerial parts per capsule	4 to 5 capsules per day
2	Herbes et Plantes	Escholzia Bio	Dry powder of flowering aerial parts	250 mg of powdered aerial parts per capsule	2 to 3 capsules a day
3	Nature et Plantes	Escholzia	Dry powder of flowering aerial parts	600 mg of powdered aerial parts per tablet	2 to 3 tablets per day
4	Pierre Fabre	Elusanes Escholzia	Dry extract of flowering aerial parts	200 mg extract per capsule Aqueous extract Drug/extract ratio: 4 – 7:1	2 tablets per day
5	PiLLe laboratoire	Phytostandard Escholzia Valériane	Dry extract of aerial flowering parts, and extract of valerian roots	80 mg of California poppy and 32 mg of valerian per tablet California poppy and valerian extracts	2 to 4 tablets per day
6	Boiron	Sommeil Pavot jaune de Californie	Liquid extract of flowering aerial parts	45% hydroalcoholic extract of flowering aerial parts 94 mg of extract per mL	5 mL per day
7	Naturalma	Escolzia	Liquid preparation of flowering aerial parts	Glycerine-water (90%) extract of herbal drug. Drug/extract ratio 10:1. 100 mg of extract per mL	2 to 6 mL per day
8	Wolada	Sommeil Pavot jaune de Californie Bio	Liquid extract of flowering aerial parts	45% hydroalcoholic extract of flowering aerial parts. No information on drug/extract ratio	0.6 to 1.2 mL per day

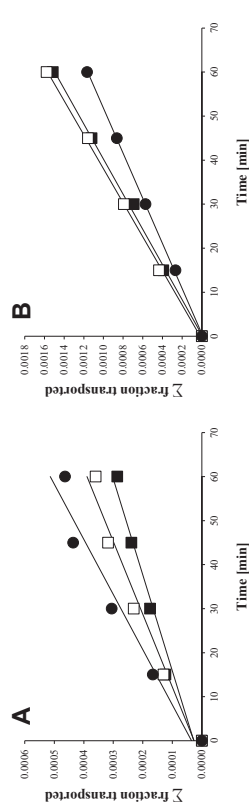


Fig. S1. Atenolol transport across Caco-2 monolayers in AB (A) and in BA direction (B) over 60 min. The cumulative fraction for three individual monolayers is shown; (■) monolayer 1, (□) monolayer 2, and (●) monolayer 3.

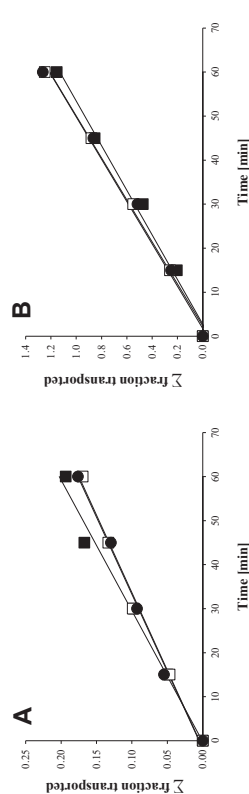


Fig. S2. Propranolol transport across Caco-2 monolayers in AB (A) and in BA direction (B) over 60 min. The cumulative fraction for three individual monolayers is shown; (■) monolayer 1, (□) monolayer 2, and (●) monolayer 3.

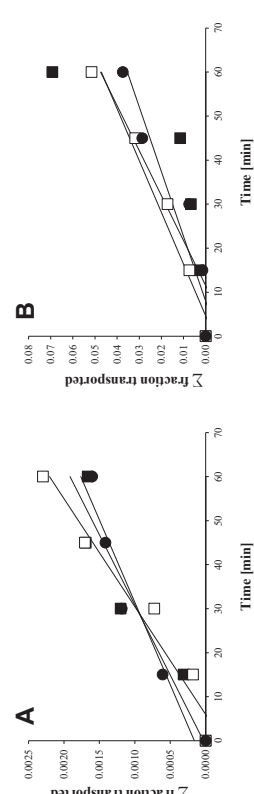


Fig. S3. Califormidine transport across Caco-2 monolayers in AB (A) and in BA direction (B) over 60 min. The cumulative fraction for three individual monolayers is shown; (■) monolayer 1, (□) monolayer 2, and (●) monolayer 3.

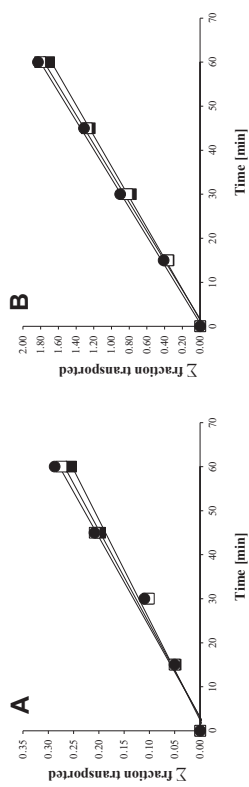


Fig. S4. Escholtzine transport across Caco-2 monolayers in AB (A) and in BA direction (B) over 60 min. The cumulative fraction for three individual monolayers is shown; (■) monolayer 1, (□) monolayer 2, and (●) monolayer 3.

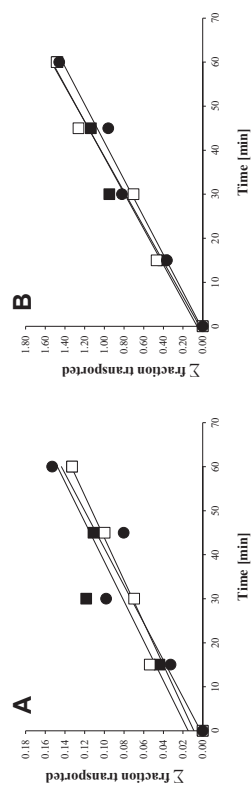


Fig. S5. Protopine transport across Caco-2 monolayers in AB (A) and in BA direction (B) over 60 min. The cumulative fraction for three individual monolayers is shown; (■) monolayer 1, (□) monolayer 2 and (●) monolayer 3.

Table S2. Transepithelial electrical resistance (TEER) values of Caco-2 cell monolayers before (n = 6) and after (n = 2) experiments, and fluorescein flux across Caco-2 cell monolayers, determined after transport experiments (n = 2).

Compounds	Pre-experiment TEER ($\Omega \cdot \text{cm}^2$) (Mean \pm SD.)	Post-experiment TEER ($\Omega \cdot \text{cm}^2$) (values of the 2 replicates)	Fluorescein flux (%) (values of the 2 replicates)
Califormidine perchlorate	255 \pm 606	225 220	0.20 0.64
Escholtzine	251 \pm 937	256 241	0.18 0.41
Protopine	288 \pm 465	260 270	0.96 0.70
Atenolol	279 \pm 809	225 235	0.29 0.51
Propranolol HCl	255 \pm 556	236 247	0.28 0.79

Table S3. Optimized MS/MS parameters for californidine perchlorate, escholtzine, protopine, atenolol, propranolol HCl and verapamil HCl, all analyzed on an Agilent UHPLC-MS/MS system

Compounds	Optimized MS/MS parameters		
	ESI mode	MRM transitions	Collision energy (eV)
Californidine perchlorate	Positive	338.1 → 235.1 (Q)	45
		338.1 → 205.0 (Q)	35
Escholtzine	Positive	324.1 → 176.1 (Q)	70
		324.1 → 293.1 (Q)	22
Protopine	Positive	354.14 → 189.1 (Q)	30
		354.14 → 149.0 (Q)	26
Atenolol	Positive	267.17 → 56.1 (Q)	30
		267.17 → 91.1 (Q)	54
Propranolol HCl	Positive	260.17 → 56.1 (Q)	26
		260.17 → 72.1 (Q)	18
Verapamil HCl (IS)	Positive	455.29 → 77.1	125

Q: Quantifier; q: Qualifier

Table S4. Optimized UHPLC parameters of all studied compounds

Compounds	Gradient	Flow rate (mL/min)	Total run time (min)	Eluent	Column	Injection vol. (µL)	Column temp. (°C)	Autosampler temp. (°C)
Californidine perchlorate	5% to 100% in 5 min, 100% for 0.5 min	0.4	7	A: Water + 0.1% FA ^a B: Methanol + 0.1% FA	Waters Acquity UPLC® HSS T3, 1.8 µm, 100 × 2.1 mm	2	45	4
Escholtzine	5% to 100% in 2 min, 100% for 1 min	0.5	5	A: Water + 0.1% FA B: Acetonitrile + 0.1% FA	Waters Acquity UPLC® HSS T3, 1.8 µm, 100 × 2.1 mm	2	45	4
Protopine	5% to 100% in 2 min, 100% for 1 min	0.5	5	A: Water + 0.1% FA B: Acetonitrile + 0.1% FA	Waters Acquity UPLC® HSS T3, 1.8 µm, 100 × 2.1 mm	2	45	4
Atenolol	5% to 100% in 2 min, 100% for 1 min	0.5	5	A: Water + 0.1% FA B: Acetonitrile + 0.1% FA	Waters Acquity UPLC® HSS T3, 1.8 µm, 100 × 2.1 mm	2	45	4
Propranolol HCl	5% to 100% in 2 min, 100% for 1 min	0.5	5	A: Water + 0.1% FA B: Acetonitrile + 0.1% FA	Waters Acquity UPLC® HSS T3, 1.8 µm, 100 × 2.1 mm	2	45	4

^aFA: Formic acid

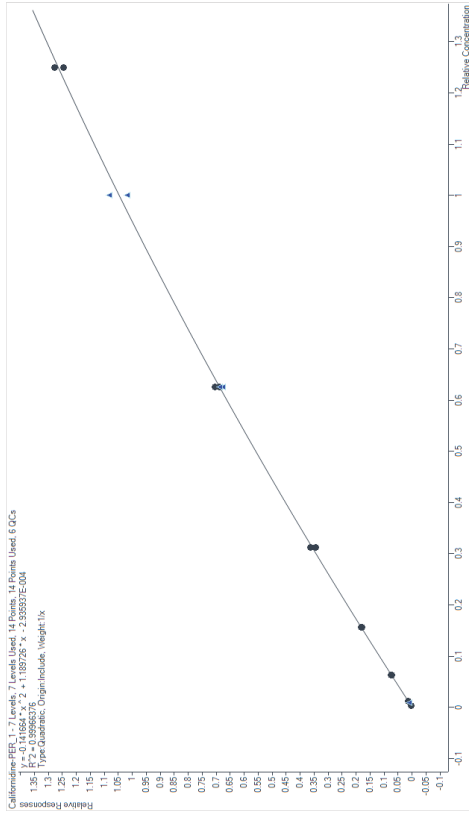


Fig. S6. Calibration curve of californidine perchlorate (calibrators are shown as crosses and quality controls are shown as squares) for quantification in California poppy herbal products

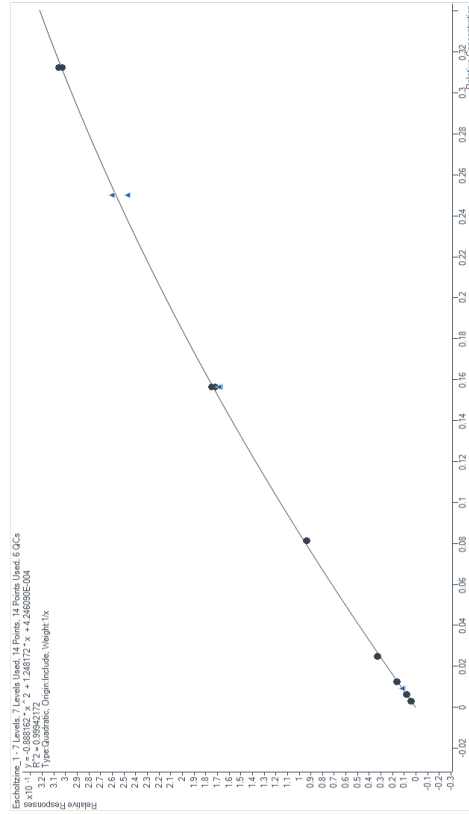


Fig. S7. Calibration curve of escholtzine (calibrators are shown as crosses and quality controls are shown as squares) for quantification in California poppy herbal products

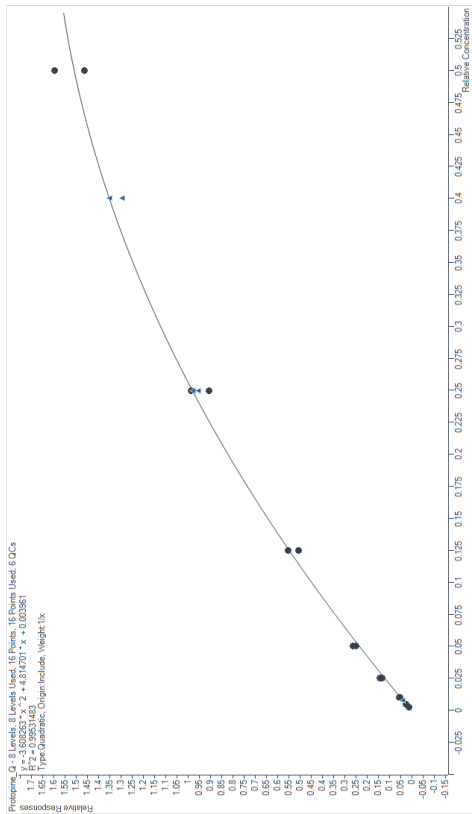


Fig. S8. Calibration curve of protopine (calibrators are shown as crosses and quality controls are shown as squares) for quantification in California poppy herbal products

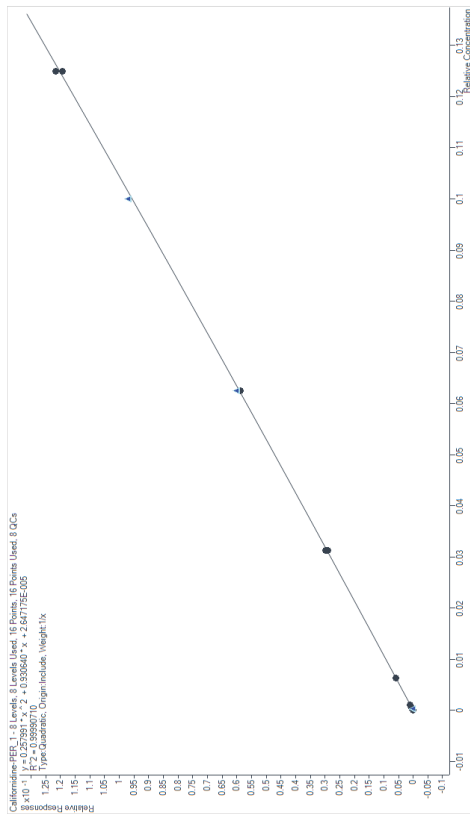


Fig. S9. Calibration curve of californidine perchlorate (calibrators are shown as crosses and quality controls are shown as squares) for quantification in Caco-2 samples

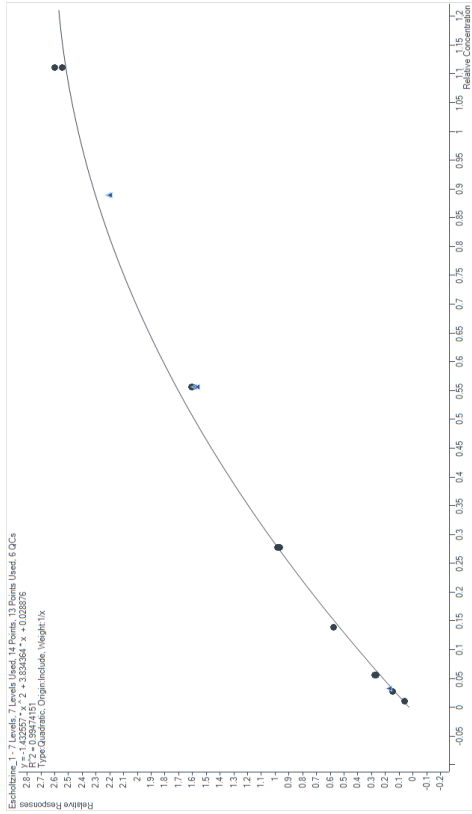


Fig. S10. Calibration curve of escholtzine (calibrators are shown as dots and quality controls are shown as triangles) for quantification in Caco-2 samples.

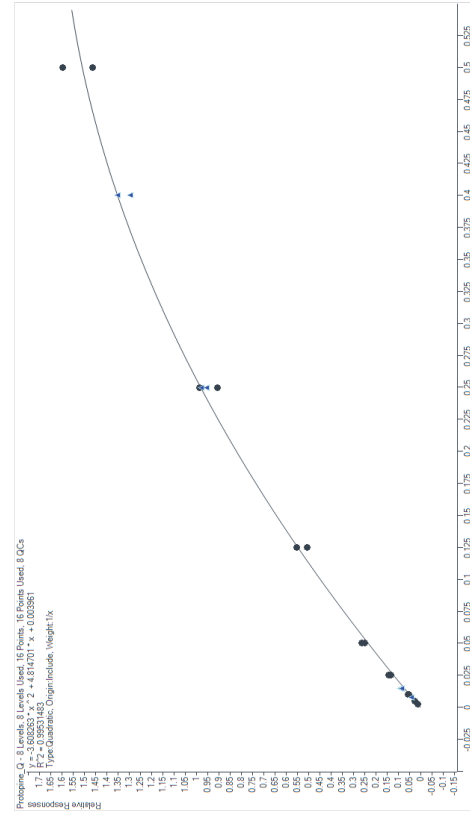


Fig. S11. Calibration curve of protopine (calibrators are shown as crosses and quality controls are shown as squares) for quantification in Caco-2 samples

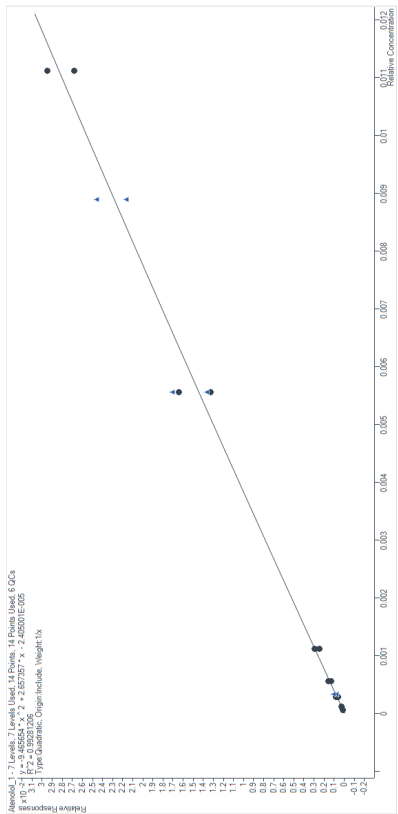


Fig. S12. Calibration curve of atenolol, low range (calibrators are shown as dots and quality controls are shown as triangles)

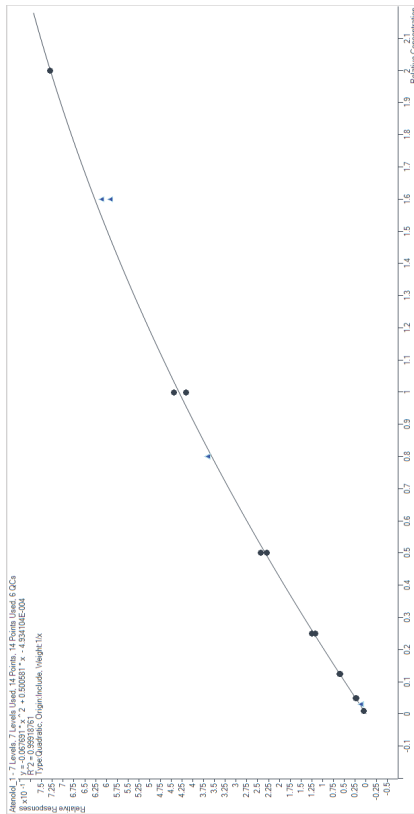


Fig. S13. Calibration curve of atenolol, high range (calibrators are shown as dots and quality controls are shown as triangles)

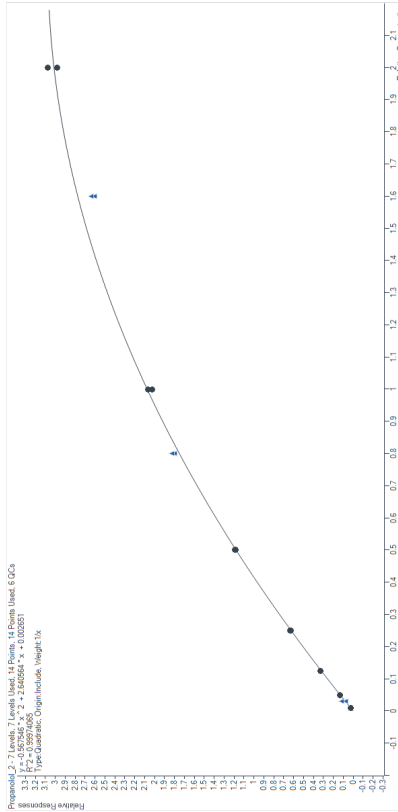


Fig. S14. Calibration curve of propranolol HCl (calibrators are shown as dots and quality controls are shown as triangles)

Table S5. Calibrators and calibration curve parameters for the determination of californidine in California poppy herbal products

Response: $A \times Conc^2 + B \times Conc + C$, 1/X weighing, Quadratic regression, included origin (n = 2)

	Concentration (ng/mL)						Regression parameters				
	2.50	10.0	50.0	125	250	500	1000	A	B	C	R ²
Mean	2.54	9.90	49.46	125	252	498	1001	-0.2694	1.7137	-0.0003	0.9995
SD	0.09	0.26	1.48	2.07	9.44	17.7	22.4	0.1806			
CV%	3.56	2.59	2.99	1.66	3.75	3.56	2.24				
RE%	1.55	-0.96	-1.08	0.09	0.81	-0.47	0.12				

Table S6. Quality control samples of californidine in California poppy herbal products (n = 2)

	QCL		QCM		QCH	
	7.50	500	10.0	20.0	65.0	125
Mean	7.45	487	760			
SD	0.57	16.5	55.6			
CV%	7.61	3.38	7.32			
RE%	-0.64	-2.56	-5.06			

Table S7. Calibrators and calibration curve parameters for the determination of escholtzine in California poppy herbal products

Response: $A \times Conc^2 + B \times Conc + C$, 1/X weighing, Quadratic regression, included origin (n = 2)

	Concentration (ng/mL)						Regression parameters				
	2.50	5.00	10.0	20.0	65.0	125	250	A	B	C	R ²
Mean	2.35	4.99	10.2	21.3	63.4	125	251	-0.9069	1.2664	0.0005	0.9994
SD	0.11	0.18	0.33	0.18	0.65	1.36	4.84	0.0265			
CV%	4.77	3.69	3.28	0.85	1.02	1.10	1.93				
RE%	-6.10	-0.17	2.20	6.59	-2.41	-0.39	0.33				

Table S8. Quality control samples of escholtzine in California poppy herbal products (n = 2)

	OCL		OCM		QCH	
	7.50	125	125	200	200	200
Mean	7.35	120	120	197	197	197
SD	0.08	1.07	1.07	10.2	10.2	10.2
CV%	1.09	0.89	0.89	5.17	5.17	5.17
RE%	-2.06	-3.68	-3.68	-1.48	-1.48	-1.48

Table S9. Calibrators and calibration curve parameters for the determination of protopine in California poppy herbal products

Response: $A \times Conc^2 + B \times Conc + C$, 1/X weighing, Quadratic regression, included origin (n = 2)

	Concentration (ng/mL)						Regression parameters			R ²	
	2.50	10.0	25.0	50.0	125	250	500	A	B		C
Mean	2.29	10.4	25.6	52.2	126	241	508	-0.6548	1.2663	0.0007	0.9991
SD	0.11	0.23	0.70	1.36	2.34	4.93	3.99	0.0010			
CV%	4.85	2.24	2.76	2.60	1.86	3.70	0.79				
RE%	-8.53	3.61	2.28	4.33	0.73	-3.56	1.54				

Table S10. Quality control samples of protopine in California poppy herbal products (n = 2)

	QCL		QCM		QCH	
	7.50	240	250	400	400	375
Mean	7.32	240	240	375	375	375
SD	0.69	13.6	13.6	4.62	4.62	4.62
CV%	9.49	5.68	5.68	1.23	1.23	1.23
RE%	-2.35	-3.83	-3.83	-6.21	-6.21	-6.21

Table S11. Calibrators and calibration curve parameters for the determination of californidine in Caco-2 samples

Response: $A \times Conc^2 + B \times Conc + C$, 1/X weighing, Quadratic regression, included origin (n = 2)

	Concentration (ng/mL)						Regression parameters			R ²	
	0.10	0.50	1.00	6.25	31.3	62.5	125	A	B		C
Mean	0.09	0.52	1.02	6.35	31.6	61.7	125	0.5205	0.9877	0.00003	0.9998
SD	0.01	0.003	0.03	0.12	0.41	0.77	1.68	0.3671			
CV%	6.31	0.56	3.07	1.95	1.31	1.24	1.34				
RE%	-6.94	4.98	2.36	1.54	1.15	-1.22	0.21				

Table S12. Quality control samples of californidine in Caco-2 samples (n = 2).

	QCL		QCM		QCH	
	0.30	62.5	62.5	100	100	99.0
Mean	0.32	61.8	61.8	99.0	99.0	99.0
SD	0.02	2.23	2.23	2.95	2.95	2.95
CV%	6.12	3.62	3.62	2.98	2.98	2.98
RE%	5.23	-1.20	-1.20	-1.03	-1.03	-1.03

Table S13. Calibrators and calibration curve parameters for the determination of escholtzine in Caco-2 samples

Response: $A \times Conc^2 + B \times Conc + C$, 1/X weighing, Quadratic regression, included origin (n = 3)

	Concentration (ng/mL)						Regression parameters			R ²	
	10.0	25.00	50.0	125	250	500	1000	A	B		C
Mean	8.76	28.7	57.4	139	251	457	1063	-1.1979	3.3765	0.0230	0.9957
SD	0.31	0.23	0.70	1.22	0.52	1.48	1.23	0.2818			
CV%	3.56	0.79	1.22	0.52	1.48	1.23	3.57				
RE%	-12.4	14.7	14.8	11.4	0.58	-8.58	6.31				

Table S14. Quality control samples of escholtzine in Caco-2 samples (n = 2).

	QCL		QCM		QCH	
	30.0	500	500	800	800	743
Mean	34.1	441	441	743	743	743
SD	0.32	9.99	9.99	21.7	21.7	21.7
CV%	0.94	2.27	2.27	2.92	2.92	2.92
RE%	13.8	-11.8	-11.8	-7.14	-7.14	-7.14

Table S15. Calibrators and calibration curve parameters for the determination of protopine in Caco-2 samples

Response: $A \times Conc^2 + B \times Conc + C$, 1/X weighing, Quadratic regression, included origin (n = 2)

	Concentration (ng/mL)						Regression parameters			R ²		
	2.50	5.00	10.0	25.0	50.0	125	250	500	A		B	C
Mean	2.50	4.76	10.16	25.4	54.0	118	249	446	-4.0896	6.2262	-0.0007	0.9946
SD	0.49	0.20	0.40	1.86	2.35	7.25	19.4	26.9	0.6807			
CV%	19.4	4.16	3.96	7.34	4.36	6.13	7.80	6.03				
RE%	0.09	-4.86	1.58	1.44	7.91	-5.37	-0.23	-10.7				

Table S16. Quality control samples of protopine in Caco-2 sample (n = 2).

	QCL		QCM		QCH	
	7.50	400	250	400	400	392
Mean	8.14	247	247	392	392	392
SD	0.15	7.88	7.88	17.5	17.5	17.5
CV%	1.86	3.19	3.19	4.5	4.5	4.5
RE%	8.60	-1.22	-1.22	-2.01	-2.01	-2.01

Table S17. Calibrators and calibration curve parameters for the determination of atenolol (high range).

Response: $A \times Conc^2 + B \times Conc + C$, 1/X weighing, Quadratic regression, included origin (n = 4)

	Concentration (ng/mL)						Regression parameters			R ²	
	10.00	50.00	125.00	250.00	500.00	1000.00	2000.00	A	B		C
Mean	10.22	46.80	123.14	251.51	509.03	988.65	2005.13	-0.07347	0.51651	-0.00021	0.99918
SD	0.60	1.85	3.58	6.20	14.06	34.59	13.85	0.00848			
CV%	5.90	3.95	2.91	2.47	2.76	3.50	0.69				
RE%	2.16	-6.40	-1.49	0.60	1.81	-1.13	0.26				

Table S18. Quality control samples of atenolol, high range (n = 4).

	OC1	OCM	OCH
	30.00	800.00	1600.00
Mean	25.76	827.17	1505.27
SD	0.87	3.74	29.58
CV%	3.39	0.45	1.97
RE%	-14.14	3.40	-5.92

Table S19. Calibrators and calibration curve parameters for the determination of atenolol (low range).
Response: $A \times Conc^2 + B \times Conc + C$, 1/X weighing, Quadratic regression, included origin (n = 4)

	Concentration (ng/mL)						Regression parameters			R ²	
	0.050	0.100	0.250	0.500	1.000	5.000	10.000	A	B		C
Mean	0.047	0.103	0.258	0.493	1.024	5.177	10.028	-9.49216	2.66480	-0.00002	0.99256
SD	0.002	0.009	0.036	0.059	0.014	0.646	0.580	0.03748	-	-	-
CV%	3.808	8.738	13.955	11.949	1.331	12.486	5.783	-	-	-	-
RE%	-5.154	2.565	3.270	-1.406	2.430	3.549	0.280	-	-	-	-

Table S20. Quality control samples of atenolol, low range (n = 4).

	OC1	OCM	OCH
	0.300	5.000	8.000
Mean	0.297	4.783	8.169
SD	0.003	0.064	0.618
CV%	0.843	1.331	7.564
RE%	-0.969	-4.346	2.116

Table S21. Calibrators and calibration curve parameters for the determination of propranolol.
Response: $A \times Conc^2 + B \times Conc + C$, 1/X weighing, Quadratic regression, included origin (n = 4)

	Concentration (ng/mL)						Regression parameters			R ²	
	10.00	50.00	125.00	250.00	500.00	1000.00	2000.00	A	B		C
Mean	9.65	50.77	127.73	250.86	503.12	981.20	2053.78	-0.60147	2.69910	0.00234	0.99977
SD	0.12	0.33	0.94	1.54	6.29	14.41	195.62	0.04797	-	-	-
CV%	1.24	0.64	0.74	0.61	1.25	1.47	9.52	-	-	-	-
RE%	-3.54	1.55	2.18	0.34	0.62	-1.88	2.69	-	-	-	-

Table S22. Quality control samples of propranolol (n = 4).

	QC1	QCM	QCH
	30.00	800.00	1600.00
Mean	34.00	830.23	1417.46
SD	4.89	11.77	35.11
CV%	14.38	1.42	2.48
RE%	13.33	3.78	-11.41

Table S23. Carry-over assessment for all analytes and corresponding internal standard (I.S.) for analysis of California Poppy preparations (n = 2)

Compound	Mean carry-over (%)
Californidine	14.15
I.S.	0.050
Escholtzine	1.490
I.S.	0.067
Protopine	4.420
I.S.	0.057

Table S24. Carry-over assessment for all analytes and corresponding internal standard (I.S.) for analysis of Caco-2 samples (n = 2)

Compound	Mean carry-over (%)
Californidine	15.22
I.S.	0.036
Escholtzine	2.929
I.S.	0.063
Protopine	5.803
I.S.	0.051
Atenolol – high range	0.702
I.S.	0.047
Atenolol – low range	5.592
I.S.	0.102
Propranolol	4.890
I.S.	0.036

Table S25. Stability of study compounds after 24 h incubation of donor 1 or 2 PolyfermS microbiota supplemented with 30% nutritive medium and 20 μ L DMSO. Values are normalized to 100%.

Compounds	Replicates		Abiotic		Female donor 1		Female donor 2	
	Replicate 1	Replicate 2	T0h	T24h	T0h	T24h	T0h	T24h
Californidine	100.0%	99.1%	100.0%	99.1%	100.0%	98.2%	100.0%	106.7%
Escholzine	Replicate 1	100.0%	100.0%	103.1%	100.0%	101.5%	100.0%	101.7%
	Replicate 2	100.0%	100.0%	103.1%	90.2%	100.0%	100.0%	93.7%
Protopine	Replicate 1	100.0%	100.0%	98.7%	100.0%	98.6%	100.0%	97.4%
	Replicate 2	100.0%	100.0%	105.0%	94.7%	100.0%	100.0%	101.6%
			100.0%	101.2%	100.0%	94.8%	100.0%	95.6%

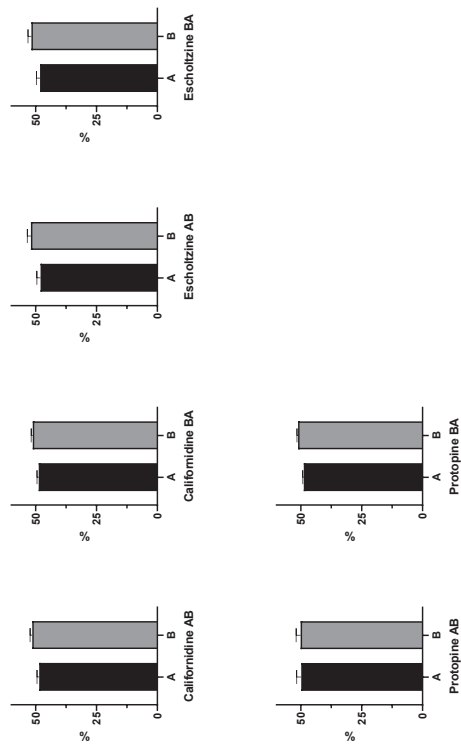


Fig. S15. Distribution of compounds in apical (A) and basolateral (B) compartments after 1 h transport experiments on cell-free inserts, with transport buffer adjusted to pH 6.5 (10 mM MES, 4.2 mM NaHCO_3 in HBSS) in apical chamber, and to pH 7.4 in basolateral chamber (25 mM HEPES, 4.2 mM NaHCO_3 in HBSS), both containing 1% DMSO. Experiments were done in apical to basolateral (AB) and basolateral to apical directions (BA). Data are expressed as percentage and mean \pm S.D. from 3 independent experiments.

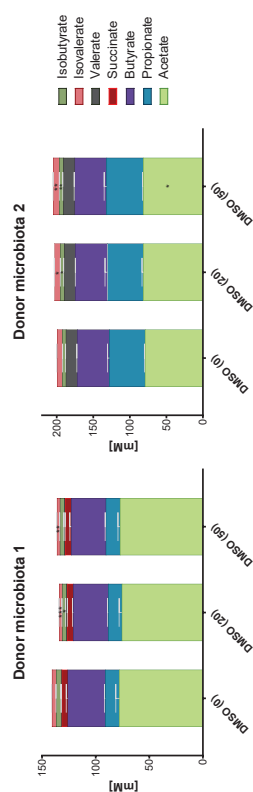


Fig. S16. Short chain fatty acid concentration after 24 h incubation of PolyfermS microbiota 1 and 2 supplemented with 30% nutritive medium and different DMSO concentrations (0, 20 or 50 μ L) that served as controls for compounds dissolved in DMSO. Averages \pm SD (n=3). Asterisks indicate significant differences in average metabolite concentration compared to DMSO (0) control (p < 0.05).

Curriculum Vitae

Antoine Chauveau

Education

04.2018 – present

Doctor of Philosophy (PhD) in Pharmaceutical Sciences, University of Basel (Switzerland)

Title: Intestinal permeability and gut microbiota interactions of phytochemicals from herbal drugs used in the treatment of depressive, anxiety and sleeping disorders

Supervisor: Prof. Dr. Matthias Hamburger

09.2015 – 09.2016

Master's Degree (MSc) in Analytical Chemistry, Aix-Marseille University (France)

09.2013 – 06.2015

Master's Degree (MSc) in Human Nutrition and Food Sciences, university of Nantes (France)

Degree jointly offered by university of Nantes (France) and ONIRIS (Nantes-Atlantic National College of Veterinary Medicine, Food Sciences and Engineering)

09.2010 – 06.2013

Bachelor's degree (BSc) in Biology, university of Poitiers (France)

3rd year completed with University of Turku in Finland (in the frame of the European Erasmus program), with English as language of courses and exams

Employment history

04.2018 – present

Researcher in Pharmaceutical Sciences (PhD candidate), University of Basel

Quantitative UHPLC-MS/MS and HPLC-UV, Caco-2 cells model and permeability studies, plant extract characterization

Practical course teaching and supervising of Master students in Drug Sciences

03.2016 – 03.2017

Bioanalyst, Bioanalytics and DMPK, F. Hoffman-La Roche, pRED, Basel

Conduct both non-regulated and GLP-regulated bioanalytical method development and validation by UHPLC-MS/MS, for PK/PD pre-clinical studies.

First 6 months (03.2016 – 09.2016) were in the frame of a Master's thesis with Aix-Marseille University (France)

01.2015 – 06.2015

Research intern, Laboratory of Nutrition Obesity and Thrombotic risk, Aix-Marseille University

Topic: Lipids metabolism, pathophysiology of dyslipidemia and bariatric surgery in humans

Main techniques: Separation of lipoproteins, Bradford assay, electrophoresis with IEF gels, GC-MS/MS.

2014 (1.5 months)

Research intern, Laboratory of Nutrition and Endocrinology, ONIRIS Nantes

Topic: Effect of polyphenols on memory loss in dogs (beagles)

Main techniques: RNA extraction, isolation of mononuclear cells, ELISA, calorimetry.

2013 (1 month)

Research intern, Laboratory of Animal Physiology, university of Turku (Finland)

Topic: Antioxidant status of *Marenzelleria* (worm from the Baltic sea) in different parts of the Turku Archipelago (Finland)

Main techniques: Colorimetric enzyme assay (GST assay), Bradford assay, tissue homogenization.

Publications

A. Chauveau, A. Geirnaert, A. Babst, A. Treyer, C. Lacroix, M. Hamburger, O. Potterat, Alkaloids in commercial preparations of California poppy – Quantification, intestinal permeability and microbiota interactions, *Biomed. Pharmacother.* 166 (2023) 115420.
<https://doi.org/10.1016/j.biopha.2023.115420>.

A. Chauveau, A. Treyer, A. Geirnaert, L. Bircher, A. Babst, V.F. Abegg, A.P. Simões-Wüst, C. Lacroix, O. Potterat, M. Hamburger, Intestinal permeability and gut microbiota interactions of pharmacologically active compounds in valerian and St. John’s wort, *Biomed. Pharmacother.* 162 (2023) 114652.
<https://doi.org/10.1016/j.biopha.2023.114652>.

M. Winker, **A. Chauveau**, M. Smieško, O. Potterat, A. Areesanan, A. Zimmermann-Klemd, C. Gründemann, Immunological evaluation of herbal extracts commonly used for treatment of mental diseases during pregnancy, *Sci. Rep.* 13 (2023) 9630.
<https://doi.org/10.1038/s41598-023-35952-5>.

D. Spiess, V.F. Abegg, **A. Chauveau**, J. Rath, A. Treyer, M. Reinehr, S. Kuoni, M. Oufir, O. Potterat, M. Hamburger, A.P. Simões-Wüst, Transplacental passage of hyperforin, hypericin, and valerenic acid, *Front. Pharmacol.* 14 (2023).
<https://doi.org/10.3389/fphar.2023.1123194>.

D. Spiess, V.F. Abegg, **A. Chauveau**, A. Treyer, M. Reinehr, M. Oufir, E. Duong, O. Potterat, M. Hamburger, A.P. Simões-Wüst, Placental passage of protopine in an *ex vivo* human perfusion system, *Planta Med.* 89 (2022) 194–207.
<https://doi.org/10.1055/a-1829-9546>.

D. Spiess, M. Winker, **A. Chauveau**, V.F. Abegg, O. Potterat, M. Hamburger, C. Gründemann, A.P. Simões-Wüst, Medicinal plants for the treatment of mental diseases in pregnancy: An *in vitro* safety assessment, *Planta Med.* 88 (2021) 1036–1046.
<https://doi.org/10.1055/a-1628-8132>.

Conferences

08.2021

Flash presentation at the 34th Seminar in Pharmaceutical Sciences “New paradigms in natural product drug discovery: Bedside to Bench ↔ Bench to Bedside”, Leysin, Switzerland

Languages

French	Native proficiency
English	Full professional proficiency
Spanish	Elementary proficiency
German	Elementary proficiency